ANALYSIS OF A SLOT PAIR ON A CONDUCTING SPHERE

CHAIWAT LEEKPAI

A THESIS SUBMITTED IN PARTIAL FULFILLMENT OF
THE REQUIREMENT FOR THE DEGREE OF
MASTER OF ENGINEERING IN ELECTRICAL ENGINEERING
SCHOOL OF GRADUATE STUDIES
KING MONGKUT'S INSTITUTE OF TECHNOLOGY LADKRABANG
2001

ISBN 974-648-093-6

หัวข้อวิทยานิพนธ์	**การวิเคราะห์สายอากาศร่องคู่บนผิวตัวนำทรงกลม**
นักศึกษา	**นายชัยวัฒน์ หลีกภัย**
รหัสประจำตัว	**41061023**
ปริญญา	**วิศวกรรมศาสตรมหาบัณฑิต**
สาขาวิชา	**วิศวกรรมไฟฟ้า**
พ.ศ.	**2544**
อาจารย์ผู้ควบคุมวิทยานิพนธ์	**รศ.ดร.โมไนย ไกรฤกษ์**

บทคัดย่อ

วิทยานิพนธ์ฉบับนี้เป็นการนำเสนอการศึกษาคุณลักษณะของสายอากาศแบบร่องเดี่ยววางนอน, ร่องเดี่ยวเอียง และร่องคู่บนผิวตัวนำทรงกลมซึ่งจะมีประโยชน์ในการศึกษาสายอากาศแบบแถวลำดับร่องบนผิวทรงกลม โดยสายอากาศจะถูกกระตุ้นโดยตรงที่ปากร่องด้วยสายส่งแกนร่วมทำให้กำหนดองค์ประกอบของสนามไฟฟ้าในแนวสัมผัสกับปากร่อง ทฤษฎีของลอเรนซ์จะถูกนำมาใช้ในการแก้ปัญหาเงื่อนไขขอบเขต จากนั้นจะใช้การแปลงระบบพิกัดในการแปลงจากกรณีของการจัดวางร่องเดี่ยวในแนวนอนไปยังการจัดวางร่องเดี่ยวทำมุมใดๆ จากนั้นจะศึกษาสายอากาศแบบร่องคู่เพื่อหาเงื่อนไขในการสร้างคลื่นโพลาไรซ์วงกลม ผลการคำนวณเชิงตัวเลขจะแสดงคุณลักษณะของสายอากาศเช่น สภาพเจาะจงทิศทาง, ความกว้างครึ่งกำลังของรูปแบบการแพร่กระจายคลื่นในสภาพเงื่อนไขต่างๆ กัน และได้สร้างสายอากาศและทดสอบคุณลักษณะต่างๆ เพื่อเปรียบเทียบและยืนยันผลการคำนวณ

Thesis Title	Analysis of a Slot Pair on a Conducting Sphere
Student	Mr. Chaiwat Leekpai
Student ID.	41061023
Degree	Master of Engineering
Programme	Electrical Engineering
Year	2001
Thesis Advisor	Assoc. Prof. Dr. Monai Krairiksh

ABSTRACT

This thesis presents characteristics of a single horizontal slot, inclined single slot and slot pair on a conducting sphere which is essential to the study of a spherical slot array antenna. The antenna is excited directly by a coaxial transmission line at the center of a slot. The tangential component of the electric field on a slot is assumed. The Lorentz reciprocity theorem is used in solving the boundary value problem. Then, the coordinate transformation can be applied to transform the fields from a single horizontal slot to an arbitrary inclined slot. Radiation from a slot pair that provides the circular polarization is investigated. Numerical results of directivity, half-power beamwidth and radiation pattern are illustrated. The antenna is fabricated and the measurement is set up to verify the numerical results.

ACKNOWLEGDEMENTS

There are many persons that contributed their help to the successful completion of this thesis without them, this thesis would never been accomplished.

A portion of the research work was conducted under the supervision of Associate Professor Monai Krairiksh, I gratefully acknowledge his contribution and support. I also appreciate his attention and stimulation the progress of this research.

I would like to appreciate to Assistant Professor Sompol Kosulvit for his useful suggestion. Also, I wish to thank Associate Professor Kraisin Songwatana for his helpful discussion on mathematics.

Special thanks are due to my senior and colleagues in Wireless Communication Laboratory, ReCCIT, especially my junior Mr. Sakchai Thongthap for his helpful in fabrication and experiment. Many thanks to Mr. Chuwong Pongcharoenpanich for improving the manuscript. Also, I would like to thank Mr. Komsak Meksamoot and Mr. Duang-arthit Srimoon for their consultants in any troubles when I studied at KMITL.

I wish to thank the National Science and Technology Development Agency (NSTDA) for partially funding this research grant and local graduate scholarship program for providing the graduate scholarship during my graduate study.

Finally, This thesis is dedicated to my parent, who has been a constant support my education throughout my life.

Chaiwat Leekpai

TABLE OF CONTENTS

TABLE OF CONTENTS (to)

TABLE OF CONTENTS (to)

LIST OF TABLES

LIST OF FIGURES

LIST OF FIGURES (to)

LIST OF FIGURES (to)

NOMENCLATURES

Symbol	
$[\hat{c}]$	Unprimed Cartesian system
$[\hat{c}']$	Primed Cartesian system
$[\hat{c}'']$	Double primed Cartesian system
$[\hat{c}''']$	Triple primed Cartesian system
$[\hat{s}]$	Unprimed spherical system
$[\hat{s}']$	Primed spherical system
$[^{c'}T^{c}]$	Transformation matrix from unprimed to primed components in Cartesian system
$[^{c''}T^{c}]$	Transformation matrix from unprimed to double primed components in Cartesian system
$[^{c''}T^{c'}]$	Transformation matrix from double to triple primed components in Cartesian system
$[^{s'}T^{c'}]$	Transformation matrix from Cartesian to spherical components in primed system
$[^{c}T^{s}]$	Transformation matrix from spherical to Cartesian components in unprimed system
$[\bar{r}']$	Radial component (r) in primed spherical system
$[\bar{r}-\bar{a}]$	Radial component ($r-a$) in unprimed spherical system

CHAPTER 1

INTRODUCTION

1.1 Literature of the Spherical Slot Antennas

Recent years have rapidly grown of wireless communication systems. In these systems, an antenna plays an important role in establishing a communication link between different destination points. With diversified applications of wireless communications, the demand of complicate antenna has increased. On the other hand, they must fulfill a number of additional requirements. Such antennas must feature improved performance, including attracting the commercial market. For a number of years, parabolic reflector antennas have been used in a variety of communication systems. These antennas are relatively easy and inexpensive to manufacture. However, their inconvenience is that they occupy a substantial volume, which makes them obtrusive in appearance. In order to attract a wider commercial market, there has been a significant more to replace parabolic antennas by low profile, light weight and more aesthetic antennas. One possible candidate is the microstrip array antenna. It has a number of the desired features such as low profile, light weight and relatively low cost to develop. However, one problem of this antenna is that it performs poor bandwidth and radiation efficiency when the required gain value is high. This is due to the lossy feed network that accompanies the array. In the search for new antennas, the concept of radial line slot array antenna (RLSA) was demonstrated and further extended by Goto and Yamamoto [1-2]. The advantages of the RLSA antenna include high radiation efficiency, low profile and easy for installation, due to its flat surface. However, it was found that the beam direction was about 30° from broadside, making the elevation angle of the beam relatively high. To lower the elevation angle, Takada *et al.* [3-4] proposed a rotating mode generator to feed the slot array antenna but the gain degradation and a more complicated feeding structure occurred. This will be affected to the subscriber located far from the equator in mobile satellite communication. To overcome the beam coverage problems, the spherical array antenna was proposed. It is one of the conformal array antenna which provides a large scanning angles with a constant gain and beamwidth. There are many types of the element which are considered to be located on the spherical surface. The turnstile dipole was proposed and optimized by Horiguchi[5-6]. Furthermore, the steerable spherical array antenna [7] used a microstrip antenna as a radiating element was also investigated. However, it is apparent that these array elements are suffered from the complicated feeding structure and the gain degradation. From these reasons, Krairiksh *et al.* [8-9] presented the spherical slot array antenna. The advantage of this antenna type is that the structure is expected to be suitable for mass production as well as the feeding structure is simple. Additionally, the cost effective of the antenna is very significant. However, the derivations of a radiation characteristic of a fundamental element have not been revealed. The general solutions of an arbitrary aperture were derived by Bailin and Silver [10]. Some results of a slot on sphere were shown by Mushiake and Webster [11]. In addition, the applications of coordinate relations derived by Sengupta [12-13] and Hoffman [14] are revised and assisted in a straightforward application. As all the reasons mentioned above, in this thesis, the rigorous formulations of a half-wave slot on sphere are demonstrated. Furthermore, the circular polarization properties of a slot pair will be discussed.

to be located on the spherical surface. The turnstile dipole was proposed and optimized by Horiguchi[5-6]. Furthermore, the steerable spherical array antenna [7] used a microstrip antenna as a radiating element was also investigated. However, it is apparent that these array elements are suffered from the complicated feeding structure and the gain degradation. From these reasons, Krairiksh *et al.* [8-9] presented the spherical slot array antenna. The advantage of this antenna type is that the structure is expected to be suitable for mass production as well as the feeding structure is simple. Additionally, the cost effective of the antenna is very significant. However, the derivations of a radiation characteristic of a fundamental element have not been revealed. The general solutions of an arbitrary aperture were derived by Bailin and Silver [10]. Some results of a slot on sphere were shown by Mushiake and Webster [11]. In addition, the applications of coordinate relations derived by Sengupta [12-13] and Hoffman [14] are revised and assisted in a straightforward application. As all the reasons mentioned above, in this thesis, the rigorous formulations of a half-wave slot on sphere are demonstrated. Furthermore, the circular polarization properties of a slot pair will be discussed.

1.2 Objective of the Thesis

The objective of this thesis is to analyze the characteristics of the half-wave slots on a conducting sphere. Firstly, the characteristics, such as radiation pattern, directivity, half-power beamwidth, of a single horizontal slot on sphere are analyzed. The parameter is the effective radius of a conducting sphere. Next, consideration of the radiation for various inclination angles of a single inclined slot on a conducting sphere by utilizing the coordinate transform is discussed. Consequently, the analysis of the circular polarization of two orthogonal slots can be tractable via the coordinate transform. The numerical results, such as co- and cross-polarization patterns and the axial ratio, are displayed. The interested parameters are the separation distances between the center of slots and the axis. Ultimately, the experiments of radiation and circular polarization characteristics of the fabricated antenna are set up to verify the theory.

Furthermore, the derivations of the vector analysis in the spherical coordinate system are shown in Appendix A. The brief of the special functions in spherical coordinate and useful series expansions are summarized in Appendix B.

CHAPTER 2

EXTERIOR ELECTROMAGNETIC FIELD FOR ARBITRARY APERTURE ON A SPHERE

In this chapter, the boundary value problems for exterior electromagnetic fields of a sphere are derived. It is shown that, outside the source region, the electromagnetic fields for spherical geometry can be decomposed into two types of modes: TE^R (transverse electric field to R mode) and TM^R (transverse magnetic field to R mode). The organizations in this chapter are as follows. Maxwell's equations in the differential form are presented first. Next, we determine the component of the electric and magnetic fields for TE^R and TM^R modes. Finally, the application of Lorentz reciprocity theorem is applied to determine the fields in the region exterior to a sphere.

2.1 Maxwell's Equations

The fundamental equations for electromagnetic field are Maxwell's equations. The equations were formulated through experiments carried out by many scientists such as Faraday, Gauss, Lenz, Coulomb, Volta and others and were led to theoretical conclusion by James Clerk Maxwell (1831-1879), a scottish physicist and mathematician. Maxwell's equations were originally written as a set of coupled, time dependent integral equations. However, only the differential forms are suitable to use in this thesis. Therefore, the differential form of Maxwell's equations with time-harmonic $e^{j\omega t}$ will be expressed here

$$\nabla \times \overline{E} = -\overline{M}_i - j\omega\overline{B} \tag{2.1a}$$

$$\nabla \times \overline{H} = \overline{J}_i + \overline{J}_c + j\omega\overline{D} \tag{2.1b}$$

$$\nabla \cdot \overline{D} = q_{ev} \tag{2.1c}$$

$$\nabla \cdot \overline{B} = q_{mv} \tag{2.1d}$$

with the continuity equation

$$\nabla \cdot \overline{J} = -j\omega q_{ev} \tag{2.1e}$$

where

$\overline{E}$: electric field intensity (volts/meter)
$\overline{H}$: magnetic field intensity (amperes/meter)
$\overline{D}$: electric flux density (coulombs/square meter)
$\overline{B}$: magnetic flux density (webers/square meter)
$\overline{J}_i$: impressed (source) electric current density (amperes/square meter)

$\overline{M}_i$: impressed (source) magnetic current density (volts/square meter)

q_{ev} : electric charge density (coulombs/cubic meter)

q_{mv} : magnetic charge density (webers/cubic meter)

The relationships among $\overline{D},\overline{E},\overline{B},\overline{H}$ and $\overline{J}$ depend on the characteristics of the medium and they are expressed by the constitutive parameters. Then, they can be expressed as

$$\overline{D} = \varepsilon\overline{E} \tag{2.2a}$$

$$\overline{B} = \mu\overline{H} \tag{2.2b}$$

$$\overline{J}_c = \sigma\overline{E} \tag{2.2c}$$

where ε,μ,σ denote the permittivity, the permeability and the conductivity of the medium, respectively.

$$\varepsilon = \varepsilon_o\varepsilon_r \tag{2.3a}$$

$$\mu = \mu_o\mu_r \tag{2.3b}$$

ε_r,μ_r are the relative permittivity and permeability which depend on the electrical properties of the medium. ε_o is the free space permittivity and equals to 8.854×10^{-12} or about $10^{-9}/36\pi$ farads per meter. In the same manner, μ_o is the free space permeability equals to $4\pi\times10^{-7}$ henries per meter. For free space the conductivity vanishes.

2.2 Wave Equation

Maxwell's equations are the coupled first-order differential equations which are difficult to solve as the boundary value problem. This problem is overcome by numerical methods such as Finite Difference Time Domain (FDTD), Finite Element Method (FEM), Method of Moments (MoM) [15-16]. The numerical methods have advantage in solving the complex geometry without higher mathematics but generally give approximate solutions. To solve the Maxwell's equations by analytical method, the Maxwell's equations are raised to the uncoupled second-order differential equations which are referred to as the wave equation. By taking the curl for both sides of (2.1a) and (2.1b) with the property of vector identity

$$\nabla\times\nabla\times\overline{A} = \nabla(\nabla\cdot\overline{A}) - \nabla^2\overline{A} \tag{2.4}$$

After rearranging (2.1a) and substituting (2.1c), the electric vector wave equation can be represented as

$$\nabla^2\overline{E} = \nabla\times\overline{M}_i + j\omega\overline{J}_i + \frac{1}{\varepsilon}\nabla q_{ev} + j\omega\mu\sigma\overline{E} - \omega^2\mu\varepsilon\overline{E} \tag{2.5}$$

In the same manner, substituting (2.1d) into (2.1b), we can write that

$$\nabla^2 \overline{H} = -\nabla \times \overline{J}_i + \sigma \overline{M}_i + j\omega\varepsilon \overline{M}_i + \frac{1}{\mu}\nabla q_{mv} + j\omega\mu\sigma\overline{H} - \omega^2 \mu\varepsilon\overline{H} \tag{2.6}$$

For the source-free ($\overline{J}_i = \overline{M}_i = q_{ev} = q_{mv} = 0$) and losses ($\sigma = 0$) medium, the vector wave equation (2.5) and (2.6) reduce, respectively, to

$$\nabla^2 \overline{E} = -\omega^2 \mu\varepsilon\overline{E} \tag{2.7a}$$

$$\nabla^2 \overline{H} = -\omega^2 \mu\varepsilon\overline{H} \tag{2.7b}$$

These equations represent three vector field components, each of which satisfies the Helmholtz or scalar wave equation.

$$\nabla^2 \psi + k^2 \psi = 0 \tag{2.8}$$

Both (2.7a)-(2.7b) and (2.8) represent the simplest forms for the wave equation.

2.3 Hertz Vector Potential

The electromagnetic fields in orthogonal coordinate systems can be determined by using the hertz vector potential as aid in obtaining the solutions for electric and magnetic fields. The hertz vector potential can be classified into two types by means of the mode generated. They are the $\overline{\Pi}$, magnetic hertz vector potential for transverse magnetic (TM) mode and $\overline{\Pi}^*$, electric hertz vector potential for transverse electric (TE) mode.

Since the spherical coordinate system does not possess an axis with constant direction, the vector wave equation can not be separated into three uncoupled scalar wave equations. It is necessary to devise the different method which is based on the selection of the Lorentz condition and the configurations are subjected to the transverse field to radial direction. After the assembly, it can be written to

Transverse magnetic to R mode: TM^R

$$\overline{E}_\Pi = \nabla \times \nabla \times (r\overline{\Pi}) \tag{2.9a}$$

$$E_r = \frac{\partial^2}{\partial r^2}(r\Pi_r) + k^2(r\Pi_r) \tag{2.9b}$$

$$E_\theta = \frac{1}{r}\frac{\partial^2}{\partial r \partial \theta}(r\Pi_r) \tag{2.9c}$$

$$E_\phi = \frac{1}{r\sin\theta}\frac{\partial^2}{\partial r \partial \phi}(r\Pi_r) \tag{2.9d}$$

$$\overline{H}_{\Pi} = -j\omega\mu\nabla\times(r\overline{\Pi}) \tag{2.10a}$$

$$H_r = 0 \tag{2.10b}$$

$$H_\theta = \frac{j\omega\varepsilon}{r\sin\theta}\frac{\partial}{\partial\phi}(r\Pi_r) \tag{2.10c}$$

$$H_\phi = \frac{-j\omega\varepsilon}{r}\frac{\partial}{\partial\theta}(r\Pi_r) \tag{2.10d}$$

and for the transverse electric to R mode: TE^R

$$\overline{E}_{\Pi^*} = -j\omega\mu\nabla\times(r\overline{\Pi}^*) \tag{2.11a}$$

$$E_r = 0 \tag{2.11b}$$

$$E_\theta = \frac{-j\omega\mu}{r\sin\theta}\frac{\partial}{\partial\phi}(r\Pi_r^*) \tag{2.11c}$$

$$E_\phi = \frac{j\omega\mu}{r}\frac{\partial}{\partial\theta}(r\Pi_r^*) \tag{2.11d}$$

$$\overline{H}_{\Pi^*} = \nabla\times\nabla\times(r\overline{\Pi}^*) \tag{2.12a}$$

$$H_r = \frac{\partial^2}{\partial r^2}(r\Pi_r^*) + k^2(r\Pi_r^*) \tag{2.12b}$$

$$H_\theta = \frac{1}{r}\frac{\partial^2}{\partial r\partial\theta}(r\Pi_r^*) \tag{2.12c}$$

$$H_\phi = \frac{1}{r\sin\theta}\frac{\partial^2}{\partial r\partial\phi}(r\Pi_r^*) \tag{2.12d}$$

where Π_r and Π_r^* satisfy the scalar wave equation in (2.8), that is

$$\nabla^2\Pi_r + k^2\Pi_r = \nabla^2\Pi_r^* + k^2\Pi_r^* = 0 \tag{2.13}$$

The solution can be constructed by the method of separation variables [17-18]. By assuming the product of solution

$$\Pi_r^{(*)} = f(r)g(\theta)h(\phi) \tag{2.14}$$

Which (2.13) can be reduced to the three scalar differential equations and can be written to

$$\left\{\frac{1}{r^2}\frac{d}{dr}\left(r^2\frac{d}{dr}\right)+\left[k^2-\frac{n(n+1)}{r^2}\right]\right\}f(r)=0 \qquad (2.15a)$$

$$\left\{\frac{1}{\sin\theta}\frac{d}{d\theta}\left(\sin\theta\frac{d}{d\theta}\right)+\left[n(n+1)-\frac{m^2}{\sin^2\theta}\right]\right\}g(\theta)=0 \qquad (2.15b)$$

and

$$\left\{\frac{d^2}{d\phi^2}+m^2\right\}h(\phi)=0 \qquad (2.15c)$$

Each of above equation is a second-order differential equation, and the solution is represented by a combination of two independent solutions.

Let us first consider (2.15a). This is a spherical Bessel equation and its solutions is given by

$$f(r)=\begin{cases} L_1 j_n(kr)+M_1 y_n(kr) & (2.16a) \\ N_1 h_n^{(1)}(kr)+P_1 h_n^{(2)}(kr) & (2.16b) \end{cases}$$

where L_1, M_1, N_1, P_1 are the arbitrary constants. In (2.16a), $j_n(kr)$ and $y_n(kr)$ are referred to, respectively, the spherical Bessel functions of the first and second kinds. They are represented to the standing wave in the radial direction. In (2.16b), $h_n^{(1)}(kr)$ and $h_n^{(2)}(kr)$ are referred to, respectively, the ordinary spherical Hankel function of the first and second kinds. They are represented to the travelling wave in the radial direction.

Next consider (2.15b). This is Legendre differential equation and its solutions are given by

$$g(\theta)=\begin{cases} L_2 P_n^m(\cos\theta)+N_2 Q_n^m(\cos\theta) & n=\text{integer} \quad (2.17a) \\ M_2 P_n^m(\cos\theta)+P_2 P_n^m(-\cos\theta) & n\neq\text{integer} \quad (2.17b) \end{cases}$$

where L_2, M_2, N_2, P_2 are the arbitrary constants. In (2.17a) and (2.17b) $P_n^m(\cos\theta)$ and $Q_n^m(\cos\theta)$ are referred to, respectively, the associated Legendre functions of the first and second kinds.

In (2.15c), this is a generally second order differential equation and the solutions are given by

$$h(\phi)=\begin{cases} L_3\cos(m\phi)+M_3\sin(m\phi) & (2.18a) \\ N_3e^{-jm\phi}+P_3e^{+jm\phi} & (2.18b) \end{cases}$$

where L_3, M_3, N_3, P_3 are the arbitrary constants.

The appropriate solution forms of f, g and h will depend on the geometry of the problems. For representing a field outside a sphere, they may take the form as can be written to

$$\prod_r^{(*)}=[L_1h_n^{(1)}(kr)+M_1h_n^{(2)}(kr)][L_2P_n^m(\cos\theta)+M_2Q_n^m(\cos\theta)] \\ [L_3\cos(m\phi)+M_3\sin(m\phi)] \qquad (2.19)$$

To form outward traveling waves and the boundary condition at infinite distance. The spherical Hankel function of a second kind $h_n^{(2)}(kr)$ is chosen and for the finite field at any value of θ, including $\theta=0,\pi$ where $Q_n^m(\cos\theta)$ possesses singularity. So that (2.19) can be reduced to

$$\prod_r^{(*)}=h_n^{(2)}(kr)P_n^m(\cos\theta)[A_{nm}\cos(m\phi)+B_{nm}\sin(m\phi)] \qquad (2.20)$$

where A_{nm} and B_{nm} are normalized coefficients to be determined. Each of field components, due to hertz vector potentials $\overline{\prod}$ and $\overline{\prod}^*$, is derived by the superposition of the fields from TE and TM modes. By substituting (2.20) to (2.9a)-(2.12d). Thus, we can write

$$E_r=\sum_n\sum_m\frac{n(n+1)}{r}h_n^{(2)}(kr)P_n^m(\cos\theta)[A_{nm}\cos m\phi+B_{nm}\sin m\phi] \qquad (2.21a)$$

$$E_\theta=\sum_n\sum_m\frac{1}{r}\frac{d}{dr}[rh_n^{(2)}(kr)]\frac{dP_n^m(\cos\theta)}{d\theta}[A_{nm}\cos m\phi+B_{nm}\sin m\phi] \\ -j\omega\mu\sum_{n'}\sum_m\frac{m}{\sin\theta}h_{n'}^{(2)}(kr)\frac{dP_{n'}^m(\cos\theta)}{d\theta}[C_{n'm}\sin m\phi-D_{n'm}\cos m\phi] \qquad (2.21b)$$

$$E_\phi=\sum_n\sum_m\frac{-m}{r\sin\theta}\frac{d}{dr}[rh_n^{(2)}(kr)]P_n^m(\cos\theta)[A_{nm}\sin m\phi-B_{nm}\cos m\phi] \\ +j\omega\mu\sum_{n'}\sum_m h_{n'}^{(2)}(kr)\frac{dP_{n'}^m(\cos\theta)}{d\theta}[C_{n'm}\cos m\phi+D_{n'm}\sin m\phi] \qquad (2.21c)$$

$$H_r=\sum_{n'}\sum_m\frac{n'(n'+1)}{r}h_{n'}^{(2)}(kr)P_{n'}^m(\cos\theta)[C_{n'm}\cos m\phi+D_{n'm}\sin m\phi] \qquad (2.21d)$$

$$H_\theta = \sum_{n'}\sum_{m}\frac{1}{r}\frac{d}{dr}[rh_{n'}^{(2)}(kr)]\frac{dP_{n'}^{m}(\cos\theta)}{d\theta}[C_{n'm}\cos m\phi + D_{n'm}\sin m\phi] - j\omega\mu\sum_{n}\sum_{m}\frac{m}{\sin\theta}h_n^{(2)}(kr)P_n^m(\cos\theta)[A_{nm}\sin m\phi - B_{nm}\cos m\phi] \quad (2.21e)$$

$$H_\phi = \sum_{n'}\sum_{m}\frac{-m}{r\sin\theta}\frac{d}{dr}[rh_{n'}^{(2)}(kr)]P_{n'}^{m}(\cos\theta)[C_{n'm}\sin m\phi - D_{n'm}\cos m\phi] - j\omega\mu\sum_{n}\sum_{m}h_n^{(2)}(kr)\frac{dP_n^m(\cos\theta)}{d\theta}[A_{nm}\cos m\phi + B_{nm}\sin m\phi] \quad (2.21f)$$

where $n^{(')}, m$ are the wave number in TM (TE) mode.

Finally, we completely derived the exterior electromagnetic fields in the spherical coordinate. However, they also have the unknown coefficients which can be easily solved from the enforcement of the boundary condition.

2.4 Lorentz Reciprocity Theorem

The Lorentz reciprocity theorem is useful for deriving the reciprocal property of the antenna [18], for deriving the orthogonal property of wave modes and so forth. Now we will discuss the property of reciprocity theorem and apply it to solve our boundary problem. Suppose that the distributions of impressed current $\bar{J}_{i1}, \bar{M}_{i1}$ give rise to field components $\bar{E}_1, \bar{H}_1$. Similarly, source current $\bar{J}_{i2}, \bar{M}_{i2}$ give rise to $\bar{E}_2, \bar{H}_2$. The individual fields satisfy Maxwell's equations as shown in (2.22a) to (2.22b).

$$\left.\begin{aligned}\nabla\times\bar{E}_1 &= -\bar{M}_{i1} - j\omega\mu\bar{H}_1\\ \nabla\times\bar{H}_1 &= \bar{J}_{i1} + j\omega\mu\bar{E}_1\end{aligned}\right\} \quad \text{for source } \bar{J}_{i1}, \bar{M}_{i1} \quad (2.22a)$$

$$\left.\begin{aligned}\nabla\times\bar{E}_2 &= -\bar{M}_{i2} - j\omega\mu\bar{H}_2\\ \nabla\times\bar{H}_2 &= \bar{J}_{i2} + j\omega\mu\bar{E}_2\end{aligned}\right\} \quad \text{for source } \bar{J}_{i2}, \bar{M}_{i2} \quad (2.22b)$$

The following scalar and dot products of (2.22a) and (2.22b) are valid.

$$\bar{E}_2\cdot\nabla\times\bar{H}_1 = \bar{E}_2\cdot\bar{J}_{i1} + j\omega\mu\bar{E}_2\cdot\bar{E}_1 \quad (2.23a)$$

and

$$\bar{H}_1\cdot\nabla\times\bar{E}_2 = -\bar{H}_1\cdot\bar{M}_{i2} - j\omega\mu\bar{H}_1\cdot\bar{H}_2 \quad (2.23b)$$

or

$$\bar{E}_1\cdot\nabla\times\bar{H}_2 = \bar{E}_1\cdot\bar{J}_{i2} + j\omega\mu\bar{E}_1\cdot\bar{E}_2 \quad (2.23c)$$

and

$$\overline{H}_2 \cdot \nabla \times \overline{E}_1 = -\overline{H}_2 \cdot \overline{M}_{i1} - j\omega\mu \overline{H}_2 \cdot \overline{H}_1 \qquad (2.23d)$$

Now by using vector identity

$$\overline{E}_2 \cdot \nabla \times \overline{H}_1 - \overline{H}_1 \cdot \nabla \times \overline{E}_2 = -\nabla \cdot (\overline{E}_2 \times \overline{H}_1) \qquad (2.24a)$$

and

$$\overline{E}_1 \cdot \nabla \times \overline{H}_2 - \overline{H}_2 \cdot \nabla \times \overline{E}_1 = -\nabla \cdot (\overline{E}_1 \times \overline{H}_2) \qquad (2.24b)$$

Subtracting (2.24b) from (2.24a) reduces to

$$\nabla \cdot (\overline{E}_1 \times \overline{H}_2 - \overline{E}_2 \times \overline{H}_1) = -\overline{E}_1 \cdot \overline{J}_{i2} + \overline{E}_2 \cdot \overline{J}_{i1} + \overline{H}_1 \cdot \overline{M}_{i2} - \overline{H}_2 \cdot \overline{M}_{i1} \qquad (2.25)$$

We now integrate both sides of (2.25) over a volume V. Then using the divergence theorem, we get

$$\iint_S (\overline{E}_1 \times \overline{H}_2 - \overline{E}_2 \times \overline{H}_1) \cdot \hat{n} ds = \iiint_V (-\overline{E}_1 \overline{J}_{i2} + \overline{E}_2 \cdot \overline{J}_{i1} + \overline{H}_1 \cdot \overline{M}_{i2} - \overline{H}_2 \cdot \overline{M}_{i1}) dv \qquad (2.26)$$

where $\hat{n}$ is a unit vector directed along the outward normal to close surface S. It is clear that the surface integral in (2.26) is zero, if the enclosed volume contains no sources.

Next, we will consider a special case by giving S to be a close surface composes of S_a and S_∞. S_a is arbitrary closed surface that encloses all the sources. We also consider another surface S_∞ extended to spherical surface with infinite radius. This event is shown in Figure 2.1. The corresponding to surface integral in (2.26) over the volume enclosed by S_a and S_∞ is zero because there are no contained source. Thus, (2.26) can be reduced to

$$\iint_{S_a + S_\infty} (\overline{E}_1 \times \overline{H}_2 - \overline{E}_2 \times \overline{H}_1) \cdot \hat{n} ds = 0 \qquad (2.27)$$

$$\iint_{S_a} (\overline{E}_1 \times \overline{H}_2 - \overline{E}_2 \times \overline{H}_1) \cdot \hat{n} ds + \iint_{S_\infty} (\overline{E}_1 \times \overline{H}_2 - \overline{E}_2 \times \overline{H}_1) \cdot \hat{n} ds = 0 \qquad (2.28)$$

From the radiation conditions at infinite point, we now apply the Sommerfeld radiation condition over S_∞ which satisfies the following equations.

$$\lim_{r \to \infty} r \left[(\hat{i}_r \times \overline{H}) + \left(\frac{\varepsilon}{\mu} \right)^{1/2} \overline{E} \right] = 0 \qquad (2.29a)$$

$$\lim_{r \to \infty} r \left[\overline{H} - \left(\frac{\varepsilon}{\mu} \right)^{1/2} (\hat{i}_r \times \overline{E}) \right] = 0 \qquad (2.29b)$$

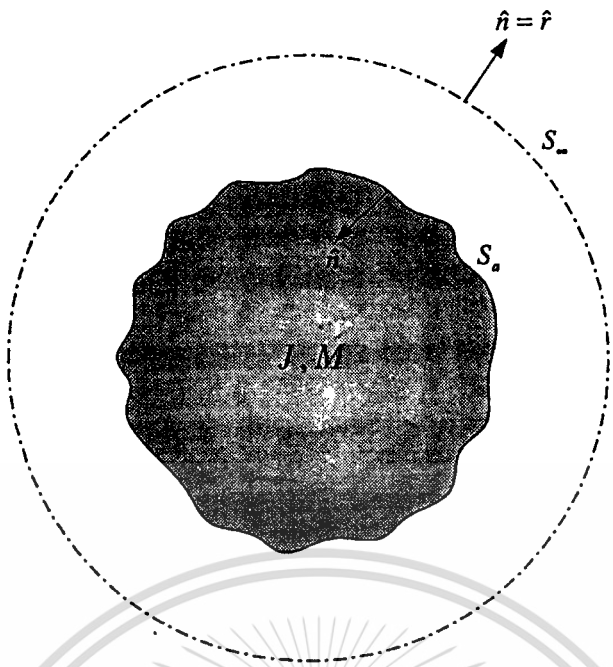

Fig. 2.1 Close surface S_a encloses all sources J and M and exterior spherical surface S_∞ with infinite radius

When we expand each component that satisfies both conditions, then, they can be written that

$$H_{\phi 1} = \left(\frac{\varepsilon}{\mu}\right)^{1/2} E_{\theta 1} \qquad H_{\theta 1} = -\left(\frac{\varepsilon}{\mu}\right)^{1/2} E_{\phi 1} \tag{2.30a}$$

$$H_{\phi 2} = \left(\frac{\varepsilon}{\mu}\right)^{1/2} E_{\theta 2} \qquad H_{\theta 2} = -\left(\frac{\varepsilon}{\mu}\right)^{1/2} E_{\phi 2} \tag{2.30b}$$

Both of fields represent outgoing plane wave. Then, we expand each component in a second term on the left-hand side of (2.28) by replacing a unit vector $\hat{n}$ with a radially outward unit vector. Therefore, we can write that

$$\iint_{S_a} (\overline{E}_1 \times \overline{H}_2 - \overline{E}_2 \times \overline{H}_1) \cdot \hat{n} ds + \iint_{S_\infty} (E_{\theta 1} H_{\phi 2} - E_{\phi 1} H_{\theta 2} - E_{\theta 2} H_{\phi 1} + E_{\phi 2} H_{\theta 1}) ds = 0 \tag{2.31}$$

Substituting (2.30a) and (2.30b) to the integration over S_∞ in (2.31). Thus it follows that the integration over infinitely spherical surface S_∞ will vanish. Finally, (2.31) reduces to

$$\iint_{S_a} (\overline{E}_1 \times \overline{H}_2 - \overline{E}_2 \times \overline{H}_1) \cdot \hat{n} ds = 0 \tag{2.32}$$

where S_a, as indicated in Figure 2.1, enclosed all sources.

2.5 Boundary Value Problem of a Sphere

In this section, we will consider the boundary value of a conducting sphere of radius "a" with a radiating aperture designated by S_{ap} on the surface as shown in Figure 2.2. On the assumption of perfectly conducting sphere with vanishing thickness, the tangential components on the surface are not zero over the radiating aperture. Thus, the boundary conditions of the electric fields are

$$E_\theta(a,\theta,\phi) = f_1(\theta,\phi) \tag{2.33a}$$

and

$$E_\phi(a,\theta,\phi) = f_2(\theta,\phi) \tag{2.33b}$$

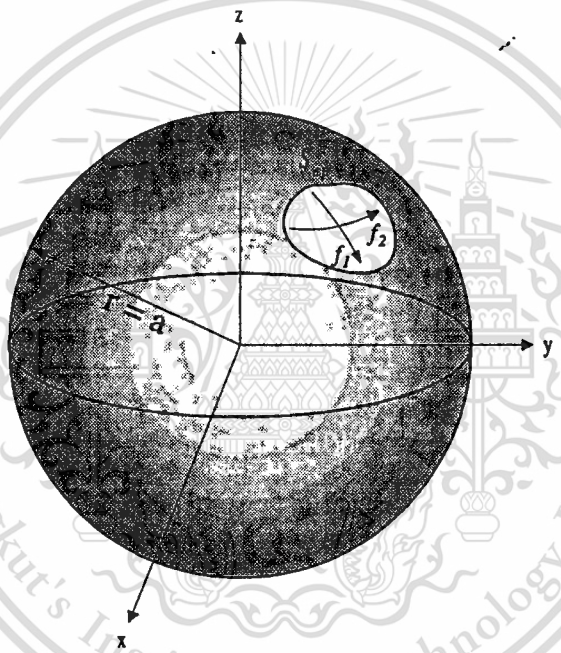

Fig. 2.2 Geometry of a sphere with arbitrary radiating aperture

To determine the unknown coefficients A_{nm}, B_{nm}, C_{nm} and D_{nm} in (2.21a)-(2.21f), we apply the Lorentz reciprocity theorem in the previous section. From the Lorentz reciprocity theorem for a source-free region, (2.32) can be rewritten as

$$\iint_{S_{ap}} (\overline{E}_1 \times \overline{H}_2)\cdot\hat{n}ds = \iint_{S_{ap}} (\overline{E}_2 \times \overline{H}_1)\cdot\hat{n}ds \tag{2.34}$$

where in this case $\hat{n}$ is the radially inward unit vector normal to the closed surface and S_{ap} is an aperture area represented in Figure 2.2. When we expand each component of (2.34), it can be written as

$$\iint_{S_{ap}} (E_{\theta 1}H_{\phi 2} - E_{\phi 1}H_{\theta 2})ds = \iint_{S_{ap}} (E_{\theta 2}H_{\phi 1} - E_{\phi 2}H_{\theta 1})ds \tag{2.35}$$

In order to determine the unknown coefficient A_{nm}, B_{nm}, C_{nm} and D_{nm}, we separate the problem into 2 cases:

1. TM mode to determine A_{nm}, B_{nm}
2. TE mode to determine C_{nm}, D_{nm}

From the integral equation in (2.35), the given boundary value $f_1(\theta,\phi)$ and $f_2(\theta,\phi)$ obviously enter into the integral on left-hand side. We use the series representation, (2.21e) to (2.21f), for $H_{\theta 1}$ and $H_{\phi 1}$ in the integral on the right-hand side. By taking $\overline{E}_2, \overline{H}_2$ to be successively even and odd or $TM_{nm(e,o)}$, $TE_{nm(e,o)}$ modes and also the orthogonal in each wave mode are used to minimize the derivations. For deep understanding, we will explain in each following case.

Case 1: $\overline{E}_2, \overline{H}_2$ are TM^R mode even and odd

Referring to (2.21a)-(2.21f), the TM^R field components can be expressed by

$$E_{r2} = \frac{n(n+1)}{r} h_n^{(2)}(kr) P_n^m(\cos\theta) \begin{Bmatrix} A_{nm}\cos m\phi \\ B_{nm}\sin m\phi \end{Bmatrix} \tag{2.36a}$$

$$E_{\theta 2} = \frac{1}{r}\left[r h_n^{(2)}(kr)\right]' \frac{dP_n^m(\cos\theta)}{d\theta} \begin{Bmatrix} A_{nm}\cos m\phi \\ B_{nm}\sin m\phi \end{Bmatrix} \tag{2.36b}$$

$$E_{\phi 2} = -m\frac{1}{r}\left[r h_n^{(2)}(kr)\right]' \frac{P_n^m(\cos\theta)}{\sin\theta} \begin{Bmatrix} A_{nm}\sin m\phi \\ -B_{nm}\cos m\phi \end{Bmatrix} \tag{2.36c}$$

$$H_{r2} = 0 \tag{2.36d}$$

$$H_{\theta 2} = -j\omega\varepsilon m h_n^{(2)}(kr) \frac{P_n^m(\cos\theta)}{\sin\theta} \begin{Bmatrix} A_{nm}\sin m\phi \\ -B_{nm}\cos m\phi \end{Bmatrix} \tag{2.36e}$$

$$H_{\phi 2} = -j\omega\varepsilon h_n^{(2)}(kr) \frac{dP_n^m(\cos\theta)}{d\theta} \begin{Bmatrix} A_{nm}\cos m\phi \\ B_{nm}\sin m\phi \end{Bmatrix} \tag{2.36f}$$

As mentioned previously, we substitute $f_1(\theta,\phi)$ and $f_2(\theta,\phi)$ in the left-hand side and use the series representation, (2.21e)-(2.21f), for $H_{\theta 1}$ and $H_{\phi 1}$ in the right-hand side of the integral. In order to determine the unknown coefficient A_{nm}, we enter $\overline{E}_2, \overline{H}_2$ by $TM_{nm(e,o)}$, (2.36b)-(2.36c) and (2.36e)-(2.36f), successively. The procedure is straightforward one and leads to (2.37) after arranging the similar terms.

$$\iint_{S_{ap}}\left[f_1(\theta,\phi)\frac{dP_n^m(\cos\theta)}{d\theta}\cos m\phi-\frac{m}{\sin\theta}f_2(\theta,\phi)P_n^m(\cos\theta)\sin m\phi\right]a^2\sin\theta d\theta d\phi$$

$$=A_{nm}\frac{\left[rh_n^{(2)}(kr)\right]'_{r=a}}{a}\int_0^{\pi}\left[\left(\frac{dP_n^m(\cos\theta)}{d\theta}\right)^2\int_0^{2\pi}\cos^2 m\phi d\phi+\frac{m^2}{\sin^2\theta}\left(P_n^m(\cos)\right)^2\int_0^{2\pi}\sin^2 m\phi d\phi\right]\sin\theta d\theta \tag{2.37}$$

Using the orthogonal properties of trigonometric and Legendre functions. These relations are written to

$$\int_0^{2\pi}\begin{Bmatrix}\cos\\ \sin\end{Bmatrix}^2 m\phi d\phi=\pi(1\pm\delta_m)\quad\text{where}\qquad \delta_m=\begin{cases}0 & m\neq 0\\ 1 & m=0\end{cases} \tag{2.38}$$

and

$$\int_0^{\pi}\left\{\frac{dP_n^m(\cos\theta)}{d\theta}\frac{dP_{n'}^m(\cos\theta)}{d\theta}+\frac{m^2}{\sin^2\theta}P_n^m(\cos\theta)P_{n'}^m(\cos\theta)\right\}\sin\theta d\theta$$

$$=\begin{cases}0 & \text{for } n\neq n'\\ \dfrac{2n(n+1)(n+m)!}{(2n+1)(n-m)!} & \text{for } n=n'\end{cases} \tag{2.39}$$

After some algebraic manipulations, then, it can be found that

$$A_{nm}=\frac{(2n+1)(n-m)!}{2n(n+1)(n+m)!}\frac{a}{\pi}\frac{\iint_{S_{ap}}\left[f_1(\theta,\phi)\frac{dP_n^m(\cos\theta)}{d\theta}\cos m\phi-\frac{m}{\sin\theta}f_2(\theta,\phi)P_n^m(\cos\theta)\sin m\phi\right]\begin{matrix}\sin\theta\\ d\theta d\phi\end{matrix}}{\frac{d}{dr}\left[rh_n^{(2)}(kr)\right]_{r=a}} \tag{2.40}$$

In the similar manner to A_{nm}, B_{nm} can be evaluated by substituting $TM_{nm(e,o)}$ of (2.36b)-(2.36c) and (2.36e)-(2.36f) for $\overline{E}_2$ and $\overline{H}_2$ of (2.35). These assemblies will lead to

$$B_{nm}=\frac{(2n+1)(n-m)!}{2n(n+1)(n+m)!}\frac{a}{\pi}\frac{\iint_{S_{ap}}\left[f_1(\theta,\phi)\frac{dP_n^m(\cos\theta)}{d\theta}\sin m\phi+\frac{m}{\sin\theta}f_2(\theta,\phi)P_n^m(\cos\theta)\cos m\phi\right]\begin{matrix}\sin\theta\\ d\theta d\phi\end{matrix}}{\frac{d}{dr}\left[rh_n^{(2)}(kr)\right]_{r=a}} \tag{2.41}$$

Case 2: $\overline{E}_2, \overline{H}_2$ are TE^R mode even and odd

Referring to (2.21a)-(2.21f), the TE^R field components can be expressed by

$$E_{r2} = 0 \tag{2.42a}$$

$$E_{\theta 2} = j\omega\mu m h_n^{(2)}(kr)\frac{P_n^m(\cos\theta)}{\sin\theta}\begin{cases} C_{nm}\sin m\phi \\ -D_{nm}\cos m\phi \end{cases} \tag{2.42b}$$

$$E_{\phi 2} = j\omega\mu h_n^{(2)}(kr)\frac{dP_n^m(\cos\theta)}{d\theta}\begin{cases} C_{nm}\cos m\phi \\ D_{nm}\sin m\phi \end{cases} \tag{2.42c}$$

$$H_{r2} = \frac{n(n+1)}{r}h_n^{(2)}(kr)P_n^m(\cos\theta)\begin{cases} C_{nm}\cos m\phi \\ D_{nm}\sin m\phi \end{cases} \tag{2.42d}$$

$$H_{\theta 2} = \frac{1}{r}\left[rh_n^{(2)}(kr)\right]'\frac{dP_n^m(\cos\theta)}{d\theta}\begin{cases} C_{nm}\cos m\phi \\ D_{nm}\sin m\phi \end{cases} \tag{2.42e}$$

$$H_{\phi 2} = \frac{-m}{r\sin\theta}\left[rh_n^{(2)}(kr)\right]'P_n^m(\cos\theta)\begin{cases} C_{nm}\sin m\phi \\ -D_{nm}\cos m\phi \end{cases} \tag{2.42f}$$

The procedures of TE^R case are in the same manner of TM^R case. The coefficient C_{nm} can be determined by substituting $\overline{E}_2$ and $\overline{H}_2$ of (2.35) by $TM_{nm(e,o)}$, (2.42b)-(2.42c) and (2.42e)-(2.42f). After some algebraic manipulations, it can be found that

$$\iint_{S_{ap}}\left[\frac{m}{\sin\theta}f_1(\theta,\phi)P_n^m(\cos\theta)\sin m\phi + f_2(\theta,\phi)\frac{dP_n^m(\cos\theta)}{d\theta}\cos m\phi\right]a^2\sin\theta d\theta d\phi$$

$$= C_{nm}j\omega\mu h_n^{(2)}(ka)\int_0^{\pi}\left[\frac{m^2}{\sin^2\theta}(P_n^m(\cos\theta))^2\int_0^{2\pi}\sin^2 m\phi d\phi + \left(\frac{dP_n^m(\cos\theta)}{d\theta}\right)^2\int_0^{2\pi}\cos^2 m\phi d\phi\right]\sin\theta d\theta \tag{2.43}$$

By applying the orthogonal properties (2.38) and (2.39), we can reduce (2.43) to (2.44).

$$C_{nm} = \frac{(2n+1)(n-m)!}{2n(n+1)(n+m)!}\frac{1}{\pi}\frac{\iint_{S_{ap}}\left[\frac{m}{\sin\theta}f_1(\theta,\phi)P_n^m(\cos\theta)\sin m\phi + f_2(\theta,\phi)\frac{dP_n^m(\cos\theta)}{d\theta}\cos m\phi\right]\sin\theta}{j\omega\mu h_n^{(2)}(ka)}d\theta d\phi \tag{2.44}$$

In the similar manner with C_{nm}, D_{nm} can be evaluated by substituting $TE_{nm(e,o)}$, (2.42b)-(2.42c) and (2.42e)-(2.42f), for $\overline{E}_2$ and $\overline{H}_2$ of (2.35). These assemblies will lead to

$$D_{nm} = \frac{(2n+1)(n-m)!}{2n(n+1)(n+m)!}\frac{1}{\pi}\frac{\iint_{S_{ap}}\left[\frac{m}{\sin\theta}f_1(\theta,\phi)\cos m\phi - f_2(\theta,\phi)\frac{dP_n^m(\cos\theta)}{d\theta}\sin m\phi\right]\sin\theta\, d\theta d\phi}{-j\omega\mu h_n^{(2)}(ka)} \tag{2.45}$$

We can observe that the unknown coefficients A_{nm}, B_{nm}, C_{nm} and D_{nm} are in the integral form of the field distribution $f_1(\theta,\phi)$ and $f_2(\theta,\phi)$ on the aperture. These formulations can be applied to a slot on sphere and will be discussed in the next chapter.

2.6 Conclusions

From Maxwell's equations, electromagnetic waves TE^R and TM^R in the source free region of the spherical structure are derived by using auxiliary Hertz vector potential. Since the radial component of Hertz vector potential satisfies the scalar wave equation, it can be solved by separation of variables method, analytically. The general solutions are in the product of

(1). The spherical Bessel function of the first and second kinds ($j_n(kr)$ and $y_n(kr)$) for a standing wave and the spherical Hankel function of the first and second kinds ($h_n^{(1)}(kr)$ and $h_n^{(2)}(kr)$) for a traveling wave.

(2). The associated Legendre function of the first and second kind ($P_n^m(\cos\theta)$ and $Q_n^m(\cos\theta)$) for the wave in θ direction

(3). The exponential function ($e^{-jm\phi}$ and $e^{+jm\phi}$) and the trigonometric functions ($\cos(m\phi)$ and $\sin(m\phi)$) for the wave in ϕ direction

To determine the unknown coefficient of exterior electromagnetic boundary value problem, we apply the Lorentz reciprocity theorem when the considered region is closed by an infinite spherical surface and a finite sphere with the assumed tangential fields on the surface. Then, the radiation conditions on the infinite spherical surface are utilized with the orthogonal properties of trigonometric and associated Legendre function. Finally, the unknown coefficients can be obtained in the integral form.

CHAPTER 3

A HORIZONTAL SLOT ON A SPHERE

As the discussion on the exterior boundary value problem in the preceding chapter, general expressions of electromagnetic fields outside a sphere has been derived in term of the tangential field distributions. Now if we consider a radiating slot instead of arbitrarily radiating aperture, the general problem of a slot on a sphere can be extract the essential radiation characteristics. The work in this chapter will start from a conducting sphere with a narrow zonal slot. After that a half-wave slot on a sphere will be considered by using the expression from the previous case. The characteristics of a half-wave slot such as radiation pattern, directivity, half power beamwidth are obtained. Numerical results of half-wave slot case are illustrated and compared with the experimental results.

3.1 Formulation for a Narrow Zonal Slot on a Sphere

Let us now consider a perfectly conducting sphere with a narrow zonal slot as illustrated in Fig. 3.1. The spherical coordinate (r,θ,ϕ) system is chosen. "a" is the radius of a sphere, $\theta = \theta_1$ is the position of the slot and 2α is the width of the slot with respect the angle θ. By assuming the narrow slot, the distribution of the electric fields on each wave mode is defined by

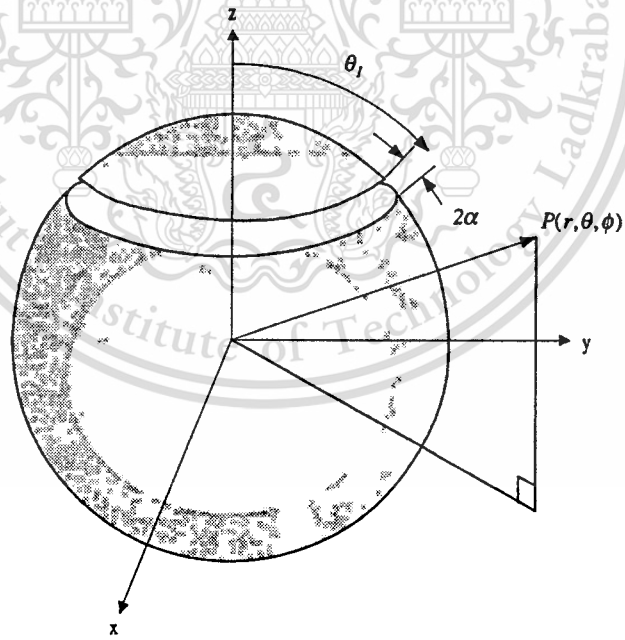

Fig. 3.1 Geometry of a sphere with a narrow zonal slot

$$E_{m\theta}(a,\theta,\phi) = \begin{cases} E_m \cos m\phi & ,\theta_1 - \alpha < \theta < \theta_1 + \alpha \\ 0 & ,0 \le \theta < \theta_1 - \alpha, \theta_1 + \alpha < \theta \le \pi \end{cases} \quad (3.1a)$$

$$E_{m\phi}(a,\theta,\phi)=0 \qquad \text{all over a sphere} \qquad (3.1b)$$

where E_m is an unknown constant to be determined. Under this condition the electromagnetic fields exterior to a sphere are easily obtained by substituting (3.1a)-(3.1b) into (2.41)-(2.42) and (2.46)-(2.47). Thus we can write that

$$A_{mn}=\frac{(2n+1)(n-m)!}{2n(n+1)(n+m)!}\frac{aE_m}{\pi}\frac{\int_0^{2\pi}\int_{\theta_1-\alpha}^{\theta_1+\alpha}[\cos^2 m\phi\,\frac{dP_n^m(\cos\theta)}{d\theta}\sin\theta]d\theta d\phi}{\frac{d}{dr}[rh_n^{(2)}(kr)]_{r=a}}$$

$$=\frac{(2n+1)(n-m)!}{2n(n+1)(n+m)!}\frac{aE_m}{\frac{d}{dr}[rh_n^{(2)}(kr)]_{r=a}}\int_{\theta_1-\alpha}^{\theta_1+\alpha}\frac{dP_n^m(\cos\theta)}{d\theta}\sin\theta d\theta \qquad (3.2a)$$

$$B_{mn}=\frac{(2n+1)(n-m)!}{2n(n+1)(n+m)!}\frac{aE_m}{\pi}\frac{\int_0^{2\pi}\int_{\theta_1-\alpha}^{\theta_1+\alpha}[\cos m\phi\sin m\phi\,\frac{dP_n^m(\cos\theta)}{d\theta}\sin\theta]d\theta d\phi}{\frac{d}{dr}[rh_n^{(2)}(kr)]_{r=a}}$$

$$=0 \qquad (3.2b)$$

$$C_{mn}=\frac{(2n+1)(n-m)!}{2n(n+1)(n+m)!}\frac{mE_m}{\pi}\frac{\int_0^{2\pi}\int_{\theta_1-\alpha}^{\theta_1+\alpha}[\cos m\phi\sin m\phi P_n^m(\cos\theta)]d\theta d\phi}{j\omega\mu h_n^{(2)}(ka)}$$

$$=0 \qquad (3.3c)$$

$$D_{mn}=\frac{(2n+1)(n-m)!}{2n(n+1)(n+m)!}\frac{mE_m}{\pi}\frac{\int_0^{2\pi}\int_{\theta_1-\alpha}^{\theta_1+\alpha}[\cos^2 m\phi P_n^m(\cos\theta)]d\theta d\phi}{-j\omega\mu h_n^{(2)}(ka)}$$

$$=-\frac{(2n+1)(n-m)!}{2n(n+1)(n+m)!}\frac{mE_m}{j\omega\mu h_n^{(2)}(ka)}\int_{\theta_1-\alpha}^{\theta_1+\alpha}P_n^m(\cos\theta)d\theta \qquad (3.3d)$$

Therefore by substituting (3.2a)-(3.2d) to (2.21a)-(2.21f) the electric and magnetic field components of $m\,th$ mode can be expressed as

$$E_{mr}(r,\theta,\phi)=-E_m\sum_{n=m}^{\infty}L_{mn}^{TM}\frac{n(n+1)}{kr}\frac{kah_n^{(2)}(kr)}{[kah_n^{(2)}(ka)]'}P_n^m(cos\theta)\cos m\phi \qquad (3.4a)$$

$$E_{m\theta}(r,\theta,\phi)=-E_m\sum_{n=m}^{\infty}\{L_{mn}^{TE}\frac{h_n^{(2)}(kr)}{h_n^{(2)}(ka)}\frac{mP_n^m(cos\theta)}{sin\theta}+L_{mn}^{TM}\frac{a}{r}\frac{[krh_n^{(2)}(kr)]'}{[kah_n^{(2)}(ka)]'}\frac{dP_n^m(cos\theta)}{d\theta}\}cosm\phi \qquad (3.4b)$$

$$E_{m\phi}(r,\theta,\phi)=E_m\sum_{n=m}^{\infty}\{L_{mn}^{TE}\frac{h_n^{(2)}(kr)}{h_n^{(2)}(ka)}\frac{dP_n^m(cos\theta)}{d\theta}+L_{mn}^{TM}\frac{a}{r}\frac{[krh_n^{(2)}(kr)]'}{[kah_n^{(2)}(ka)]'}\frac{mP_n^m(cos\theta)}{sin\theta}\}sinm\phi \tag{3.4c}$$

$$H_{mr}(r,\theta,\phi)=-j\sqrt{\frac{\varepsilon}{\mu}}E_m\sum_{n=m}^{\infty}L_{mn}^{TE}\frac{n(n+1)}{kr}\frac{h_n^{(2)}(kr)}{h_n^{(2)}(ka)}P_n^m(cos\theta)sinm\phi \tag{3.4d}$$

$$H_{m\theta}(r,\theta,\phi)=-j\sqrt{\frac{\varepsilon}{\mu}}E_m\sum_{n=m}^{\infty}\{L_{mn}^{TE}\frac{[krh_n^{(2)}(kr)]'}{[krh_n^{(2)}(ka)]}\frac{dP_n^m(cos\theta)}{d\theta}-L_{mn}^{TM}\frac{a}{r}\frac{[krh_n^{(2)}(kr)]}{[kah_n^{(2)}(ka)]'}\frac{mP_n^m(cos\theta)}{sin\theta}\}sinm\phi \tag{3.4e}$$

$$H_{m\phi}(r,\theta,\phi)=-j\sqrt{\frac{\varepsilon}{\mu}}E_m\sum_{n=m}^{\infty}\{L_{mn}^{TE}\frac{[krh_n^{(2)}(kr)]'}{[krh_n^{(2)}(ka)]}\frac{mP_n^m(cos\theta)}{sin\theta}-L_{mn}^{TM}\frac{[kah_n^{(2)}(kr)]}{[kah_n^{(2)}(ka)]'}\frac{dP_n^m(cos\theta)}{d\theta}\}cosm\phi \tag{3.4f}$$

where

$$\left[krh_n^{(2)}(kr)\right]'=\frac{\partial}{\partial(kr)}\left[krh_n^{(2)}(kr)\right] \tag{3.5}$$

$$L_{mn}^{TE}=-\frac{2n+1}{2n(n+1)}\frac{(n-m)!}{(n+m)!}\int_{\frac{\pi}{2}-\alpha}^{\frac{\pi}{2}+\alpha}mP_n^m(cos\theta)d\theta \tag{3.6}$$

and

$$L_{mn}^{TM}=-\frac{2n+1}{2n(n+1)}\frac{(n-m)!}{(n+m)!}\int_{\frac{\pi}{2}-\alpha}^{\frac{\pi}{2}+\alpha}\frac{dP_n^m(cos\theta)}{d\theta}\sin\theta d\theta \tag{3.7}$$

The total electromagnetic fields outside a sphere is obtained from the summation all of $m\,th$ mode contribution. By doing this, it can be shown that

$$E_r=\sum_{m=0}^{\infty}E_{mr}\qquad E_\theta=\sum_{m=0}^{\infty}E_{m\theta}\qquad E_\phi=\sum_{m=0}^{\infty}E_{m\phi} \tag{3.8a}$$

$$H_r=\sum_{m=0}^{\infty}H_{mr}\qquad H_\theta=\sum_{m=0}^{\infty}H_{m\theta}\qquad H_\phi=\sum_{m=0}^{\infty}H_{m\phi} \tag{3.8d}$$

Then it is reasonable to define the amplitude of $m\,th$ mode of the voltage gap along the narrow slot. So it can be written that

$$V_m=\int_{\theta_1-\alpha}^{\theta_1+\alpha}E_m a d\theta=2a\alpha E_m \tag{3.9}$$

When the observer is at infinite distance, the far zone fields radiate from a sphere can be evaluated. It is clever to replace the spherical Hankel function with an asymptotic

expression for large parameter. The asymptotic expression of the spherical Hankel function can be approximated by

$$h_n^{(2)}(kr) \sim \frac{j^{n+1}}{kr} e^{-jkr} \tag{3.10a}$$

and

$$\left[krh_n^{(2)}(kr)\right]' \sim j^{n+1}\left[\frac{(n+1)}{hr} - j\right]e^{-jkr} \tag{3.10b}$$

In the far zone the total fields of (3.4a) through (3.4f) can be reduced, by replacing the spherical Hankel function with its asymptotic form (3.10a)-(3.10b) to (3.4a)-(3.4f). So that the radiated fields will be written to

$$E_{mr}(r,\theta,\phi) \approx 0 \tag{3.11a}$$

$$E_{m\theta}(r,\theta,\phi) \approx -\frac{e^{-jkr}}{r}\frac{V_m}{ka}\sum_{n=m}^{\infty}(j)^n\left\{j\frac{L_{mn}^{TE}}{2\alpha}\frac{1}{h_n^{(2)}(ka)}\frac{mP_n^m(\cos\theta)}{\sin\theta} + \frac{L_{mn}^{TM}}{2\alpha}\frac{ka}{[kah_n^{(2)}(ka)]'}\frac{dP_n^m(\cos\theta)}{d\theta}\right\}\cos m\phi \tag{3.11b}$$

$$E_{m\phi}(r,\theta,\phi) \approx \frac{e^{-jkr}}{r}\frac{V_m}{ka}\sum_{n=m}^{\infty}(j)^n\left\{j\frac{L_{mn}^{TE}}{2\alpha}\frac{1}{h_n^{(2)}(ka)}\frac{dP_n^m(\cos\theta)}{d\theta} + \frac{L_{mn}^{TM}}{2\alpha}\frac{ka}{[kah_n^{(2)}(ka)]'}\frac{mP_n^m(\cos\theta)}{\sin\theta}\right\}\sin m\phi \tag{3.11c}$$

$$H_{mr}(r,\theta,\phi) \approx 0 \tag{3.11d}$$

$$H_{m\theta}(r,\theta,\phi) \approx -\sqrt{\frac{\varepsilon}{\mu}}E_{m\phi}(r,\theta,\phi) \tag{3.11e}$$

$$H_{m\phi}(r,\theta,\phi) \approx \sqrt{\frac{\varepsilon}{\mu}}E_{m\theta}(r,\theta,\phi) \tag{3.11f}$$

3.2 Formulation for a Half-Wave Slot on a Sphere

To analyze the radiation of a half-wave slot on a sphere, the theoretical investigation for such slot is not easy. However if the aperture field distribution along the slot is assumed, the calculations of radiation pattern are not difficult because all the formulations are already derived in the preceding section.

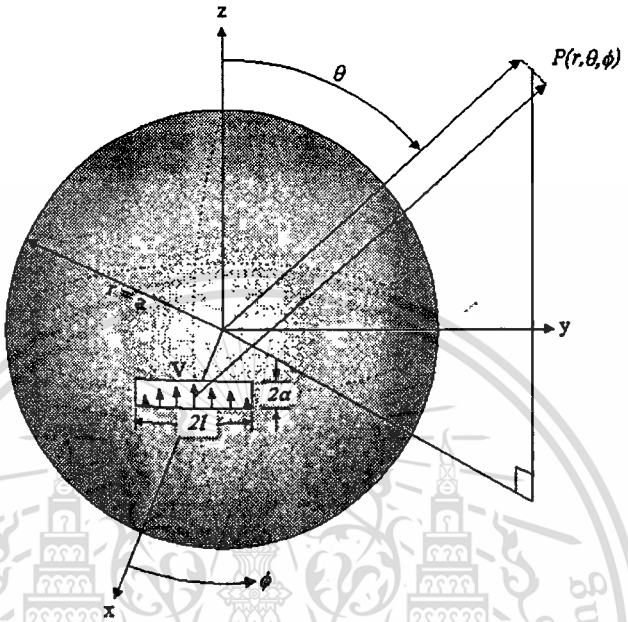

Fig. 3.2 A half-wave slot on a sphere

Now, Let us consider a horizontal half-wave slot located on the equator of a sphere as illustrated in Fig. 3.2. In this case a sinusoidal voltage distribution reasonably expressed by the following equation.

$$V(\phi)=\begin{cases} V\sin[\frac{2\pi}{\lambda}(l-a|\phi|)] & |a\phi|\le l \\ 0 & |a\phi|>l \end{cases} \tag{3.12}$$

In the other way, the voltage at the aperture can be obtained by the fourier expansion of the voltage modes.

$$V(\phi)=\sum_{m=0}^{\infty}V_m\cos m\phi \tag{3.13}$$

To find the magnitude in each voltage mode, the orthogonal property is necessary. So the multiplying the cosine function and integrating both sides are done. Therefore we can write that

$$\sum_{m=0}^{\infty}V_m\int_0^{2\pi}\cos m\phi\cos n\phi d\phi = V\int_{-l/a}^{l/a}\sin\left[\frac{2\pi}{\lambda}(l-a|\phi|)\right]\cos n\phi d\phi \tag{3.14}$$

and because

$$\int_0^{2\pi} \cos m\phi \cos n\phi d\phi = \begin{cases} 0 & m \neq n \\ \pi & m = n \neq 0 \end{cases} \tag{3.15}$$

then it can be shown that

$$V_m = \frac{2V}{(1+\delta_m)\pi} \int_0^{l/a} \sin[\frac{2\pi}{\lambda}(l - a\phi)] \cos m\phi d\phi \tag{3.16}$$

or

$$V_m = \frac{2V}{(1+\delta_m)\pi} \left[\sin kl \left(\frac{\sin\frac{(ka-m)l}{a}}{ka-m} + \frac{\sin\frac{(ka+m)l}{a}}{ka+m} \right) + \cos kl \left(\frac{\cos\frac{(ka-m)l}{a} - 1}{ka-m} + \frac{\cos\frac{(ka+m)l}{a} - 1}{ka+m} \right) \right] \tag{3.17}$$

$$= \begin{cases} \frac{V}{\pi ka}(1 - \cos kl) & m = 0 \\ \frac{V}{\pi} \frac{2ka}{(ka)^2 - m^2} [\cos(m\frac{l}{a}) - \cos kl] & m \neq ka, m \neq 0 \\ \frac{V}{\pi} \frac{l}{a} \sin kl & m = ka \end{cases} \tag{3.18}$$

From (3.18), we can find the coefficient of each voltage mode. By substituting (3.18) to (3.11a)-(3.11f), one can find the radiated fields of a half-wave slot on a sphere.

3.3 Directivity, Half-power Beamwidth and Front-to-back Ratio

One very important radiation characteristic of an antenna that described how much it can concentrate energy to the desired direction over the other directions is called directivity. It is defined as the ratio of the radiation intensity in a certain direction to the average radiation intensity, or

$$D = \frac{4\pi U_{\max}}{P_{rad}} \tag{3.19}$$

where D is directivity, $U_{\max}$ represents the maximum radiation intensity, P_{rad} is the total radiation power. The radiation intensity can be expressed by

$$U(\theta,\phi)=\frac{1}{2\eta}\left[\left|E_\theta(\theta,\phi)\right|^2+\left|E_\phi(\theta,\phi)\right|^2\right] \tag{3.20}$$

where

η = intrinsic impedance of the medium (for free space $\eta_o = 120\pi\ \Omega$)

E_θ, E_ϕ = far-zone electric field components of the antenna

The total radiated power is obtained by integrating the radiation intensity over all angles around the antenna, defined by

$$P_{rad}=\int_0^{2\pi}\int_0^{\frac{\pi}{2}} U(\theta,\phi)\sin\theta d\theta d\phi \tag{3.21}$$

The other two parameters describing the radiation patterns of the antenna are Half-power beamwidth (HPBW) and front-to-back ratio.

Half-power beamwidth (HPBW) is the angle subtended by the half-power points of the main lobe.

Front-to-back ratio is the ratio between the peak amplitudes of the main and back lobes, usually expressed in decibels.

3.4 Numerical Results

The numerical results of radiation characteristic of a half-wavelength slot on sphere are demonstrated in this section by using the expressions that are formulated in the preceding sections. The radiation characteristics which will be revealed consist of radiation pattern, directivity, half-power beamwidth and front-to-back ratio at various spherical radii.

3.4.1 Radiation Pattern

From the radiated field derived in the preceding section, the radiation in H plane and E plane for the effective radius (ka) from 1 to 100, which corresponding to a equal $10/\pi$, $20/\pi$, $30/\pi$, $40/\pi$ and $50/\pi$ of the operating wavelength, are illustrated in Fig.3.3 and Fig.3.4, respectively. Consider now the radiation characteristics, we assume the slot length is a half-wavelength and slot width is narrow. It is possible to approximate only E_θ in (3.8a) exist and is plotted for the various effective radii. They are saw that, for the H-plane pattern, the larger the effective radius the narrower the beamwidth and the lower the back lobe. At $ka = 1$, the radiated field is very close to the omnidirection and the change in $ka = 20$ become significantly observable. The estimation 3 dB beamwidth of 82 degree and 11 dB front-to-back ratio has been obtained. After $ka = 20$, it can be seen that the patterns are a little change. However, the front-to-back ratio is substantially larger from 15 dB at $ka = 40$ to 22 dB at $ka = 100$. In another plane, similar results are also obtained for various ka. As can be seen, at $ka = 1$ the radiation pattern is still close to omnidirection. For a larger ka, the results are not significantly changed. However, the ripples of the back lobe are higher when the effective radius is larger.

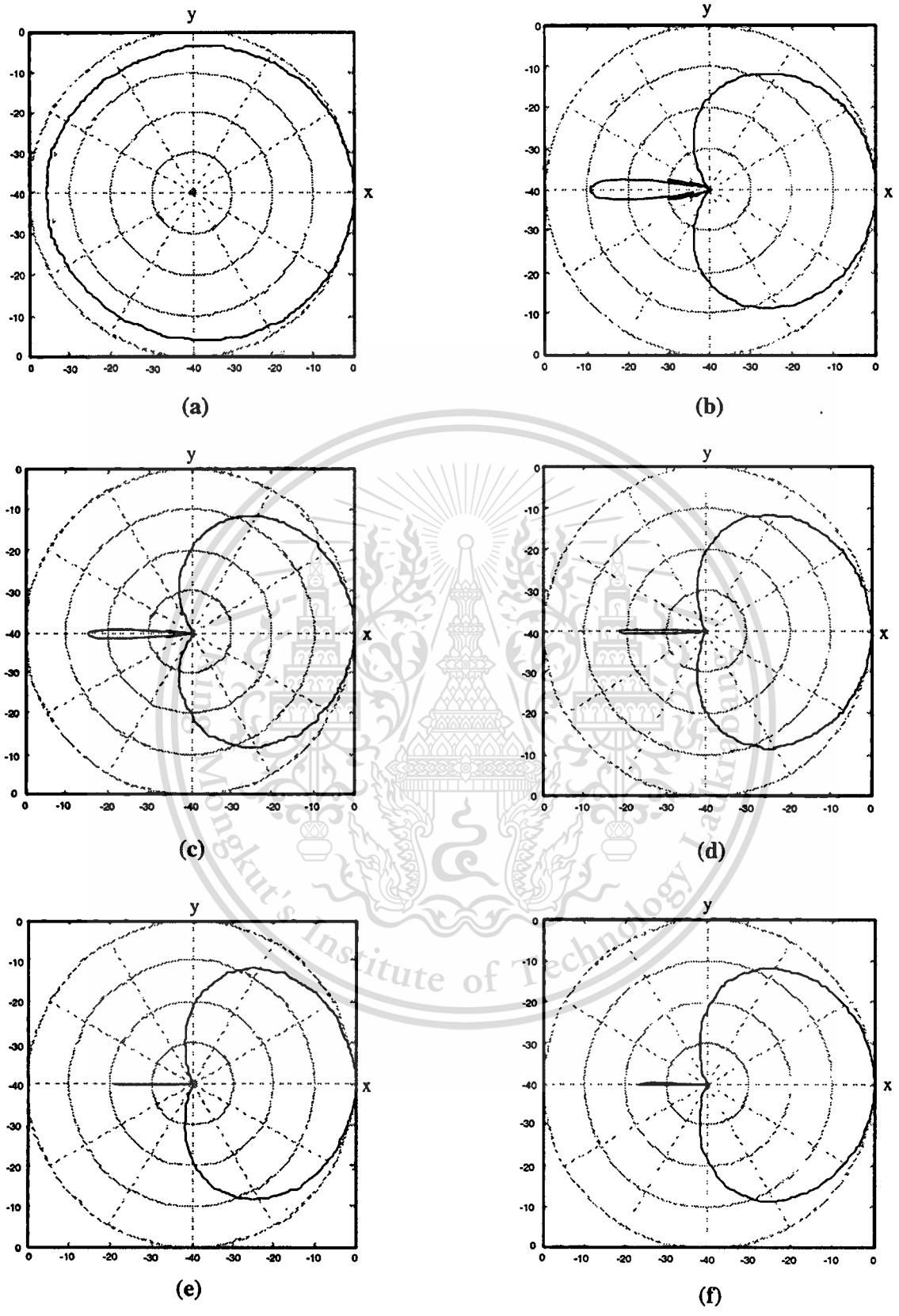

Fig. 3.3 Radiation pattern in H-plane of a half-wave slot on a sphere with various sizes of *ka*

(a) *ka=1* (b) *ka=20* (c) *ka=40* (d) *ka=60* (e) *ka=80* (f) *ka=100*

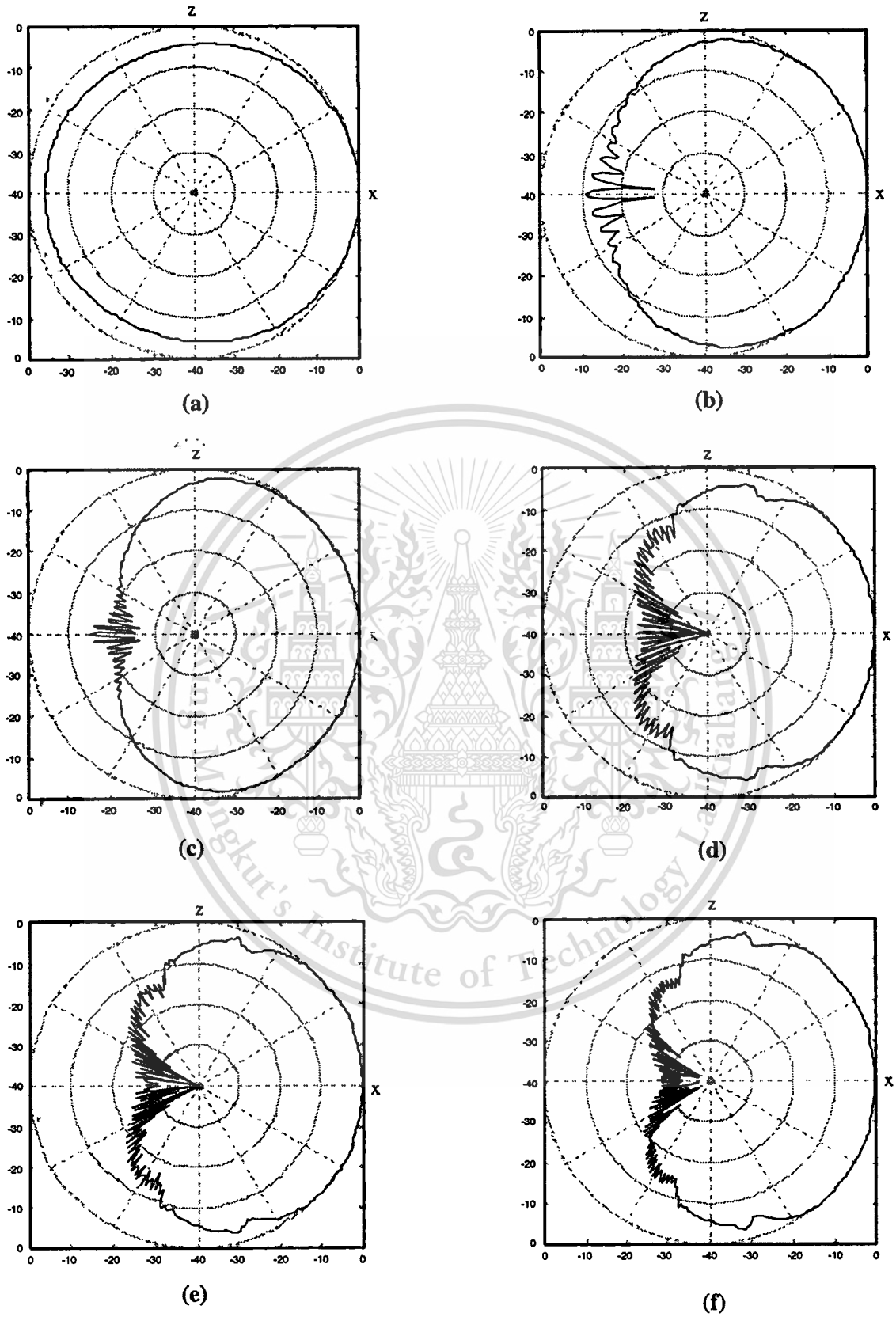

Fig. 3.4 Radiation pattern in E-plane of a half-wave slot on a sphere with various sizes of *ka*

(a) *ka=1* (b) *ka=20* (c) *ka=40* (d) *ka=60* (e) *ka=80* (f) *ka=100*

3.4.2 Directivity

Fig.3.5 illustrates the directivity as the function of the effective spherical radius. The directivity of *2.51* dBi can be accomplished at the effective radius of *1* and rapidly increase to *4.10* dBi at $ka = 40$ after this the directivity is slightly increasing.

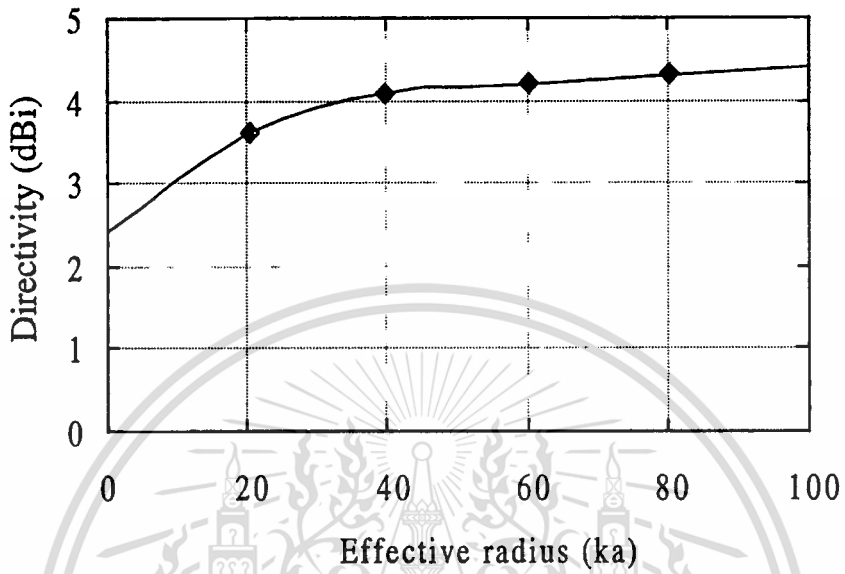

Fig. 3.5 Directivity of a slot on a sphere

3.4.3 Half-power Beamwidth

The half-power beamwidth is defined to specify the merit of the antenna. Fig.3.6 illustrates the half-power beamwidth versus the effective radius. It is obvious that for the effective radius is equal to *1*, the half-power beamwidth is *146* degree and decrease rapidly until to *79* degree at the effective radius of *40*. For the larger effective radius than *40*, the half-power beamwidth become a constant at *78* degrees.

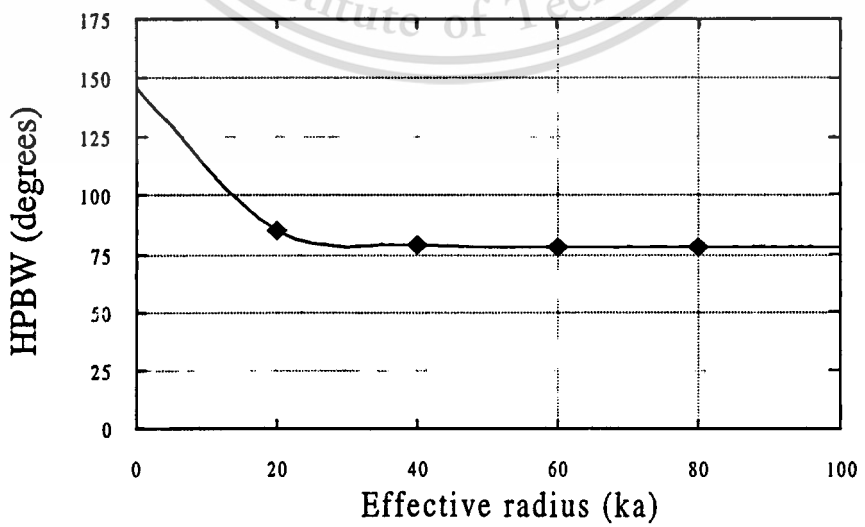

Fig.3.6 Half-power beamwidth of a slot on a sphere

3.4.4 Front-to-back Ratio

In the investigation, the front-to-back ratio is the significant parameter to select the spherical radius. From Fig.3.7, it can be seen that the front-to-back ratio is low for the small radius and increase as the large size of the sphere.

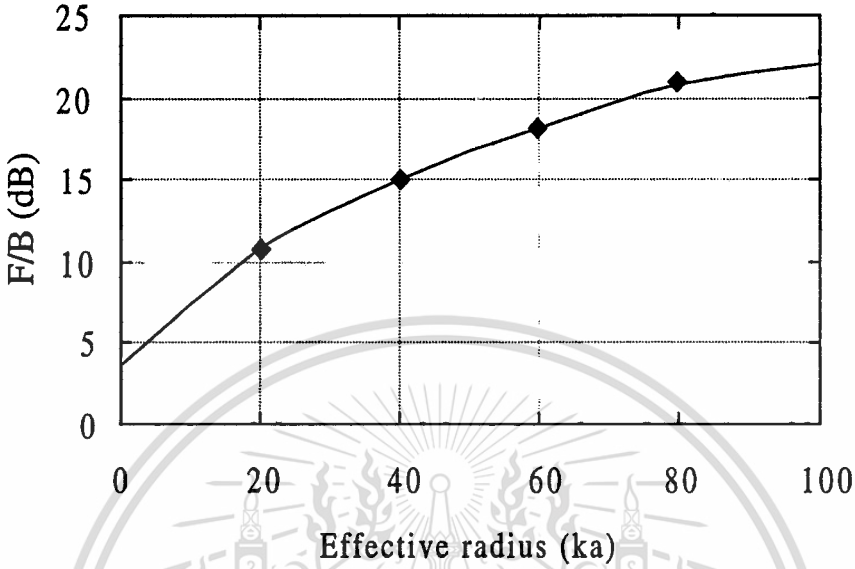

Fig.3.7 Front-to-back ratio of a lot on a sphere

3.5 Experimental Results

To verify the theoretical results, the antenna prototype is composed of 2 hemispheres which are contacted by aluminium foil around the outer circumference. Respectively, the slot length and width are *2.69* cm and *1.50* mm. The antenna is excited by probe at the bottom of a sphere and perpendicular to a slot length. The experiment is set up at the operating frequency of *5.58* GHz for $ka = 8.57$ ($a = 7.34$ cm). This antenna has SWR of *1.8*. The photograph of the prototype antenna is shown in Fig. 3.8. The antenna far-field test site is set up with the distance of *1.10* m which is greater than twice of the far field range. The antenna under test is connected to port 1 of the HP-8510C network analyzer to transmit the waves and is rotated at *2* degrees per step. A conical horn is connected to port 2 of the network analyzer to measure the received signal strength. The radiation pattern from experiment is plotted and compared with the calculation as illustrated in Fig.3.9.

We find generally good agreement, except for some discrepancies in the relative magnitudes of minor lobe region. These may be come from some imperfect fabrications or the effect of multipath waves due to imperfect free space test site.

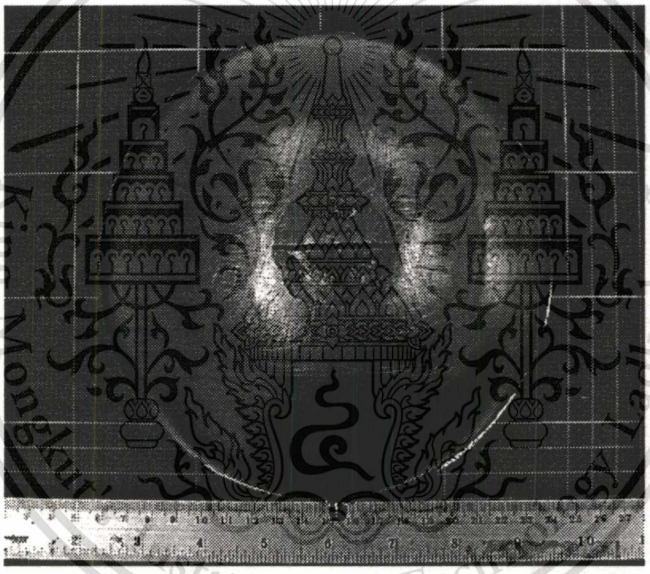

Fig.3.8 Photograph of the prototype antenna with $ka = 8.57$

3.6 Conclusions

From the theoretical aspects as derived in the previous chapter by assuming the tangential field components on the aperture, the theoretical formulation of a slot on a sphere can be investigated. The numerical results of radiation characteristic such as radiation pattern, half-power beamwidth, front-to-back ratio and directivity are demonstrated. It is apparent that the narrower the half-power beamwidth the higher front-to-back ratio and the higher the directivity can be obtained by using the larger the effective radius of a sphere at a constant slot dimension. However, the size of a sphere can be chosen according to the cost effective and the radiation property requirement. Finally, the experiment is set up to confirm the theoretical ones.

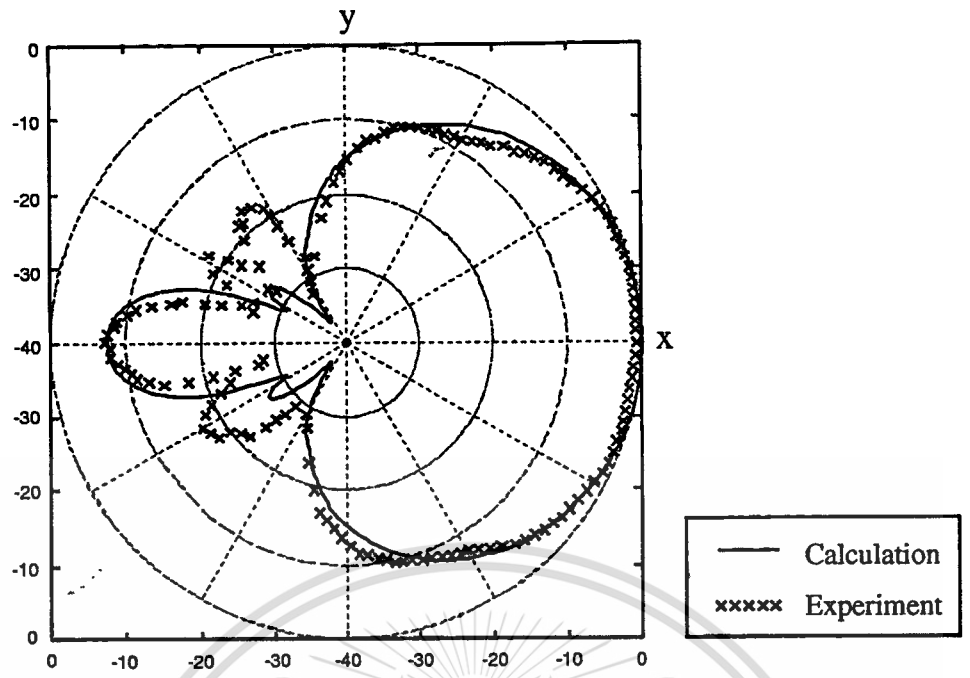

H-Plane (xy cut, $\theta = 90^{\circ}$)

(a)

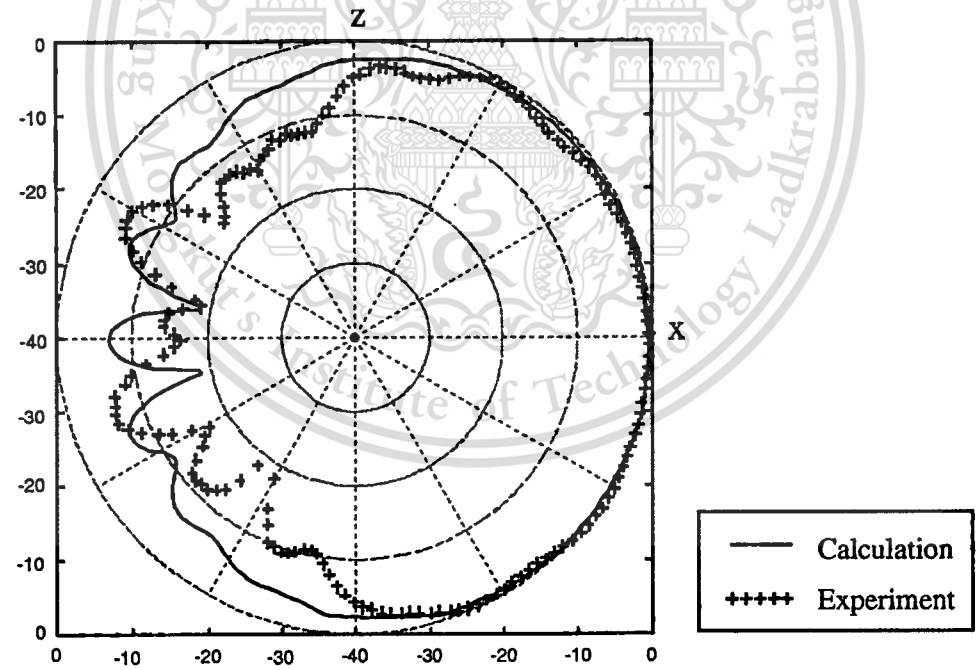

E-Plane (xz cut, $\phi = 0^{\circ}$)

(b)

Fig.3.9 Radiation pattern comparison between theoretical and experimental results of a slot on a sphere for $ka = 8.57$.
(a) H-plane
(b) E-plane

CHAPTER 4

AN INCLINED SLOT ON A SPHERE

In this chapter we explained the radiation characteristics of an inclined slot on a sphere. From the theoretical aspects of a half-wave slot on a sphere in the preceding chapter, the relations between a half-wave horizontal and inclined slot on a sphere are explained in a comprehensive derivation. The contents are divided into two parts, the first deals with using the Euler angle rotation to rotate an object in the space and transform the component from one to other coordinate systems. The second part, we develop the governing coordinate transform for an inclined slot on a sphere. Finally, the numerical results of radiation pattern are presented at the various inclined angles and the experiment is set up to validate the numerical results.

4.1 The Euler Angle

In general the calculation of radiation characteristics of a spherical array antenna faces some difficulties because the antenna pattern and the feed element coordinate do not coincide. Consequently, the idea of an array factor times the element pattern collapses. However the pattern can be obtained by rotating pattern direction into the coordinate of each element pointing in a difference directions. In many designs and measurements for example mechanics, robotics, image processing etc., they are necessary to use a coordinate transformation that relates the Cartesian and spherical components each other.

This obstruction can be achieved by using the Euler rotation angle. It composes of Cartesian and spherical Euler angles. The Cartesian Euler angle is utilized to obtain the rotation matrix of the unit components between antenna and rotated coordinate system. The spherical Euler angle is applied to calculate the position angle in the space with different coordinate systems. The definitions for each case are explained in the subsequent sections.

4.1.1 The Cartesian Euler Angle

Let us consider two Cartesian coordinate systems, triple primed system (x''', y''', z''') and unprimed system (x, y, z) as shown in Fig.4.1. These Cartesian systems are related via three rotations that involve the use of matrix of cosines and the rotating angle are so called Cartesian Euler angle [19-21]. The final coordinate system (x''', y''', z''') is developed in three steps. We start from unprimed system (x, y, z) then sequential rotating through angle L, M and N to the triple primed system. All of the operations will be described step by step.

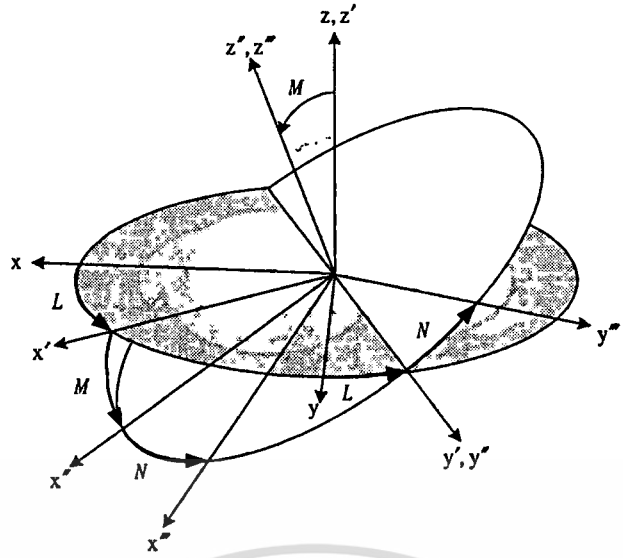

Fig. 4.1 Cartesian Euler angle

1. The $x'-, y'-, z'-$axes are rotated about the $z-$axis through an angle L counterclockwise relative to x, y, z. (The $z-$and $z'-$axes coincide.) as shown in Fig.4.2.

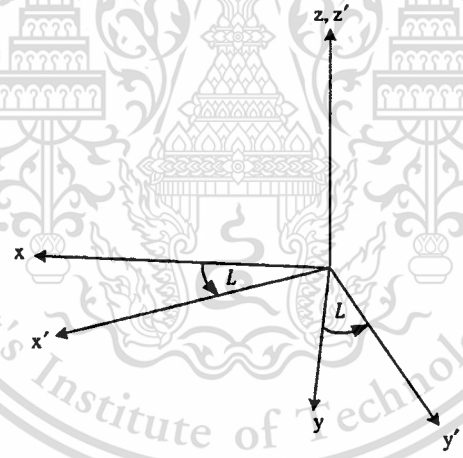

Fig. 4.2 Rotation about z'-axis through angle L

The transformation equation can be shown that

$$[\hat{c}'] = [{}^{c'}T^{c}][\hat{c}] \tag{4.1a}$$

or equivalent to

$$\begin{bmatrix} x' \\ y' \\ z' \end{bmatrix} = \begin{bmatrix} \cos L & \sin L & 0 \\ -\sin L & \cos L & 0 \\ 0 & 0 & 1 \end{bmatrix} \begin{bmatrix} x \\ y \\ z \end{bmatrix} \tag{4.1b}$$

2. The $x''-, y''-, z''-$axes are rotated about the $y'-$axis through an angle M counterclockwise relative to x', y', z'. (The $y'-$and $y''-$axes coincide.) as shown in Fig.4.3.

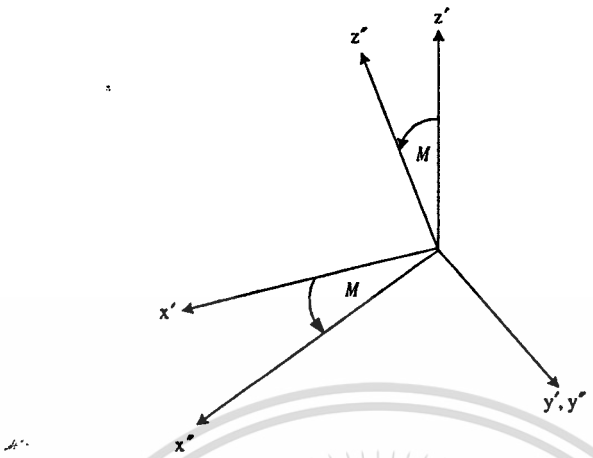

Fig. 4.3 Rotation about y'-axis through angle M

The transformation equation can be shown that

$$[\hat{c}''] = [{}^{c''}T^{c'}][\hat{c}'] \tag{4.2a}$$

or equivalent to

$$\begin{bmatrix} x'' \\ y'' \\ z'' \end{bmatrix} = \begin{bmatrix} \cos M & 0 & -\sin M \\ 0 & 1 & 0 \\ \sin M & 0 & \cos M \end{bmatrix} \begin{bmatrix} x' \\ y' \\ z' \end{bmatrix} \tag{4.2b}$$

3. The $x'''-, y'''-, z'''-$axes are rotated about the $z''-$axis through an angle N counterclockwise relative to x'', y'', z''. (The $z''-$and $z'''-$axes coincide.) as shown in Fig.4.4.

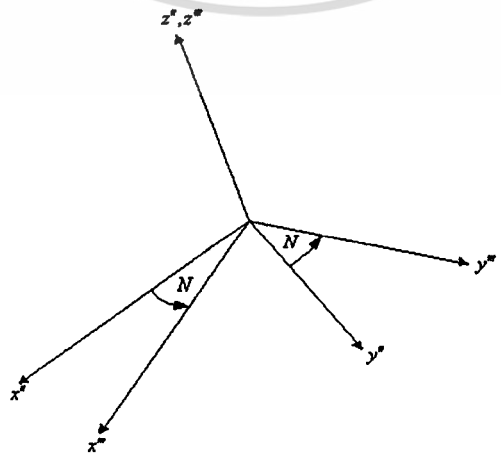

Fig. 4.4 Rotation about z'-axis through angle N

The transformation equation can be shown that

$$[\hat{c}'''] = [{}^{c''}T^{c'}][\hat{c}''] \tag{4.3a}$$

or equivalent to

$$\begin{bmatrix} x''' \\ y''' \\ z''' \end{bmatrix} = \begin{bmatrix} \cos N & \sin N & 0 \\ -\sin N & \cos N & 0 \\ 0 & 0 & 1 \end{bmatrix} \begin{bmatrix} x'' \\ y'' \\ z'' \end{bmatrix} \tag{4.3b}$$

After successively performing three rotations, we arrive to the following transformation equation (4.4a) among the unit components of Cartesian coordinate system.

$$[\hat{c}'''] = [{}^{c''}T^{c'}][{}^{c'}T^{c}][\hat{c}] = [{}^{c''}T^{c}][\hat{c}] \tag{4.4a}$$

or equivalent to

$$\begin{bmatrix} x''' \\ y''' \\ z''' \end{bmatrix} = \begin{bmatrix} \cos N & \sin N & 0 \\ -\sin N & \cos N & 0 \\ 0 & 0 & 1 \end{bmatrix} \begin{bmatrix} \cos M & 0 & -\sin M \\ 0 & 1 & 0 \\ \sin M & 0 & \cos M \end{bmatrix} \begin{bmatrix} \cos L & \sin L & 0 \\ -\sin L & \cos L & 0 \\ 0 & 0 & 1 \end{bmatrix} \begin{bmatrix} x \\ y \\ z \end{bmatrix} \tag{4.4b}$$

where

$$[{}^{c''}T^{c}] = \begin{bmatrix} \cos N \cos M \cos L - \sin N \sin L & \cos N \cos M \sin L + \sin N \cos L & -\cos N \sin M \\ -\sin N \cos M \cos L - \cos N \sin L & -\sin N \cos M \sin L + \cos N \cos L & \sin N \sin M \\ \sin M \cos L & \sin M \sin L & \cos M \end{bmatrix} \tag{4.4c}$$

Note that if Euler angle changes the coordinate system representation, but does not rotate the object. So, it means that the pointing direction still be the same in both coordinates. The applications of constant direction are the main point of coordinate transformation and will be discussed in the succeeding sections.

4.1.2 The Spherical Euler Angle

The spherical Euler angle [22-23] is different from Cartesian Euler angle because they are easy to visualize. In addition no matrix operations are required to convert angle from one coordinate system to other systems. We will start to consider two right-handed Cartesian coordinate systems with a common origin. We point out that the primed meridian runs from $+z$-axis through the $+x$-axis to the $-z$-axis, as

shown in Fig.4.5. A point in the space can be described by (x, y, z) or (r, θ, ϕ) coordinate system.

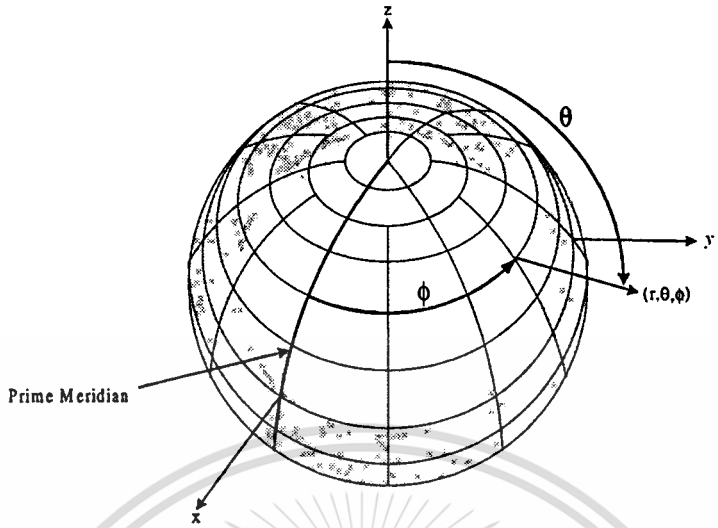

Fig.4.5 Spherical coordinate and the primed meridian

We start from the system, as shown in Fig.4.6, where the space angle in (r, θ, ϕ) or (x, y, z) is known. The (r', θ', ϕ') or (x', y', z') is the target system. The prime and unprimed systems are related by the spherical Euler angle α, β and γ that rotate the prime system to coincide with the unprimed system.

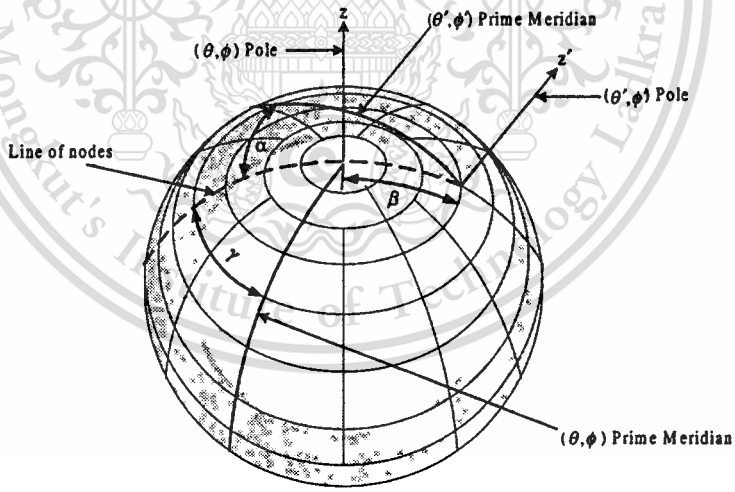

Fig. 4.6 Prime and unprimed coordinate a sphere, showing coordinate system and Euler angle α, β and γ

To derive the relationship between primed and unprimed coordinate, we apply some spherical trigonometry properties and the geometry is shown in Fig.4.7. By the law of cosine yields

$$\cos\theta = \cos\theta'\cos\beta + \sin\theta'\sin\beta\cos(\phi' - \alpha) \tag{4.5}$$

The angle ϕ'' is redefined by

$$\phi'' = \pi - (\phi - \gamma) \tag{4.6}$$

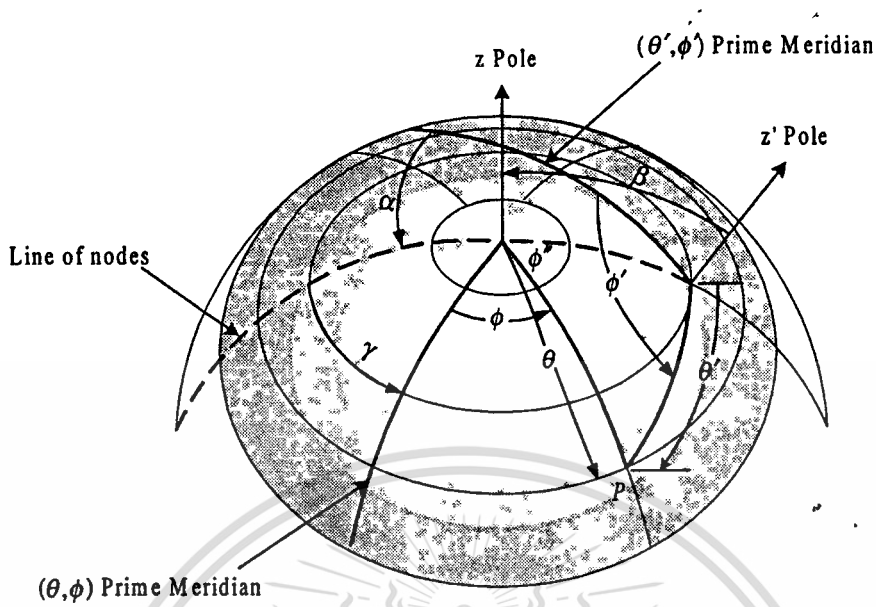

Fig. 4.7 Derivation geometry of a spherical Euler angle

Again applying the law of cosines

$$\cos\theta' = \cos\beta\cos\theta + \sin\beta\sin\theta\cos\phi'' \tag{4.7}$$

Applying the law of sine yields

$$\frac{\sin\phi''}{\sin\theta'} = \frac{\sin(\phi' - \alpha)}{\sin\theta} \tag{4.8}$$

From (4.6), we find that

$$\cos\phi'' = -\cos(\phi + \gamma) \tag{4.9a}$$

$$\sin\phi'' = \sin(\phi + \gamma) \tag{4.9b}$$

Therefore, from (4.8), we write

$$\sin\phi'' = \sin(\phi + \gamma) = \frac{\sin\theta'\sin(\phi' - \alpha)}{\sin\theta} \tag{4.10}$$

From (4.7), we write

$$-\cos\phi'' = \cos(\phi + \gamma) = \frac{\cos\theta\cos\beta - \cos\theta'}{\sin\theta\sin\beta} \tag{4.11}$$

Dividing (4.11) by (4.10) gives

$$\tan(\phi+\gamma)=\frac{\sin\theta'\sin(\phi'-\alpha)\sin\beta}{\cos\theta\cos\beta-\cos\theta'} \tag{4.12}$$

By substituting (4.5) into (4.12) yields

$$\tan(\phi+\gamma)=\frac{\sin\theta'\sin\beta\sin(\phi'-\alpha)}{\cos\beta[\cos\theta'\cos\beta+\sin\theta'\sin\beta\cos(\phi'-\alpha)]-\cos\theta'} \tag{4.13}$$

This will be simplified to

$$\tan(\phi+\gamma)=\frac{\sin\theta'\sin(\phi'-\alpha)}{\cos\beta\sin\theta'\cos(\phi'-\alpha)-\sin\beta\cos\theta'} \tag{4.14}$$

Using (4.5) and (4.14) the unknown (θ',ϕ') can be evaluated when the other parameters are defined. Visualizing the Euler angle may be confusing and it is important to rotate the angle α,β and γ in the correct order of the right-hand direction. To transform an angle from (θ',ϕ') to (θ,ϕ), it can be described by

1. Rotating the sphere an angle of α until the prime meridian crosses the $+z$-axis.
2. Moving an angle of β along the Line of Nodes until $+z'$- and $+z$-axes coincide.
3. Rotating an additional angle γ until the two prime meridians coincide.

4.2 Coordinate Transformation of a Spherical Array Antenna

Having derived the Euler angle rotation both Cartesian and sphere in the preceding sections, we next will apply all materials to calculate the radiation pattern of array elements on a sphere. Firstly, we introduce the global and local coordinate system. The global coordinate system will be designated by unprimed Cartesian (x,y,z), or unprimed spherical coordinate (r,θ,ϕ) and the local coordinate system will be designated by primed Cartesian (x',y',z') or primed spherical coordinate (r',θ',ϕ') system. While calculating an antenna pattern, we hold the space direction constant in unprimed coordinate system and iterating calculation over the element array, local or primed coordinate, to calculate the total electromagnetic waves. In the following section, we will apply the Euler angle to evaluate the relations between the unit vectors in global and local coordinates with the same and different origins.

4.2.1 The Global and Local Coordinates with the Same Origin

Let us consider two primed and unprimed coordinate systems with the same origin as depicted in Fig.4.8. We assume the element as a slot and the orientation of a slot can be described by angle A,B and C that are employed to define the Cartesian Euler angle. Angle A describes a counterclockwise rotation about the z-axis, then angle B defines a counterclockwise rotation about the y-axis. Sequentially, angle C is rotated about the x'-axis which will take the unprimed coordinate coincide with primed coordinate system. After complete rotating the three transformation matrices,

we arrive to the transformation equations among the unit Cartesian components. From section 4.1, we can write the transformation matrix as

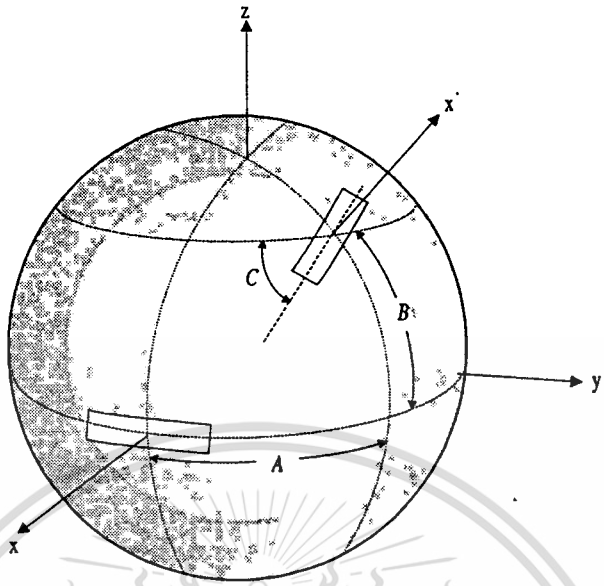

Fig. 4.8 Geometry of global and local coordinates locate on the same origin showing the Cartesian Euler angle A, B and C

$$\begin{bmatrix}\hat{x}'\\ \hat{y}'\\ \hat{z}'\end{bmatrix}=\begin{bmatrix}1 & 0 & 0\\ 0 & \cos C & \sin C\\ 0 & -\sin C & \cos C\end{bmatrix}\begin{bmatrix}\cos B & 0 & -\sin B\\ 0 & 1 & 0\\ \sin B & 0 & \cos B\end{bmatrix}\begin{bmatrix}\cos A & \sin A & 0\\ -\sin A & \cos A & 0\\ 0 & 0 & 1\end{bmatrix}\begin{bmatrix}\hat{x}\\ \hat{y}\\ \hat{z}\end{bmatrix} \quad (4.15)$$

or it can be alternately written by

$$[\hat{c}']=[{}^{c'}T^{c}][\hat{c}] \quad (4.16)$$

where

$$[{}^{c'}T^{c}]=\begin{bmatrix}\cos B\cos A & \cos B\sin A & -\sin B\\ \sin C\sin B\cos A & \sin C\sin B\sin A+\cos C\cos A & \sin C\sin B\\ \cos C\sin B\cos A+\sin C\sin A & \cos C\sin B\sin A-\cos A\sin C & \cos C\cos B\end{bmatrix}$$

After multiplication and expansion (x', y', z') in term of (r', θ', ϕ') then (4.15) yields

$$\begin{bmatrix}r'\sin\theta'\cos\phi'\\ r'\sin\theta'\sin\phi'\\ r'\cos\theta'\end{bmatrix}=\begin{bmatrix}\cos B\cos A & \cos B\sin A & -\sin B\\ \sin C\sin B\cos A & \sin C\sin B\sin A+\cos C\cos A & \sin C\sin B\\ \cos C\sin B\cos A+\sin C\sin A & \cos C\sin B\sin A-\cos A\sin C & \cos C\cos B\end{bmatrix}\cdot\begin{bmatrix}r\sin\theta\cos\phi\\ r\sin\theta\sin\phi\\ r\cos\theta\end{bmatrix} \quad (4.17)$$

In calculating the radiation pattern, the far field condition can be written as

$$r = r' \approx \infty \tag{4.18}$$

Then we expand each component in (4.17) by applying the condition in (4.18). The relation between primed and unprimed coordinate can be obtained as shown in (4.19a) through (4.19c).

$$\sin\phi' = \frac{\sin C \sin B \sin\theta \cos(\phi - A) + \cos C \sin\theta \sin(\phi - A) + \sin A \cos B \cos\theta}{\sin\theta'} \tag{4.19a}$$

$$\cos\phi' = \frac{\cos B \sin\theta \cos(\phi - A) - \sin B \cos\theta}{\sin\theta'} \tag{4.19b}$$

$$\cos\theta' = \cos C \sin B \sin\theta \cos(\phi - A) - \sin C \sin\theta \sin(\phi - A) + \cos C \cos B \cos\theta \tag{4.19c}$$

Our next task is to derive the relation between unit component $(\hat{r}', \hat{\theta}', \hat{\phi}')$ and $(\hat{r}, \hat{\theta}, \hat{\phi})$ which can be represented by (4.20).

$$[\hat{s}'] = [{}^{s'}T^{c'}][{}^{c'}T^{c}][{}^{c}T^{s}][\hat{s}] \tag{4.20}$$

After substituting the transformation matrix $[{}^{s'}T^{c'}], [{}^{c'}T^{c}]$ and $[{}^{c}T^{s}]$, it can be explicitly written as follow

$$\begin{bmatrix} \hat{r}' \\ \hat{\theta}' \\ \hat{\phi}' \end{bmatrix} = \begin{bmatrix} \sin\theta'\cos\phi' & \sin\theta'\sin\phi' & \cos\theta' \\ \cos\theta'\cos\phi' & \cos\theta'\sin\phi' & -\sin\theta' \\ -\sin\phi' & \cos\phi' & 0 \end{bmatrix}$$
$$\cdot \begin{bmatrix} \cos B\cos A & \cos B\sin A & -\sin B \\ \sin C\sin B\cos A & \sin C\sin B\sin A + \cos C\cos A & \sin C\sin B \\ \cos C\sin B\cos A + \sin C\sin A & \cos C\sin B\sin A - \cos A\sin C & \cos C\cos B \end{bmatrix}$$
$$\cdot \begin{bmatrix} \sin\theta\cos\phi & \cos\theta\cos\phi & -\sin\phi \\ \sin\theta\sin\phi & \cos\theta\sin\phi & \cos\phi \\ \cos\theta & -\sin\theta & 0 \end{bmatrix} \begin{bmatrix} \hat{r} \\ \hat{\theta} \\ \hat{\phi} \end{bmatrix} \tag{4.21}$$

We finally expand (4.21) to determine the $\hat{\theta}'$ and $\hat{\phi}'$ in term of $\hat{\theta}$, $\hat{\phi}$ via the applications of (4.19a) through (4.19c) with a condition of constant radial direction. After taking a laborious derivation, we obtain (4.22a) and (4.22b).

$$\hat{\phi}' = \frac{\left(\begin{array}{c} -\frac{1}{4}\sin C\sin 2B\sin 2\theta\cos^2(\phi - A) - \sin C\cos^2 B\cos^2\theta\cos(\phi - A) \\ -\sqrt{2}\cos(45-\phi)(\frac{1}{4}\sin C\sin 2B\sin A\sin 2\theta\cos(\phi - A) - \sin C\sin^2 B\sin A\cos^2\theta) \\ -\cos C\sin B\sin(\phi - A) - \sin C\sin^2\theta\cos(\phi - A) \end{array}\right)}{\sin\theta'}\hat{\theta}$$

$$+\frac{\left(\begin{array}{c} \frac{1}{4}\sin C\sin 2B\sin 2(\phi - A)\sin\theta + \cos C\cos B\sin\theta \\ +\frac{\sqrt{2}}{2}\sin(45-\phi)\sin C\sin 2B\sin A\sin\theta\cos(\phi - A) \\ -\cos C\sin B\cos\theta\cos(\phi - A) + \sin C\cos^2 B\cos\theta\sin(\phi - A) \end{array}\right)}{\sin\theta'}\hat{\phi} \tag{4.22a}$$

$$\hat{\theta}' = \frac{\left(\begin{array}{c} \frac{1}{4}\sin C\sin 2B\sin 2(\phi - A)\sin\theta + \cos C\cos B\sin\theta \\ +\frac{\sqrt{2}}{2}\sin(45-\phi)\sin C\sin 2B\sin A\sin\theta\cos(\phi - A) \\ -\cos C\sin B\cos\theta\cos(\phi - A) + \sin C\cos^2 B\cos\theta\sin(\phi - A) \end{array}\right)}{\sin\theta'}\hat{\theta}$$

$$-\frac{\left(\begin{array}{c} -\frac{1}{4}\sin C\sin 2B\sin 2\theta\cos^2(\phi - A) - \sin C\cos^2 B\cos^2\theta\cos(\phi - A) \\ -\sqrt{2}\cos(45-\phi)(\frac{1}{4}\sin C\sin 2B\sin A\sin 2\theta\cos(\phi - A) - \sin C\sin^2 B\sin A\cos^2\theta) \\ -\cos C\sin B\sin(\phi - A) - \sin C\sin^2\theta\cos(\phi - A) \end{array}\right)}{\sin\theta'}\hat{\phi} \tag{4.22b}$$

In summary, expression (4.22a) and (4.22b) are useful to calculate the radiation field of the inclined slot on a sphere that will be concentrated in the succeeding sections. Observing that the unknown parameter θ' can be successfully archived from spherical Euler angle in section 4.1.2.

4.2.2 The Global and Local Coordinates with the Different Origin

In some cases, the global and local coordinates are not located in the same origin [13] because the feed element and its origin are located on the surface of a sphere. Hence, not only the rotation is involved but also the translation. As depicted in Fig.4.9, the antenna element on the surface of a sphere is located at (a,ζ,ξ) with the field point is designated by $P(r',\theta',\phi')$ and the polar axis z' is oriented along the

radial direction, also the x'-axis is taken in the $z-z'$ plane. These are related through two rotations and one translation by using the Cartesian Euler angle.

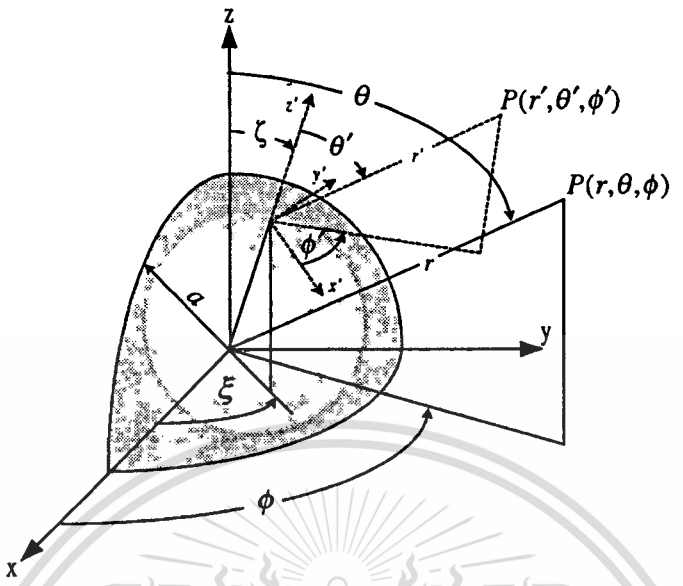

Fig. 4.9 Geometry of global and local coordinates locate on a different origin

Next, we will theoretical investigate the transformation procedure. For the rotation processes, we firstly rotate about z-axis through an angle ξ in a counterclockwise sense. Then, the y-axis is rotated through an angle ζ in a clockwise sense. As the results, the Fig.4.10 can be obtained.

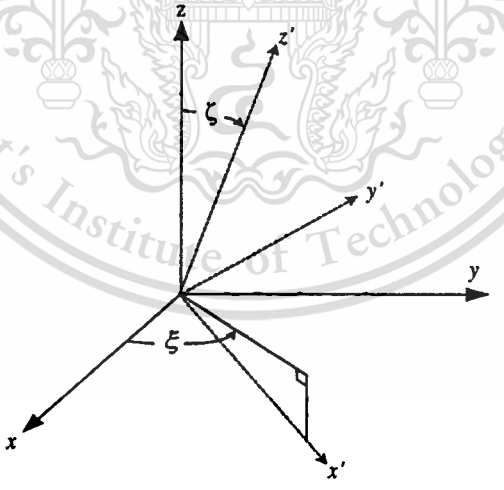

Fig. 4.10 Rotation about z- and y-axis through an angle ξ and ζ

With two aforementioned rotations, from the Cartesian Euler section 4.1.1, the transformation equation can be written by

$$\begin{bmatrix} x' \\ y' \\ z' \end{bmatrix} = \begin{bmatrix} \cos\varsigma & 0 & -\sin\varsigma \\ 0 & 1 & 0 \\ \sin\varsigma & 0 & \cos\varsigma \end{bmatrix} \begin{bmatrix} \cos\xi & \sin\xi & 0 \\ -\sin\xi & \cos\xi & 0 \\ 0 & 0 & 1 \end{bmatrix} \begin{bmatrix} x \\ y \\ z \end{bmatrix} \tag{4.23a}$$

After some multiplications yield

$$\begin{bmatrix} x' \\ y' \\ z' \end{bmatrix} = \begin{bmatrix} \cos\varsigma\cos\xi & \cos\varsigma\sin\xi & -\sin\varsigma \\ -\sin\xi & \cos\xi & 0 \\ \sin\varsigma\cos\xi & \sin\varsigma\sin\xi & \cos\varsigma \end{bmatrix} \begin{bmatrix} x \\ y \\ z \end{bmatrix} \tag{4.23b}$$

or equivalent to

$$[\hat{c}'] = [{}^{c'}T^{c}][\hat{c}] \tag{4.23c}$$

Another important transformation is translation concerns the move of origin from one position to others. Hence, the global and local coordinate systems will have a different location. By considering Fig.4.11, if the observation point $P(r,\theta,\phi)$ in unprimed coordinates and $P(r',\theta',\phi')$ in primed coordinate are the same point then the relationship of radial direction between two coordinates can be given by (4.24).

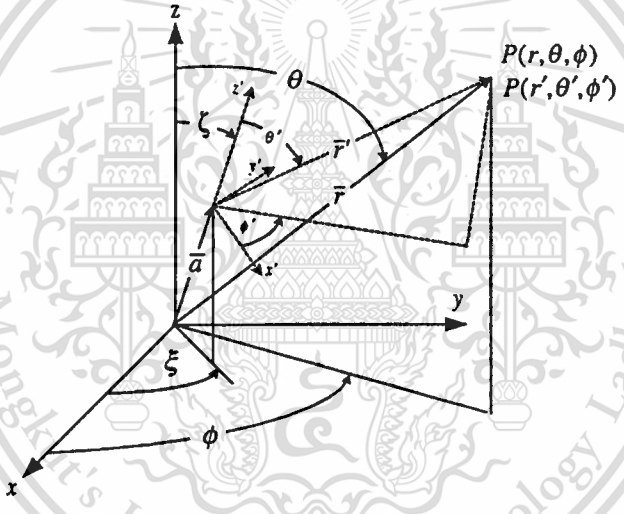

Fig. 4.11 Derivation geometry when global and local coordinate have a different origin

$$[\bar{r}'] = [{}^{c'}T^{c}][\bar{r} - \bar{a}] \tag{4.24}$$

Expanding the radial component to Cartesian component, then (4.24) can be written to (4.25).

$$\begin{bmatrix} r'\sin\theta'\cos\phi' \\ r'\sin\theta'\sin\phi' \\ r'\cos\theta' \end{bmatrix} = \begin{bmatrix} \cos\varsigma\cos\xi & \cos\varsigma\sin\xi & -\sin\varsigma \\ -\sin\xi & \cos\xi & 0 \\ \sin\varsigma\cos\xi & \sin\varsigma\sin\xi & \cos\varsigma \end{bmatrix} \begin{bmatrix} r\sin\theta\cos\phi - a\sin\varsigma\cos\xi \\ r\sin\theta\sin\phi - a\sin\varsigma\sin\xi \\ r\cos\theta - a\cos\varsigma \end{bmatrix} \tag{4.25}$$

The Cartesian component of $\bar{r}'$ can then be written separately, this means that for the x' component

$$r'\sin\theta'\cos\phi' = \cos\varsigma\cos\xi(r\sin\theta\cos\phi - a\sin\varsigma\cos\xi) + \cos\varsigma\sin\xi(r\sin\theta\sin\phi - a\sin\varsigma\sin\xi) - \sin\varsigma(r\cos\theta - a\cos\varsigma) \tag{4.26a}$$

and the y' component

$$r'\sin\theta'\sin\phi' = -\sin\xi(r\sin\theta\cos\phi - a\sin\varsigma\cos\xi) + \cos\xi(r\sin\theta\sin\phi - a\sin\varsigma\sin\xi) \tag{4.26b}$$

and finally, the z' component

$$r'\cos\theta' = \sin\varsigma\cos\xi(r\sin\theta\cos\phi - a\sin\varsigma\cos\xi) + \sin\varsigma\sin\xi(r\sin\theta\sin\phi - a\sin\varsigma\sin\xi) + \cos\varsigma(r\cos\theta - a\cos\varsigma) \tag{4.26c}$$

In the far field observation, we can assume the condition (4.27), this is

$$r \approx r' \approx \infty \tag{4.27}$$

With the applications of (4.27) and applying to (4.26a) through (4.26c) with some algebraic manipulations give (4.28a)-(4.28c).

$$\cos\phi' = \frac{\cos\varsigma\sin\theta\cos(\phi-\xi) - \sin\varsigma\cos\theta}{\sin\theta'} \tag{4.28a}$$

$$\sin\phi' = \frac{\sin\theta\sin(\phi-\xi)}{\sin\theta'} \tag{4.28b}$$

$$\cos\theta' = \sin\varsigma\sin\theta\cos(\phi-\xi) + \cos\varsigma\cos\theta \tag{4.28c}$$

So far we have been able to write out the relative angle between primed and unprimed coordinates. We shall now use the matrix notation to describe the relations between unit components. Starting with the matrix notation as can be written to

$$[\hat{s}'] = [{}^{s'}T^{c'}][{}^{c'}T^{c}][{}^{c}T^{s}][\hat{s}] \tag{4.29}$$

Expansion of each terms in (4.29), then becomes to

$$\begin{bmatrix}\hat{r}'\\ \hat{\theta}'\\ \hat{\phi}'\end{bmatrix} = \begin{bmatrix}\sin\theta'\cos\phi' & \sin\theta'\sin\phi' & \cos\theta'\\ \cos\theta'\cos\phi' & \cos\theta'\sin\phi' & -\sin\theta'\\ -\sin\phi' & \cos\phi' & 0\end{bmatrix}\begin{bmatrix}\cos\varsigma\cos\xi & \cos\varsigma\sin\xi & -\sin\varsigma\\ -\sin\xi & \cos\xi & 0\\ \sin\varsigma\cos\xi & \sin\varsigma\sin\xi & \cos\varsigma\end{bmatrix} \cdot \begin{bmatrix}\sin\theta\cos\phi & \cos\theta\cos\phi & -\sin\phi\\ \sin\theta\sin\phi & \cos\theta\sin\phi & \cos\phi\\ \cos\theta & -\sin\theta & 0\end{bmatrix}\begin{bmatrix}\hat{r}\\ \hat{\theta}\\ \hat{\phi}\end{bmatrix} \tag{4.30}$$

We finally expand (4.30) to determine the $\hat{\theta}', \hat{\phi}'$ in terms of $\hat{\theta}$ and $\hat{\phi}$ via the applications of (4.28a) through (4.28c) with a condition of constant radial direction. After taking a laborious derivation, we obtain (4.31a) through (4.31b).

$$\hat{\theta}' = -\frac{\cos\theta \sin\varsigma \cos(\phi - \xi) - \sin\theta \cos\varsigma}{\sin\theta'} \hat{\theta} + \frac{\sin\varsigma \sin(\phi - \xi)}{\sin\theta'} \hat{\phi} \tag{4.31a}$$

$$\hat{\phi}' = -\frac{\sin\varsigma \sin(\phi - \xi)}{\sin\theta'} \hat{\theta} - \frac{\cos\theta \sin\varsigma \cos(\phi - \xi) - \sin\theta \cos\varsigma}{\sin\theta'} \hat{\phi} \tag{4.31b}$$

In a similar way with the previous section, the expression (4.31a) and (4.31b) are useful to calculate the radiation field via spherical unit vector. Observing that the unknown parameter θ' can successfully be archived from spherical Euler rotation in section 4.1.2 as well.

4.3 Radiation Characteristics of an Inclined Slot on a Sphere

Here, there is sufficient information to apply the relationship in the preceding section to derive the radiation characteristics of an inclined slot on a sphere as illustrated in Fig. 4.12. The slot is rotated about x-axis through an angle β in a clockwise sense. The spherical Euler angle α and γ are -90° and 90°, respectively. For mapping point from primed to unprimed coordinate, we can solve from (4.5) and (4.14) that is for the x-y plane (fixed $\theta = 90^\circ$), we obtain

$$\phi' = \tan^{-1}(\cos\beta \tan\phi) \tag{4.32a}$$

$$\theta' = \tan^{-1}(\cot\beta \csc\phi') \tag{4.32b}$$

and the x-z plane (fixed $\phi = 0^\circ$ or $\phi = 180^\circ$)

$$\theta' = \cos^{-1}(\cos\theta \cos\beta) \tag{4.33a}$$

$$\phi' = \sin^{-1}\left(\frac{-\tan\beta}{\tan\theta'}\right) \tag{4.33b}$$

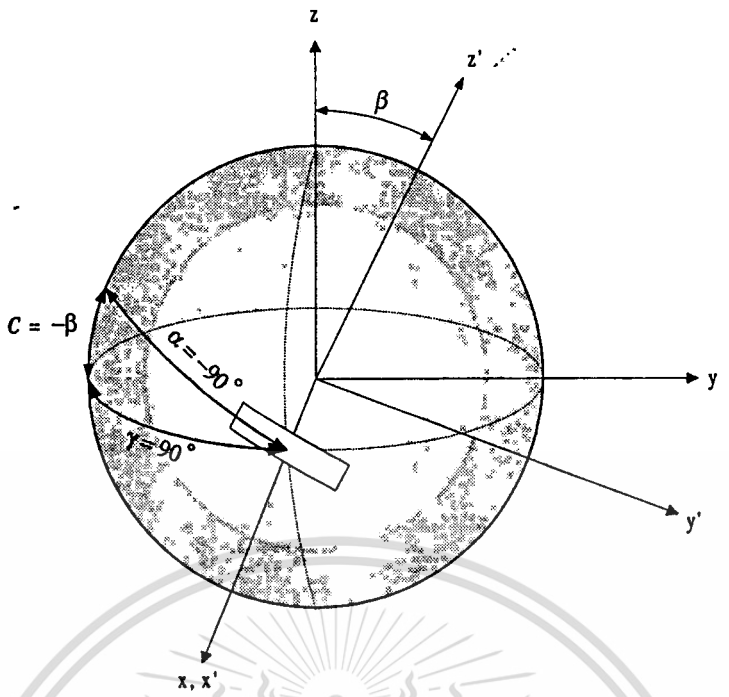

Fig. 4.12 Geometry configuration of an inclined slot on a sphere showing a spherical Euler angle α, β and γ

Due to the symmetry of the structure, the patterns can be calculated in the x-z plane only. Note that the value of (4.33a) and (4.33b) in each quadrant can be obtained from Table 4.1.

Table 4.1 Formulation to evaluate θ' and ϕ' in the x-z plane

θ (degree), $\phi = 0^\circ$	θ' (degree)	ϕ' (degree)
$0^\circ \rightarrow 90^\circ = d$	$\cos^{-1}[\cos\theta\cos\beta]$	$\tan^{-1}\left[\dfrac{-\tan\beta}{\tan\theta'}\right]$
$90^\circ \rightarrow 180^\circ$ $= 90^\circ + d$	$90^\circ + \sin^{-1}[\sin d\cos\beta]$	$\sin^{-1}\left[\dfrac{\sin\beta\sin d}{\cos[\sin^{-1}(-\sin d\cos\beta)]}\right]$
θ (degree), $\phi = 180^\circ$	θ' (degree)	ϕ' (degree)
$0^\circ \rightarrow 90^\circ = d$	$\cos^{-1}[\cos\theta\cos\beta]$	$90^\circ + \cos^{-1}\left[\dfrac{-\tan\beta}{\tan\theta'}\right]$
$90^\circ \rightarrow 180^\circ$ $= 90^\circ + d$	$90^\circ - \sin^{-1}[-\sin d\cos\beta]$	$180^\circ - \sin\left[\dfrac{\sin\beta\sin d}{\cos[\sin^{-1}(-\sin d\cos\beta)]}\right]$

When comparing with the rotation angle in section 4.2.1, we obtain $C = -\beta$ with A and B equal to zero. Thus (422a) and (4.22b) can be reduced to (4.34a)-(4.34b).

$$\hat{\theta}' = \frac{\sin\theta\cos C + \cos\theta\sin C\sin\phi}{\sin\theta'}\hat{\theta} + \frac{\sin C\cos\phi}{\sin\theta'}\hat{\phi} \tag{4.34a}$$

$$\hat{\phi}' = \frac{-\sin C\cos\phi}{\sin\theta'}\hat{\theta} + \frac{\sin\theta\cos C + \cos\theta\sin C\sin\phi}{\sin\theta'}\hat{\phi} \tag{4.34b}$$

It is evident from the above that the E_θ and E_ϕ in the unprimed coordinate system can be determined by multiplying (4.34a) by E'_θ and (4.34b) by E'_ϕ in the primed coordinate. The total field structures can be expressed as

$$E_\theta(r,\theta,\phi) = \frac{\sin\theta\cos C + \cos\theta\sin C\sin\phi}{\sin\theta'}E'_\theta(r',\theta',\phi') - \frac{\sin C\cos\phi}{\sin\theta'}E'_\phi(r',\theta',\phi') \tag{4.35a}$$

$$E_\phi(r,\theta,\phi) = \frac{\sin C\cos\phi}{\sin\theta'}E'_\theta(r',\theta',\phi') + \frac{\sin\theta\cos C + \cos\theta\sin C\sin\phi}{\sin\theta'}E'_\phi(r',\theta',\phi') \tag{4.35b}$$

We note that even though our solutions consist of only one rotating step. However, they can be accounted for the higher rotating step as well.

4.4 Numerical Results

Calculation of the radiation pattern of a half-wave inclined slot on a sphere is performed by utilizing the formulation in chapter 3 with (4.35a) and (4.35b), also the mapping angle from primed and unprimed coordinates can be determined from Table 4.1. Only x-z plane pattern will be considered in this case since the symmetry of the structure. The separation into individual field components is chosen to compare the theory. As shown in Fig.4.13, the numerical patterns at $ka = 10$ show that by stepping C from 0° to 45°, only E_θ-component exist at $C = 0^\circ$. While the stepping C is higher, E_ϕ-component is gradually increasing until $C = 15^\circ$ the different strength between E_θ and E_ϕ-components will be 11.349 dB and become 0 dB at $C = 45^\circ$ in the broadside. After passing 45°, E_ϕ-component will become a dominant and E_θ will be steadily decreased. At $C = 75^\circ$, E_ϕ-component will be 11.349 dB over E_θ-component and until $C = 90^\circ$ E_ϕ-component only exists.

Also shown in Fig.4.14 is the radiation characteristic of an inclined slot on a sphere at $ka = 20$. The results of comparison E_θ- and E_ϕ-components at $C = 15^\circ$, 45° and 75° are the similar way with the previous case except the more ripples are significantly observed at the back lobes.

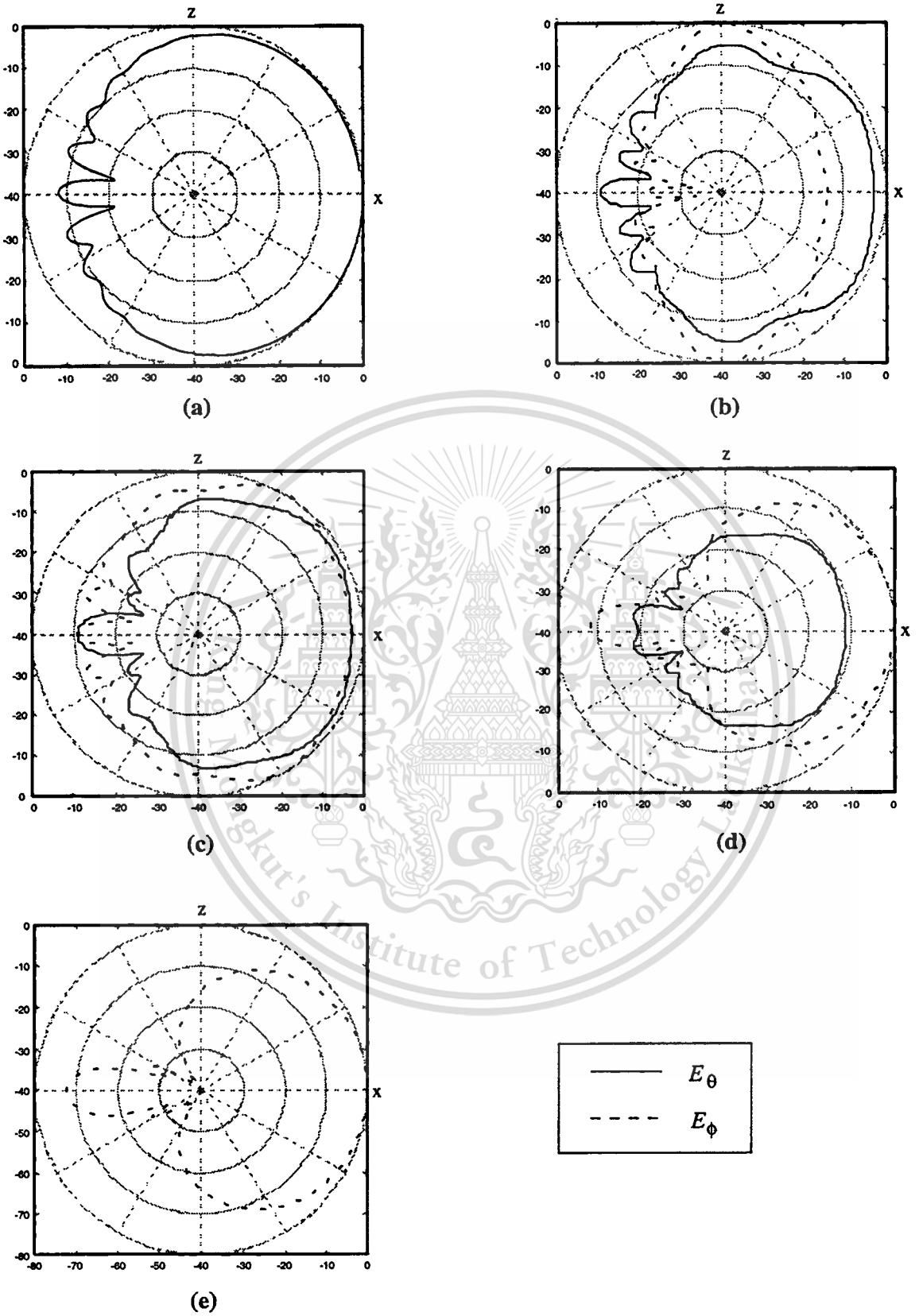

Fig. 4.13 Radiation pattern in x-z plane of a half-wave inclined slot on a sphere at *ka=10* with various inclined angles
(a) *c=0°* (b) *c=15°* (c) *c=45°* (d) *c=75°* (e) *c=90°*

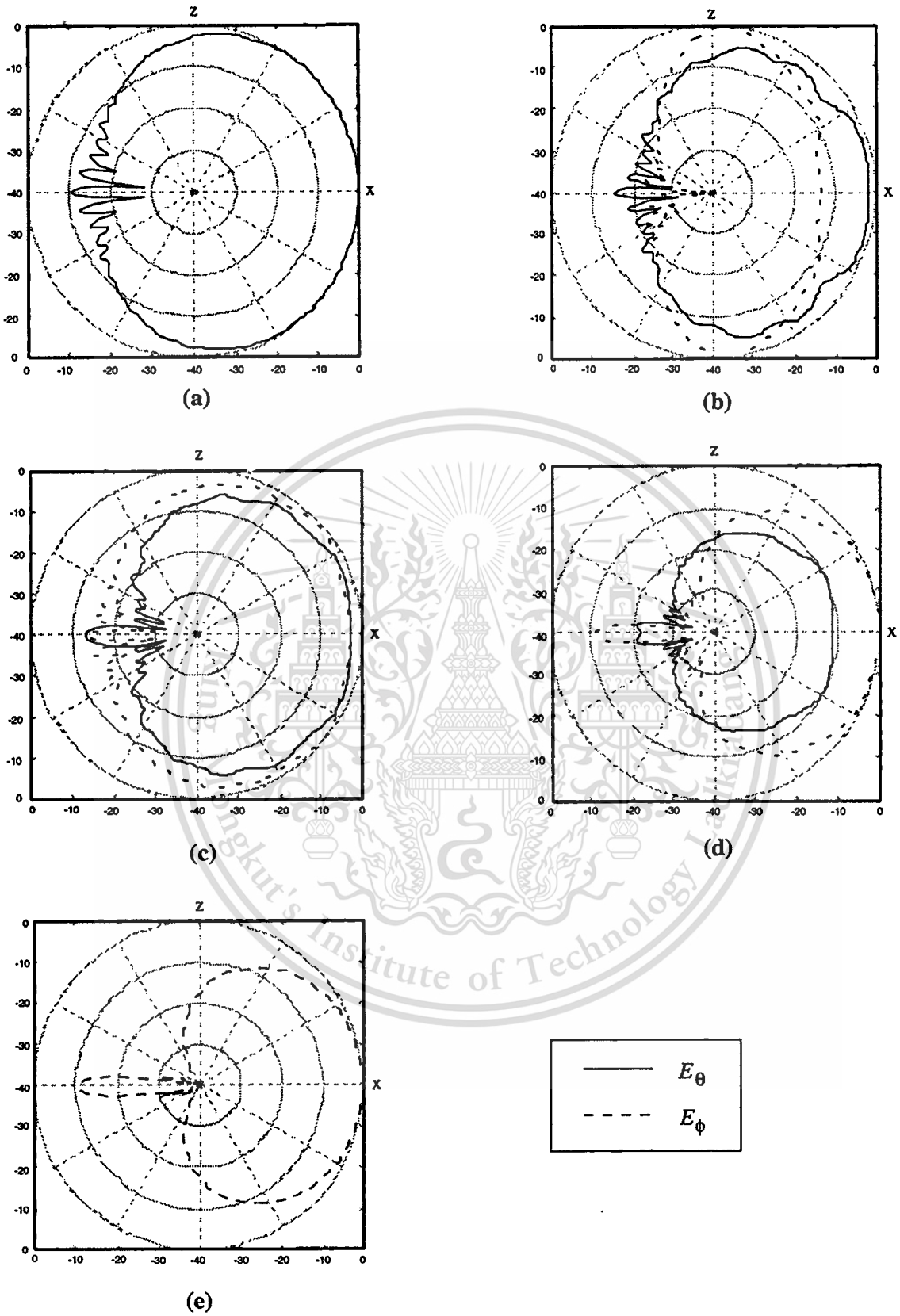

Fig. 4.14 Radiation pattern in x-z plane of a half-wave inclined slot on a sphere at *ka=20* with various inclined angles
(a) *c=0°* (b) *c=15°* (c) *c=45°* (d) *c=75°* (e) *c=90°*

4.5 Experimental Results

The prototype of an inclined slot on a sphere in the measurement of this chapter are used the same specification that was already explained in chapter 3. The antenna under test is rotated to an inclined angle with the measurement being taken in the Fresnel zone. The electric field components E_θ and E_ϕ are measured and the relative values of each other are calculated at the inclined angle $15^\circ, 45^\circ$ and 75°.

From the comparison results of the radiation pattern at $C = 15^\circ$, it is shown in Fig.4.15. It should be noted that the E_θ-component agrees reasonably well with the computation. However, the experimental result of E_ϕ-component demonstrates the asymmetric patterns as predicted by the theory. This may be come from some imperfect fabrications or the effect of multipath waves due to imperfect free space test site. However, it should be to point out that in the main beam direction, the measurement of E_θ-component differs as much as 12.13 dB from the E_ϕ-component that is close to the theory.

In Fig.4.16 shows the comparison of a radiation pattern at $C = 45^\circ$. Good agreement is obtained for both E_θ- and E_ϕ-components. The pattern of theory and experiment are similar except ripples at the back lobes.

Fig.4.17 compares the results at $C = 75^\circ$ from the theory and experiment. However, it is also good to point out that the difference between E_θ and E_ϕ components is approximately 12.45 dB at the main beam and well agreement with the theory.

As the results are reported in this section, the radiation patterns have been plotted versus angle. There are some discrepancies of the minor component at $C = 15^\circ$ and 75°. This will be searched to improve in the future work.

4.6 Conclusions

This chapter has described the radiation characteristics of a half-wave inclined slot on a sphere utilizing the formulations that have been derived in chapter 3. We have seen that the coordinate transformation plays an important role in rotated antenna radiation pattern. It composes of Cartesian and spherical Euler coordinate. The numerical results presented have been compared with the corresponding result from the measurement and are in well agreement in the strong components and some discrepancies in weak component. The comparisons of electric field components at various inclined angles are illustrated. It is evident that the variably field strength is obviously observed when the inclined angle is changed and also it is not depend on the effective radius (ka). Subsequently, the experiments are set up to verify the theoretical principle.

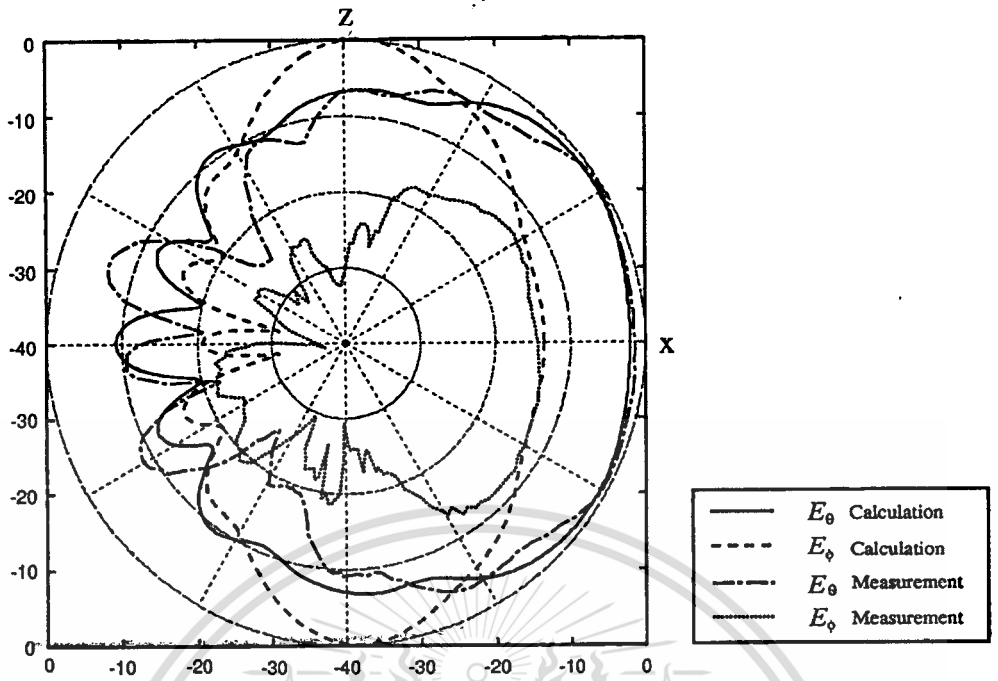

Fig. 4.15 x-z plane radiation pattern comparison between theoretical and experimental results of a slot on a sphere for $ka = 8.57$ at $C = 15^\circ$

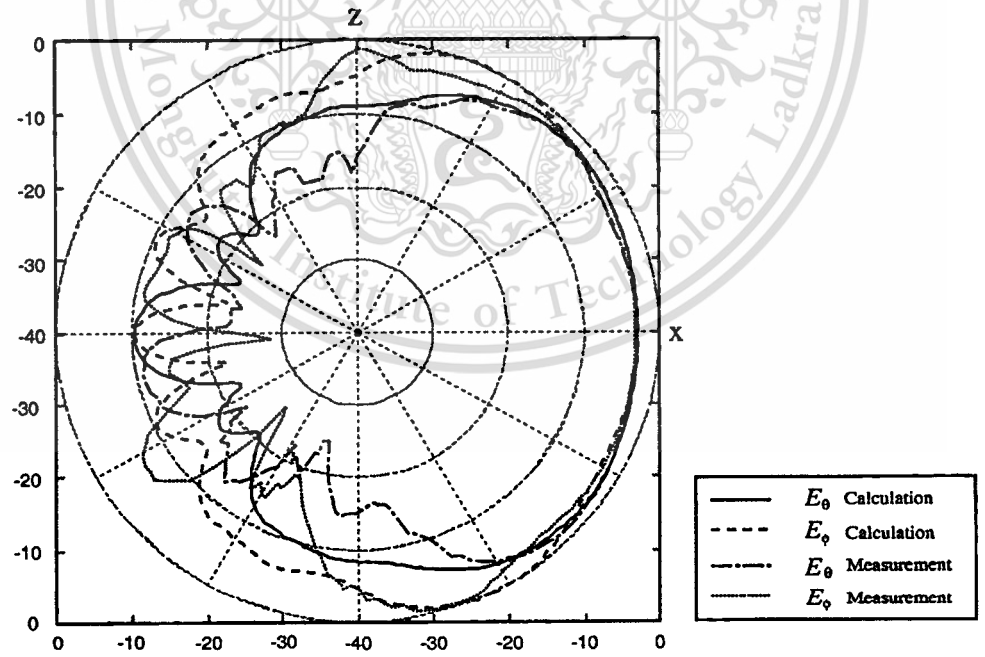

Fig. 4.16 x-z plane radiation pattern comparison between theoretical and experimental results of a slot on a sphere for $ka = 8.57$ at $C = 45^\circ$

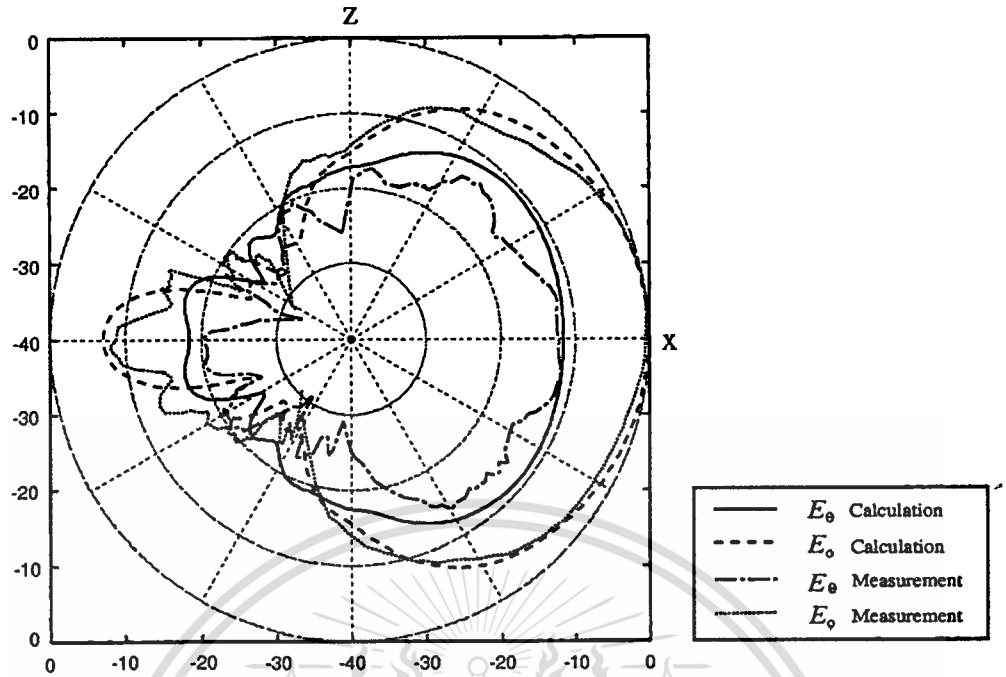

Fig. 4.17 x-z plane radiation pattern comparison between theoretical and experimental results of a slot on a sphere for $ka = 8.57$ at $C = 75^\circ$

CHAPTER 5

A SLOT PAIR ON A SPHERE

The purpose of this chapter is to study the theoretical expressions and measurement of circularly polarized characteristics of a slot pair on a sphere. The study is undertaken to evaluate the merits of two perpendicular slots providing circularly polarized radiation and the beam coverage area. The mutual coupling effect between the slots is neglected. In addition, the individual slot is assumed the tangential field distribution on the aperture. The applications of coordinate transformation in the previous chapter are useful. At the end of the chapter, the discussion on the effects of amplitude and phase error on the co- and cross-polarization and the axial ratio will be addressed. Finally, the measurement results are presented to demonstrate the usefulness of the proposed antenna configuration.

5.1 Antenna Structure

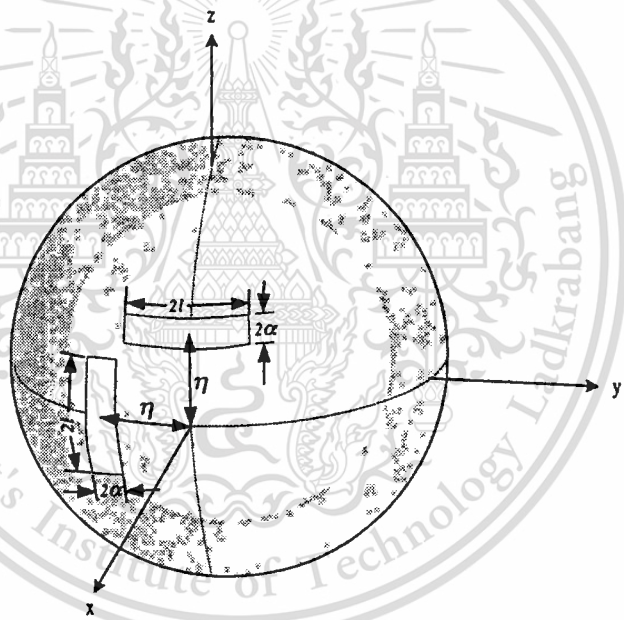

Fig 5.1 Geometry of a slot pair on a sphere

The fundamental structure of a slot pair on sphere with radius of "a" consists of two orthogonal slots. The narrow edge of each slot has a dimension "2α" and the wide edge has a length of "$2l$". Having seen that all of the parameters are the same with the prototype in preceding chapters. In addition, η is the separation between the center of slot and the x-axis. A circular polarization is obtained by adding linearly polarized slot placed perpendicular to each other, exciting them with a quadrature phase and equal amplitude [24-26]. The equal amplitude is produced by 2 way power divider and a quadrature phase is provided by adjusting an extra quarter-wavelength ($\lambda_g/4$ where λ_g is the wavelength in a transmission line) section from a common transmission line before exciting the slots.

With the application of coordinate transformation in the previous chapter, the relations between the rotated and antenna coordinate system are accomplished by the spherical Euler angle α, β and γ. The rotation paths of slot 1 are shown in Fig. 5.2 where only the y-axis is rotated through an angle η in a clockwise sense. The Euler angle are $\alpha = 0^\circ$, $\gamma = 0^\circ$ and $\beta = \eta$. It appears that the structure of problem is symmetry, so that only the x-z plane will be considered. We note that the value of (4.33a) and (4.33b) in each quadrant can be obtained from Table 5.1.

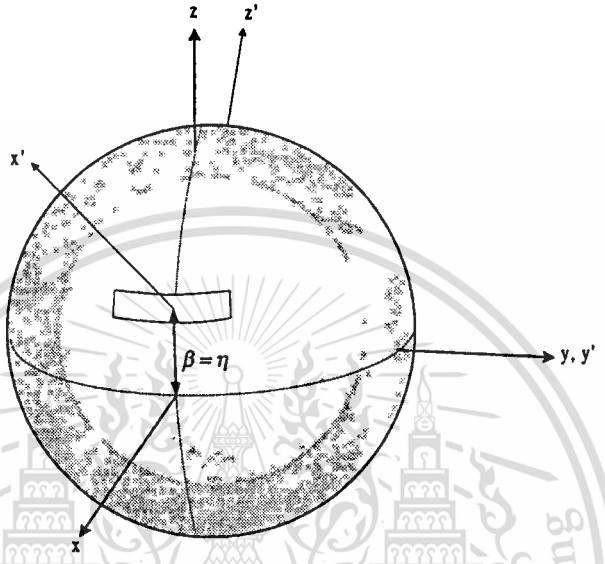

Fig. 5.2 Rotation path of slot 1 showing $\beta = \eta$

Table 5.1 Formulation to evaluate θ' and ϕ' of slot 1 in the x-z plane

θ (degree), $\phi = 0^\circ$	θ' (degree)	ϕ' (degree)
$0^\circ \rightarrow 180^\circ = d$	$\beta + d$	$\tan^{-1}\left[\dfrac{-\tan\beta}{\tan\theta'}\right]$
θ (degree), $\phi = 180^\circ$	θ' (degree)	ϕ' (degree)
$0^\circ \rightarrow 180^\circ = d$	$\cos^{-1}[\cos\theta\cos\beta]$	$90^\circ + \cos^{-1}\left[\dfrac{-\tan\beta}{\tan\theta'}\right]$

For the slot 2 the rotating procedures are displayed in Fig.5.3. The rotation process, we firstly rotate about x axis through 90 degrees in a counterclockwise sense. Then, the y axis is rotated through an angle η in a clockwise sense until the primed and unprimed coordinate systems are coincided. The relations between the rotated and antenna coordinate system are accomplished by the spherical Euler angle α, β and γ. In this case, the Euler angle $\alpha = 90^\circ$, $\beta = 0^\circ$ and $\gamma = -90^\circ + \eta$. We note that the value of (4.33a) and (4.33b) in each quadrant can be obtained from Table 5.2.

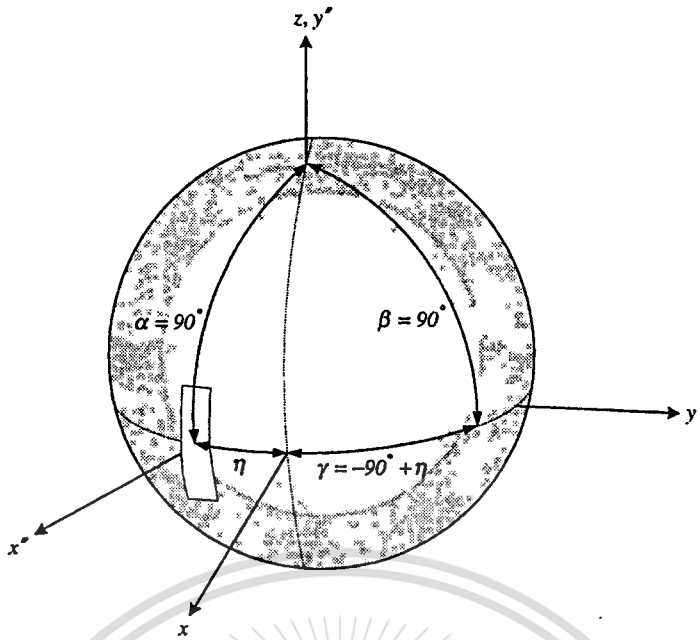

Fig. 5.3 Rotation path of slot 2 showing $\alpha = 90^{\circ}$, $\beta = 0^{\circ}$ and $\gamma = -90^{\circ} + \eta$

Table 5.2 Formulation to evaluate θ'' and ϕ'' in the x-z plane

θ (degree), $\phi = 0^{\circ}$	θ''(degree)	ϕ''(degree)
$0^{\circ} \rightarrow 90^{\circ} = d$	$90^{\circ} + \cos^{-1}\left[\frac{}{\sqrt{\cos^2\eta + \sin^2\eta\cos^2 d}}\right]$	$\sin^{-1}\left[\frac{\cos d}{\sqrt{\cos^2\eta + \sin^2\eta\cos^2 d}}\right]$
$90^{\circ} \rightarrow 180^{\circ}$ $= 90^{\circ} + d$	$90^{\circ} + \cos^{-1}\left[\frac{}{\sqrt{\cos^2\eta + \sin^2\eta\sin^2 d}}\right]$	$360^{\circ} - \sin^{-1}\left[\frac{\sin d}{\sqrt{\cos^2\eta + \sin^2\eta\sin^2 d}}\right]$
θ (degree), $\phi = 180^{\circ}$	θ''(degree)	ϕ''(degree)
$0^{\circ} \rightarrow 90^{\circ} = d$	$\sin^{-1}\left[\frac{\sqrt{\cos^2\eta}}{\sqrt{+\sin^2\eta\cos^2\theta}}\right]$	$90^{\circ} + \cos^{-1}\left[\frac{\cos d}{\sqrt{\cos^2\eta + \sin^2\eta\cos^2 d}}\right]$
$90^{\circ} \rightarrow 180^{\circ}$ $= 90^{\circ} + d$	$\sin^{-1}\left[\frac{\sqrt{\cos^2\eta}}{\sqrt{+\sin^2\eta\sin^2 d}}\right]$	$180^{\circ} - \sin\left[\frac{\sin d}{\sqrt{\cos^2\eta + \sin^2\eta\sin^2 d}}\right]$

In general the definition of right-hand circular polarization (RHCP) and left-hand circular polarization (LHCP) are simply defined by the rotating of the electric field may be observed at a given position in space as a function of increasing time. The fields may be either a right-hand and left-hand rotation, corresponding to the direction of the finger with respect to the right or left hand when the thumb is pointing in the direction of propagation of the wave.

In this chapter, we consider the right-hand circular polarization (RHCP) as a reference polarization. In this case the excited phase of slot 1 will lead slot 2 by 90°, then the total components of the electric field from a pair of slots can be written that

$$\overline{E}_{tot}(\theta,\phi)=\left[E_{\theta 1}(\theta,\phi)+jE_{\theta 2}(\theta,\phi)\right]\hat{\theta}+\left[E_{\phi 1}(\theta,\phi)+jE_{\phi 2}(\theta,\phi)\right]\hat{\phi} \quad (5.1)$$

where

$$E_{\theta 1}(r,\theta,\phi)=\frac{\sin\theta\cos\eta-\cos\theta\sin\eta\cos\phi}{\sin\theta'}E'_{\theta}(r',\theta',\phi')-\frac{\sin\eta\sin\phi}{\sin\theta'}E'_{\phi}(r',\theta',\phi') \quad (5.2a)$$

$$E_{\phi 1}(r,\theta,\phi)=\frac{\sin\eta\sin\phi}{\sin\theta'}E'_{\theta}(r',\theta',\phi')+\frac{\sin\theta\cos\eta-\cos\theta\sin\eta\cos\phi}{\sin\theta'}E'_{\phi}(r',\theta',\phi') \quad (5.2b)$$

$$E_{\theta 2}(r,\theta,\phi)=\frac{\sin\theta\cos\eta+\cos\theta\sin\eta\cos\phi}{\sin\theta''}E''_{\theta}(r'',\theta'',\phi'')+\frac{\sin\eta\sin\phi}{\sin\theta''}E''_{\phi}(r'',\theta'',\phi'') \quad (5.2c)$$

$$E_{\phi 2}(r,\theta,\phi)=-\frac{\sin\eta\sin\phi}{\sin\theta''}E''_{\theta}(r'',\theta'',\phi'')+\frac{\sin\theta\cos\eta+\cos\theta\sin\eta\cos\phi}{\sin\theta''}E''_{\phi}(r'',\theta'',\phi'') \quad (5.2d)$$

Where

E'_{θ}, E'_{ϕ} for the wave components in prime coordinate

E''_{θ}, E''_{ϕ} for the wave components in double prime coordinate

5.2 Co- and Cross-polarization Pattern

With the advent of the large communications satellites which employ frequency re-use to increase the channel capacity. There has become a need for an accurate determining the cross-polarization performance of polarization diversity antennas [27-28]. The levels of isolation between orthogonal channel of both the ground antenna and the satellite antenna are critical parameter for frequency reuse systems, and the antennas are designed to have low cross-polarization characteristics. For this reason, the main point in this section is devoted to consider the co- and cross-polarization pattern characteristics of a slot pair on a sphere.

For RHCP when the wave propagating in the r-direction, we defined the co-polarization by a co-polar unit vector of the form

$$\overline{co}(\theta,\phi)=\frac{(\hat{\theta}-j\hat{\phi})}{\sqrt{2}} \quad (5.3)$$

and correspondingly for LHCP the cross-polar unit vector of the form

$$\overline{xp}(\theta,\phi)=\frac{(\hat{\theta}+j\hat{\phi})}{\sqrt{2}} \tag{5.4}$$

The co- and cross-polarization far-fields functions $\overline{E}_{co}(\theta,\phi)$ and $\overline{E}_{xp}(\theta,\phi)$ are found by dot operation of the $\overline{E}_{tot}$ and the complex conjugate of co- and cross-polarization unit vectors $\overline{co}(\theta,\phi)$ and $\overline{xp}(\theta,\phi)$ as can be written by

$$E_{co}(\theta,\phi)=\overline{E}_{tot}(\theta,\phi)\cdot\overline{co^{*}}(\theta,\phi) \tag{5.5}$$

$$E_{xp}(\theta,\phi)=\overline{E}_{tot}(\theta,\phi)\cdot\overline{xp^{*}}(\theta,\phi) \tag{5.6}$$

After substituting (5.1) and (5.3)-(5.4) in (5.5) and (5.6), we can write that

$$E_{co}(\theta,\phi)=\frac{[E_{\theta 1}(\theta,\phi)+jE_{\theta 2}(\theta,\phi)]}{\sqrt{2}}+j\frac{[E_{\phi 1}(\theta,\phi)+jE_{\phi 2}(\theta,\phi)]}{\sqrt{2}} \tag{5.7}$$

$$E_{xp}(\theta,\phi)=\frac{[E_{\theta 1}(\theta,\phi)+jE_{\theta 2}(\theta,\phi)]}{\sqrt{2}}-j\frac{[E_{\phi 1}(\theta,\phi)+jE_{\phi 2}(\theta,\phi)]}{\sqrt{2}} \tag{5.8}$$

5.3 Polarization of Electromagnetic Waves

In general, any electromagnetic wave can be envisioned as having polarization components. The two field components are relatively independent of one another in amplitude and phase. It is not possible to sum the vectors into a single direction containing the entire signal power because the vectors are not mutually in phase. The magnitude and phase are changed rapidly with time, so the sum vectors traces out an ellipse whose eccentricity and the orientation depend on the relative magnitudes and phases of the components. The electric field traces an ellipse around the axis occur the maximum value $E_{\max}$ and minimum value $E_{\min}$ one-quarter period later, as shown in Fig.5.4. The axial ratio for a desired circular polarization of the electromagnetic wave is defined by [29-30] and can be written to

$$AR(dB)=20\log_{10}\left|\frac{E_{\max}}{E_{\min}}\right| \tag{5.9}$$

In addition to the magnitude of the polarization ellipse, the sense of polarization (RHCP and LHCP) also may be synthesized. By using the circular components the axial ratio may be defined by

$$AR(dB)=20\log_{10}\left|\frac{E_{RHCP}+E_{LHCP}}{E_{RHCP}-E_{LHCP}}\right| \tag{5.10}$$

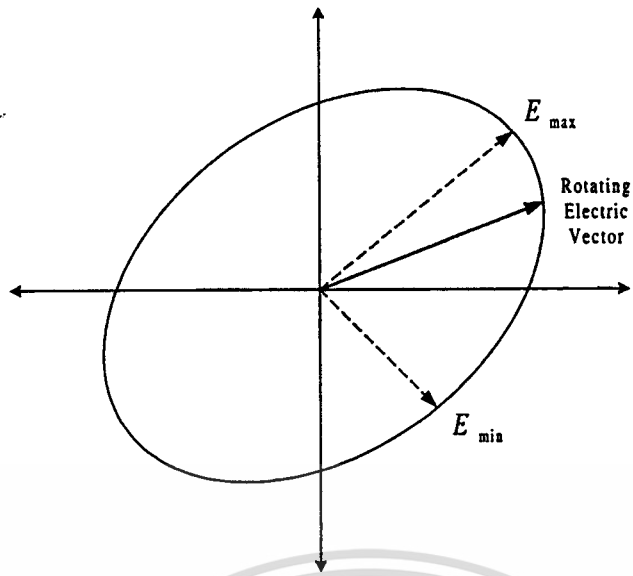

Fig. 5.4 General case of elliptical polarization

Each component of the circular polarization are expressed as

$$E_{LHCP}^2 = \frac{1}{2}(E_\theta^2 + E_\phi^2) - E_\theta E_\phi \sin\Delta\phi \tag{5.11}$$

$$E_{RHCP}^2 = \frac{1}{2}(E_\theta^2 + E_\phi^2) + E_\theta E_\phi \sin\Delta\phi \tag{5.12}$$

Where $\Delta\phi$ is a relative phase difference between E_θ and E_ϕ. Substituting (5.11) and (5.12) to (5.10), then we obtained [31]

$$AR(dB) = 10\log_{10}\left[\frac{|E_\theta|^2 + |E_\phi|^2 + \left(|E_\theta|^4 + |E_\phi|^4 + 2|E_\theta|^2|E_\phi|^2\cos 2\Delta\phi\right)^{1/2}}{|E_\theta|^2 + |E_\phi|^2 - \left(|E_\theta|^4 + |E_\phi|^4 + 2|E_\theta|^2|E_\phi|^2\cos 2\Delta\phi\right)^{1/2}}\right]^{1/2} \tag{5.13}$$

where

$$E_\theta(\theta,\phi) = E_{\theta 1}(\theta,\phi) + jE_{\theta 2}(\theta,\phi) \tag{5.14}$$

and

$$E_\phi(\theta,\phi) = E_{\phi 1}(\theta,\phi) + jE_{\phi 2}(\theta,\phi) \tag{5.15}$$

We note that for an ideally circularly polarized wave the axial ratio is unity $(0\,dB)$.

5.4 Polarization Measurement

There are several techniques for measuring the polarization characteristics of an antenna [32-35]. Some techniques measure amplitude only but some measure both amplitude and phase relative between the field components. Nevertheless, One technique is suitable for some antennas than for others, and there is no best method for measuring polarization. It is common to use the antenna under test to transmit and to use certain standard antennas, or one antenna whose polarization is known, as receivers. In this experiment, the polarization pattern method is selected because it is a rapid testing. Only the amplitude will be recorded and the accuracy is acceptable. In this method, a rotating linearly polarized antenna, such as half-wavelength dipole antenna, is connected to a receiver to measure the field intensity. Let the wave be approaching (out of page). Then, the receiving antenna is spun in the plane of the page, the field intensity observe at each position is proportional to the maximum component of electric fields in the direction of the antenna. Such measurements of the incident wave with a linearly spinning dipole do not yield the polarization ellipse of the wave but rather its polarization pattern, as shown in Fig.5.5. Thus, if the tip of the electric field describes the polarization ellipse shown in Fig.5.5 (dashed line), the variation measured with a linearly polarized receiving antenna is given by the polarization pattern in Fig.5.5 (solid line). The maximum (r_{max}) and minimum (r_{min}) and the tilt angle (τ) of the polarization ellipse are used in the calculation of the polarization pattern properties.

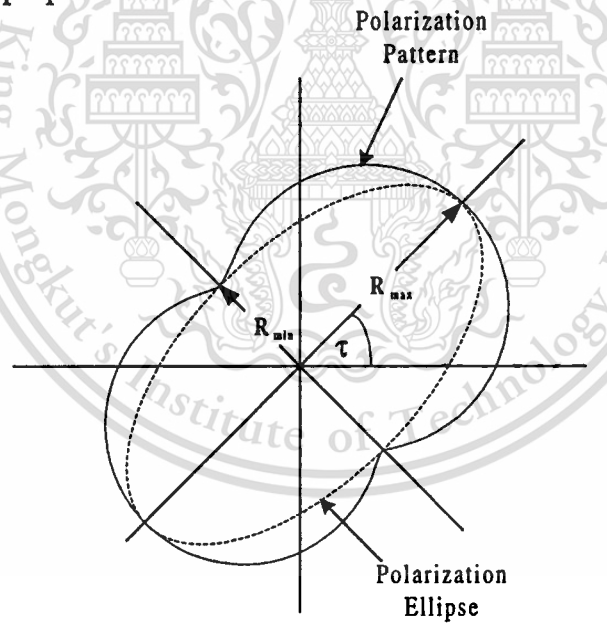

Fig. 5.5 Polarization pattern for measuring axial ratio and tilt angle of the polarization ellipse

To determine the direction of the rotation of electric field an auxiliary measurement is necessary. Such as, the output of two circularly polarized antennas with equal gain, opposite sense could be compared. The rotation direction of electric field then corresponds to the polarization of the antenna with the larger response. The axial ratio of the antenna under test is proportional to the ratio of maximum and minimum amplitude of filed components. The axial ratio of the polarization ellipse of Fig.5.5 is

$$AR = \frac{R_{\max}}{R_{\min}} \tag{5.16}$$

Thus, by specifying AR, τ and the rotation direction of electric field the polarization characteristics of Fig.5.5 are completely described.

5.5 The Effects of Amplitude and Phase Deviation

In this section, we will consider the effects of amplitude and phase deviation [36-38]. In the single polarized system, the impurity of polarized wave reduced the system performance. Also, in the dual-polarized applications polarization imperfection leads to isolation degradation. As shown in the preceding sections, the circular polarization is generated by using two linearly polarized slots. It is important to known how accurate the two linear excitations need to relative to each other.

Consider θ-polarized plane wave of a unit amplitude and ϕ-polarized plane wave of a amplitude $jAe^{j\Delta\phi}$, both propagating in the positive r-direction. The combined wave can be written by

$$\overline{E}_{tot} = E_\theta \hat{\theta} + E_\phi \hat{\phi} = \hat{\theta} - jAe^{j\Delta\phi}\hat{\phi} \tag{5.17}$$

Observing that it is a right hand circular polarization when $A=1$ and $\Delta\phi = 0$. When we define the RHCP as a co-polarization, the co- and cross-polarization are evaluated and written by

$$E_{co} = (1 + Ae^{j\Delta\phi})/\sqrt{2} \tag{5.18a}$$

$$E_{xp} = (1 - Ae^{j\Delta\phi})/\sqrt{2} \tag{5.18b}$$

We then define the relative cross-polar level (RCL) as a ratio of the cross-polarized component to the co-polarized component of the wave.

$$RCL = \left|\frac{E_{xp}}{E_{co}}\right| = \left|\frac{1 - Ae^{j\Delta\phi}}{1 + Ae^{j\Delta\phi}}\right| \tag{5.19}$$

For a desired circular polarization the axial ratio (AR) in dB and the amplitude of the co- and cross-polarization are related by

$$(AR)_{dB} = 10\log\left[\frac{|E_{co}| + |E_{xp}|}{|E_{co}| - |E_{xp}|}\right]^2 \tag{5.20}$$

or

$$(AR)_{dB} = 20\log\left[\frac{1 + RCL}{1 - RCL}\right] \tag{5.21}$$

5.5.1 Amplitude Deviation

The effects from the amplitude error are discussed in this subsection. We consider the case that there are only amplitude deviation and $\Delta\phi = 0$. By assuming the amplitude deviation is small. Then, by using one of the series expansions in Appendix B, we get

$$A = 10^{(A)_{dB}/20} = e^{(A)_{dB}\ln 10/20} \approx 1 + \frac{\ln 10}{20}(A)_{dB} = 1 + 0.115(A)_{dB} \qquad (5.22)$$

Substituting (5.22) into (5.19), RCL is expressed in dB as

$$(RCL)_{dB} \approx -25 + 20\log|(A)_{dB}| \qquad (5.23)$$

The axial ratio is found by using (5.9) with $E_{\max} = 1$ and $E_{\min} = A$ or opposite. Thus

$$(AR)_{dB} = |(AR)_{dB}| \qquad (5.24)$$

The graphs represent (5.23) and (5.24) are illustrated in Fig. 5.6 and Fig. 5.7, respectively.

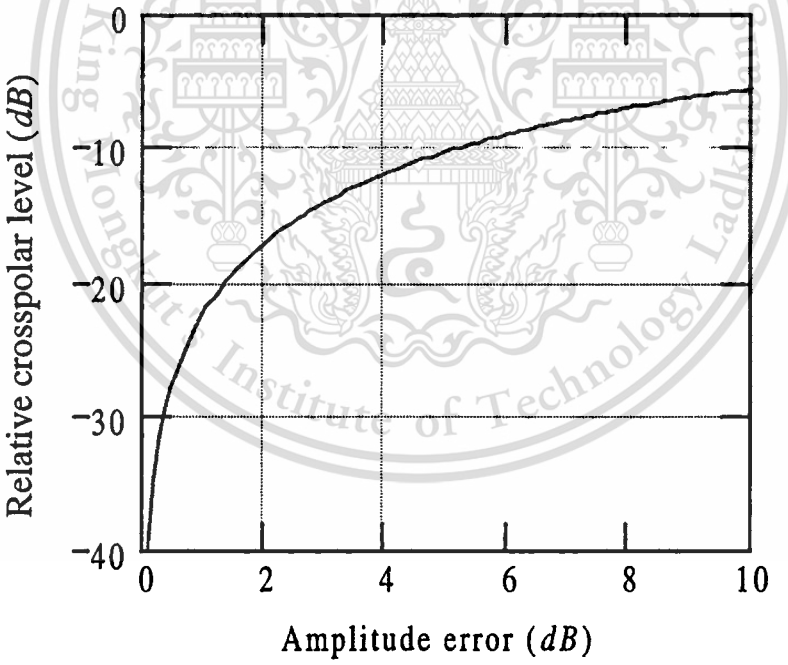

Fig. 5.6 Amplitude error of circular polarization excitation versus relative cross-polar level

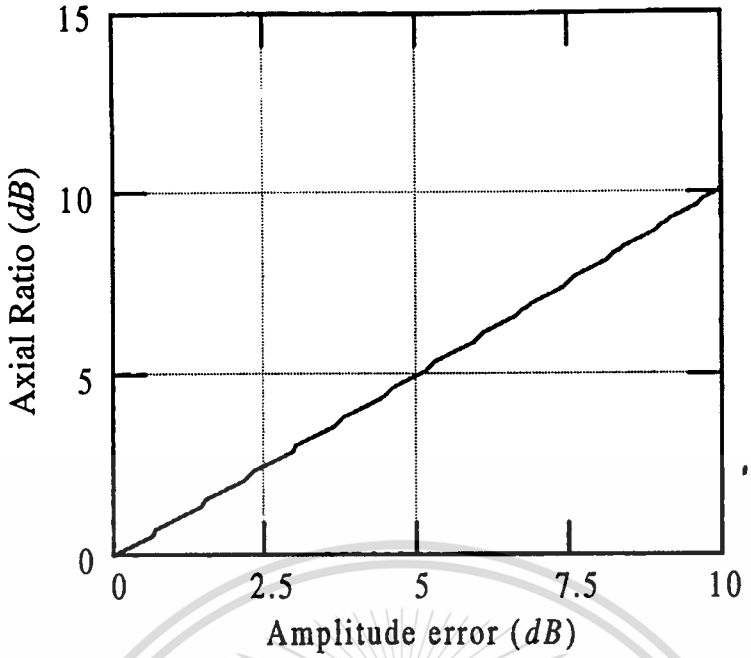

Fig. 5.7 Amplitude error of circular polarization excitation versus axial ratio

5.5.2 Phase Deviation

The effects from the phase error are discussed in this subsection. We consider the case that there are only phase deviation and $A=1$. By assuming the phase deviation is small. Then, by using one of the series expansions in Appendix B, we get

$$Ae^{j\Delta\phi} = e^{j\Delta\phi} \approx 1 + j(\Delta\phi)_{rad} = 1 + j\frac{\pi}{180}(\Delta\phi)^{\circ} \qquad (5.25)$$

Using (5.25) in (5.19), the RCL can be reduces to

$$RCL \approx \left|\frac{E_{xp}}{E_{co}}\right| = \left|\frac{-j(\Delta\phi)_{rad}}{2 + j(\Delta\phi)_{rad}}\right| = \frac{(\Delta\phi)_{rad}}{\sqrt{4 + (\Delta\phi)^2_{rad}}} = \frac{\pi}{360}(\Delta\phi)^{\circ} \qquad (5.26)$$

(5.26) is then expressed in dB. Then, we can write that

$$(RCL)_{dB} = 20\log XP = -41 + 20\log\left|\Delta\phi^{\circ}\right| \qquad (5.27)$$

The axial ratio in dB due to the phase errors can rapidly be calculated by substituting (5.27) in (5.21) and the series expansions in Appendix B, we get

$$(AR)_{dB} \approx 20\log\left[1 + 2\left|\frac{E_{xp}}{E_{co}}\right|\right] \approx 20(\log e)\frac{\pi}{180}|\Delta\phi| = \left|(\Delta\phi)^{\circ}\right|/6.6 \qquad (5.28)$$

The graphs represent (5.27) and (5.28) are illustrated in Fig. 5.8 and Fig. 5.9, respectively

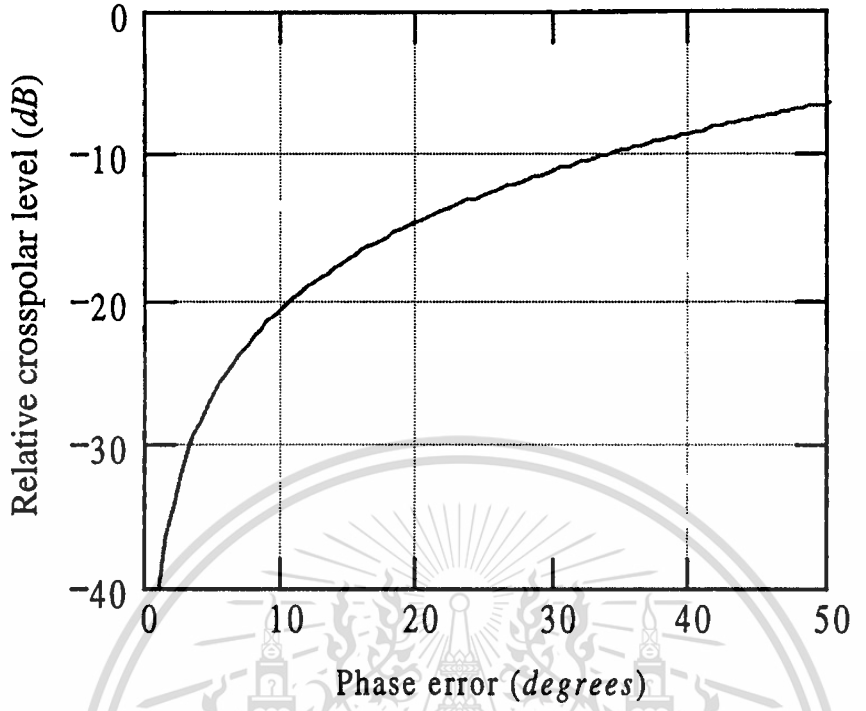

Fig. 5.8 Phase error of circular polarization excitation versus relative cross-polar level

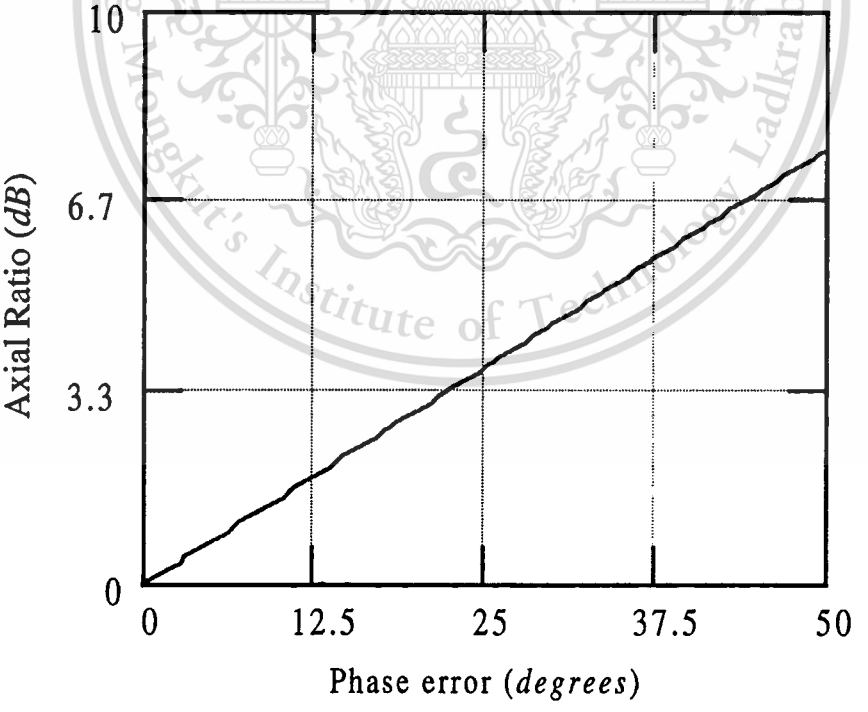

Fig. 5.9 Phase error of circular polarization excitation versus axial ratio

5.6 Numerical Results

For the results presented in this section, the co- and cross-polarization patterns and the axial ratio of a slot pair on sphere at $ka = 10$ and 20, the radius (a) of a sphere is equal to 7.64 cm and the three cases of the separation angle η are considered.

5.6.1 Co- and Cross-polarization Patterns

The co-polar (RHCP) and the cross-polar (LHCP) in x-z plane radiation patterns for two values of ka are shown in Fig. 5.10 and 5.11. The results are normalized with respect to the maximum value of the co-polarization (RHCP), which for all cases consider here occurs at $\theta = 90^\circ, \phi = 0^\circ$. In general, the higher effective radius (ka) will increase in the relative cross-polar level (RCL). When the value of θ close to broadside direction, the lower value of RCL is achieved. As expected, for $\theta = 90^\circ$, there is no cross-polar radiation and so $(RCL)_{dB} \rightarrow -\infty$ dB.

Fig. 5.10 shows the co- and cross-polarization patterns as a function of η and for $ka = 10$ and various values of θ in degrees. The results illustrate that the increment of η will slightly arise in the RCL. Moreover, these variations will be significantly observable when $ka = 20$. As shown in Fig. 5.11 where the positive $(RCL)_{dB}$ can be achieved over the range $48^\circ < \theta < 130^\circ$ for $\eta = 2$ cm and $60^\circ < \theta < 123^\circ$ for $\eta = 2.5$ cm.

5.6.2 Axial Ratios

The demonstrations of the axial ratio being plotted versus the observation angle θ in x-z plane are shown in Fig. 5.12 and 5.13. It is seen that at $\theta = 90^\circ, \phi = 0^\circ$ has a minimum axial ratio both in $ka = 10$ and 20. At close to the broadside direction, the rapid degradation in the axial ratio of $ka = 20$ is significantly observable than $ka = 10$. In each case, the larger η the faster change of the circular to elliptic polarization. This may be due to the symmetry of the structure is destroyed. In Fig. 5.12, at $ka = 10$, the 3 dB pattern bandwidth at $\eta = 1.5, 2.0$ and 2.5 cm are found to be $47, 33$ and 25 degrees, respectively. In addition, at $ka = 20$ as shown in Fig. 5.13, the 3 dB pattern bandwidth at $\eta = 1.5, 2.0$ and 2.5 cm are found to be $22, 16$ and 12 degrees, respectively. These results indicate that higher ka will lower the axial ratio pattern bandwidth.

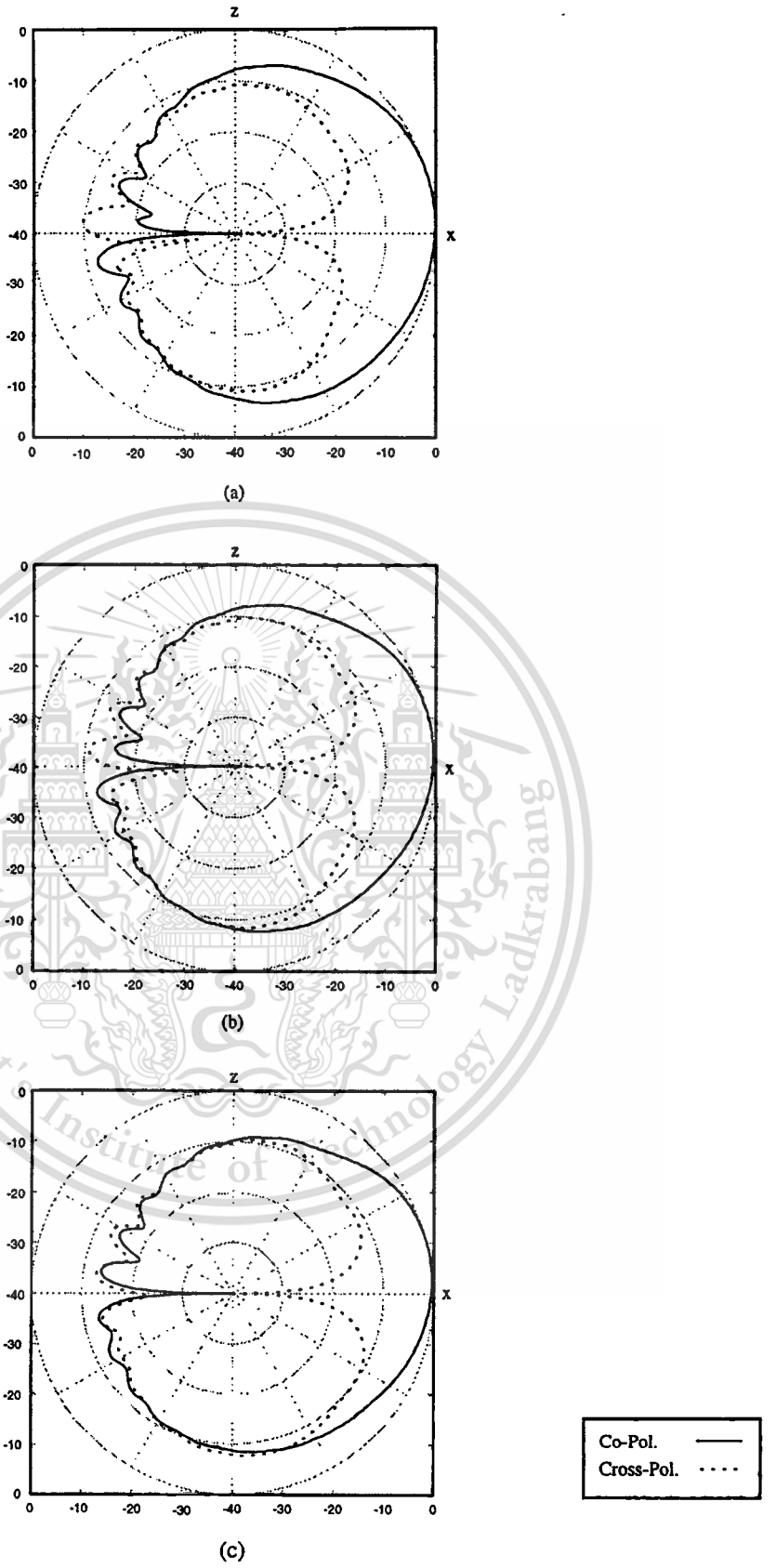

Fig. 5.10 Radiation pattern in x-z plane of a slot pair on a sphere at *ka=10 (a=7.64 cm)* with various parameter η
(a) η= *1.5 cm* (b) η= *2.0 cm* (c) η= *2.5 cm*

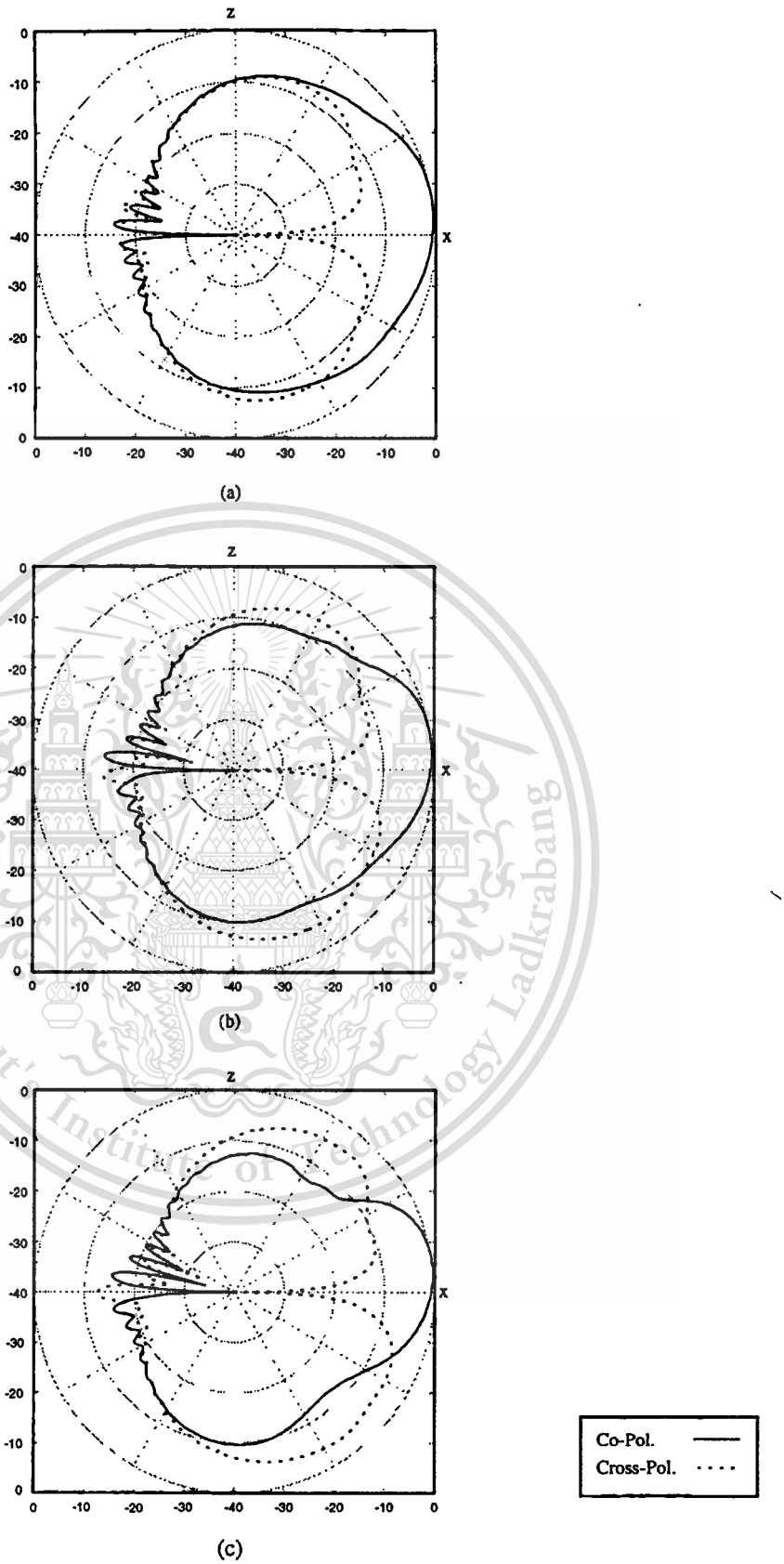

Fig. 5.11 Radiation pattern in x-z plane of a slot pair on a sphere at *ka=20 (a=7.64 cm)* with various parameter η
(a) η= *1.5 cm* (b) η= *2.0 cm* (c) η= *2.5 cm*

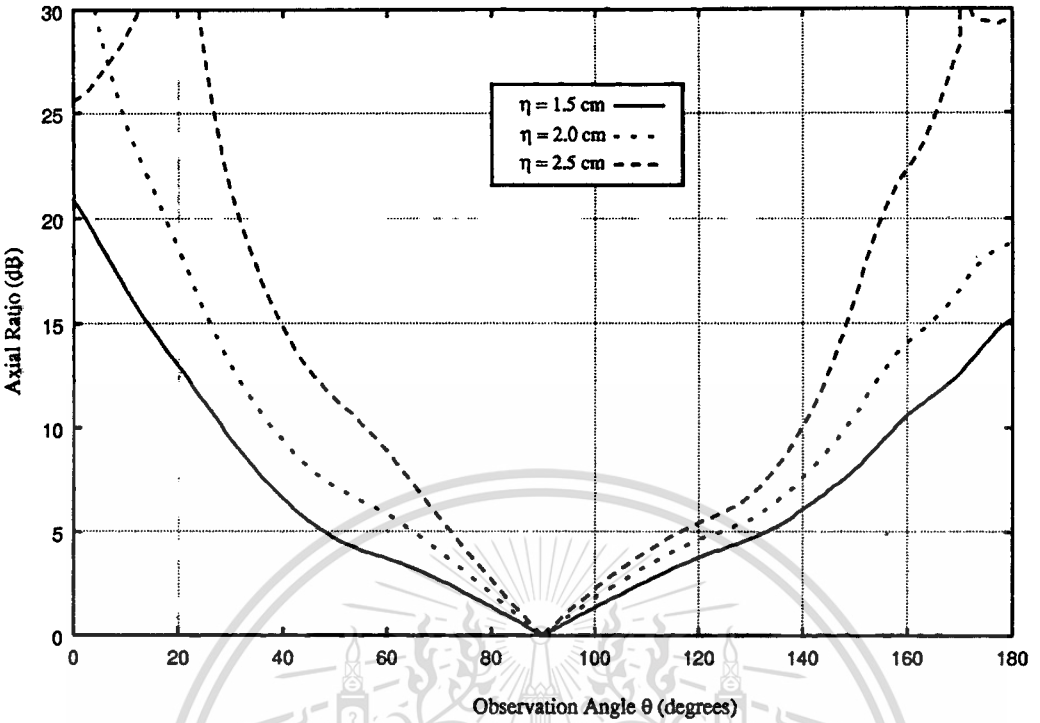

Fig. 5.12 Axial ratio in x-z plane of a slot pair on a sphere at $ka = 10$ ($a = 7.64$ cm) with various parameter η

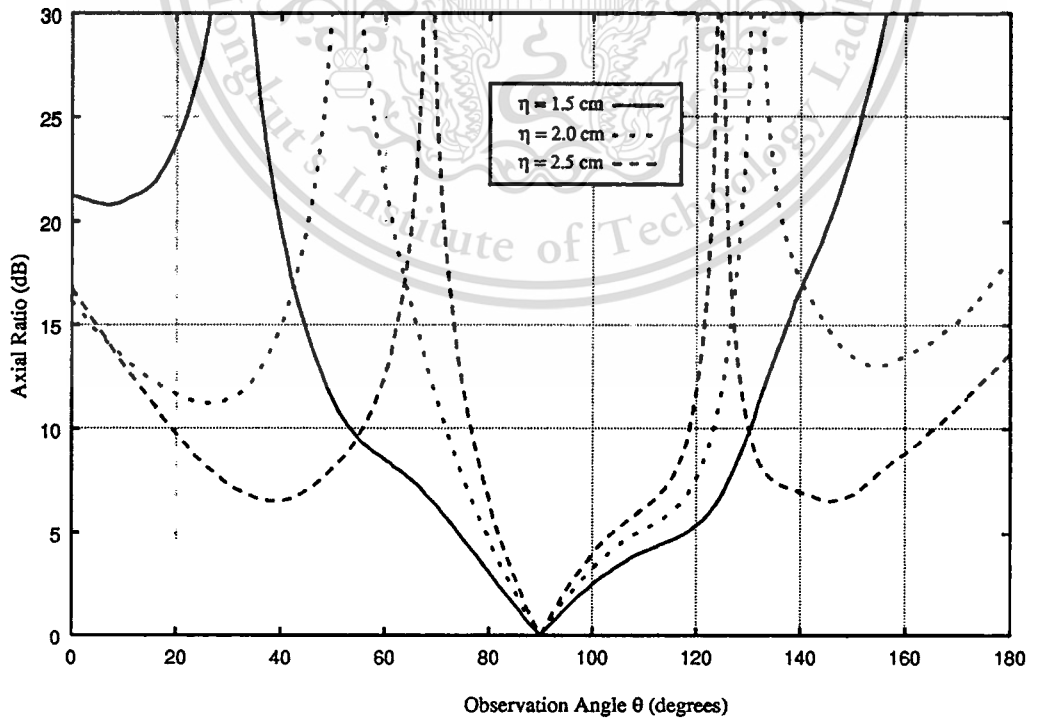

Fig. 5.13 Axial ratio in x-z plane of a slot pair on a sphere at $ka = 20$ ($a = 7.64$ cm) with various parameter η

5.7 Experimental Results

5.7.1 Co- and Cross-polarization patterns

An experimental validation of the antenna design is performed. The helix antenna is used as a receiving antenna. In order to determine the cross-polarized isolation, three helix antennas are fabricated, two of them are LHCP and another one is RHCP antenna. In the measurement, the LHCP helix antennas are used as the reference then by replacing one of them with a RHCP helix antenna and the received signal is recorded. With this data, the comparison of the co- and cross-polarization can be achieved. As the method mentioned above, the result of the cross-polarized isolation from the measurement is in the order of *14* dB.

The antenna under test is a slot pair on a sphere excited by two coaxial lines at the apertures. For the reason to generate a RHCP, an extra quarter-wavelength section of transmission line is excited at slot 2. The RG-223/U coaxial lines are used in the measurement and the wave velocity is approximately *86* % of wave propagation in the free space. The antenna prototype is built at the operating frequency of 5 GHz for $ka = 8$ ($a = 7.64$ cm) with the slot length and width are *3.0* cm and *1.50* mm, respectively. The equal amplitude is obtained by trying to match SWR of each slot as close as possible. The figure of this prototype is displayed in Fig. 5.14.

Fig. 5.14 Photograph of a slot pair on a sphere excited by coaxial line with radius 7.64 cm and $\eta = 2.5$ cm

Then, the antenna far-field test site is set up at the testing distance *1.10* m which is greater than a far-field distance. The antenna under test is connected to port 1 of the HP-8510C network analyzer to transmit the waves and is rotated *2* degrees per step. The co- and cross-polarization helix antennas are connected to port 2 of the network analyzer to measure the received signal strength. After that the antenna under test is rotated to transmit the signal to a receiving antenna. This measurement setup is shown in Fig. 5.15. Consequently, the co- and cross-polarization patterns are plotted and compare with the calculation as illustrated in Fig.5.16.

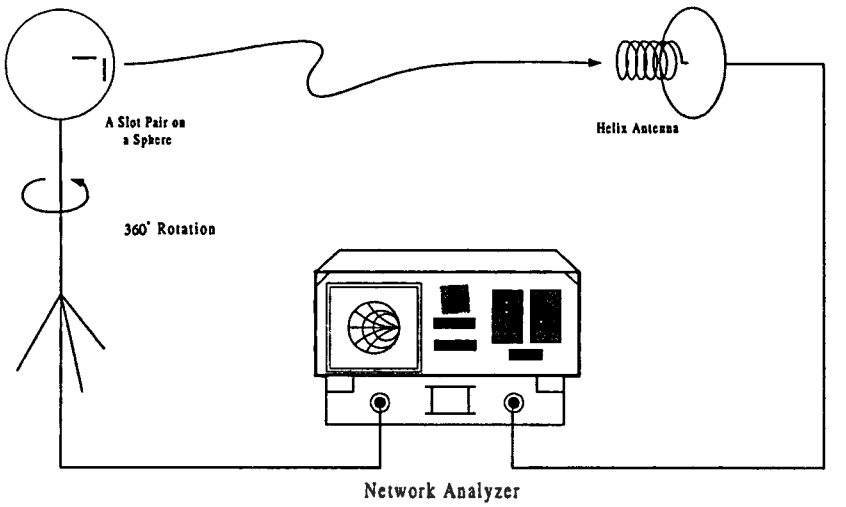

Fig. 5.15 Experiment setup to measure the radiation pattern of a slot pair on a sphere

Fig. 5.16 and 5.17 show the normalized electric far-field component co- and cross-polarization radiated by a slot pair on a sphere in the x-z plane. One can observe that, in the co-polar pattern, the computed pattern follows closely the measurement from $\theta = 30^{\circ}$ to 170° at $\eta = 2.5$ cm and $\theta = 20^{\circ}$ to 140° at $\eta = 3.0$ cm. In the cross-polar pattern, it shows that the discrepancy of the theoretical and experimental data is still high. This error may be due to the effects of the mutual coupling between the radiating slots are not taken into account and the multipath waves due to the imperfect free space test site.

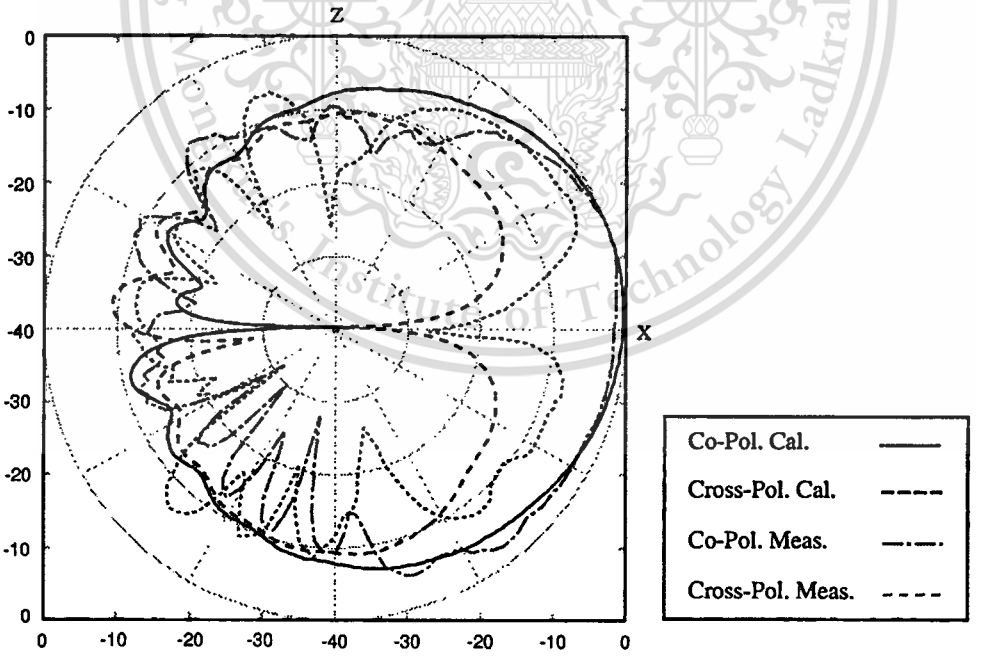

Fig. 5.16 Radiation pattern comparison in the x-z plane between theory and experiment at $ka = 8$ ($a = 7.64$ cm) with $\eta = 2.5$ cm

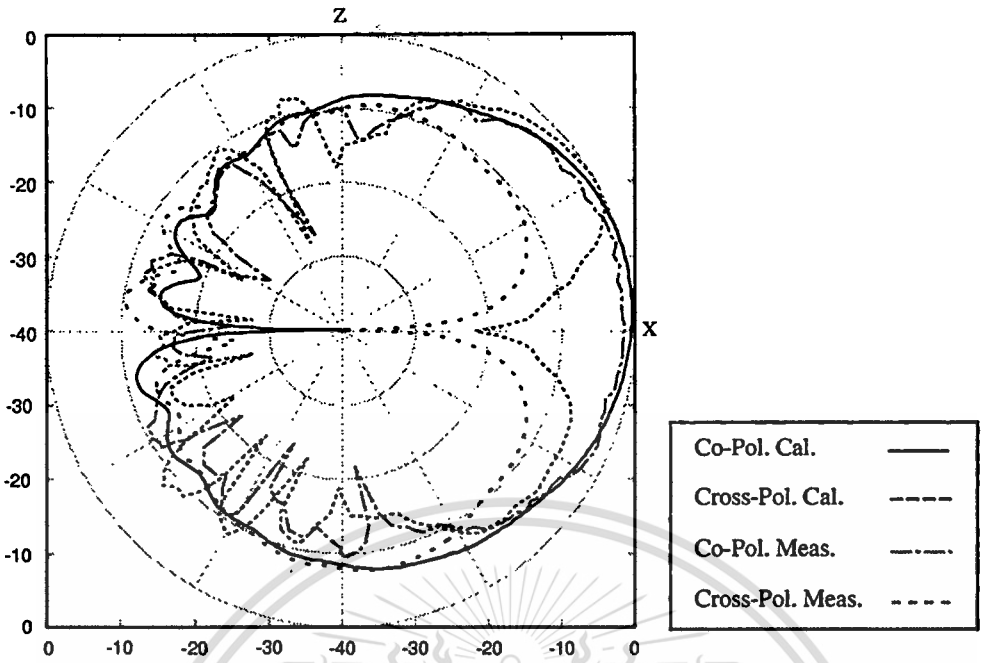

Fig. 5.17 Radiation pattern comparison in the x-z plane between theory and experiment at $ka = 8\,(a = 7.64$ cm) with $\eta = 3.0$ cm

5.7.2 Axial Ratios

Instead of helix antenna, the half-wave dipole is placed as a receiving antenna in the experiment. A dipole antenna with conductor thickness of *0.1* cm is showing in Fig.5.18. The antenna under test rotated *10* degrees per step to transmit the waves. At each step, the dipole antenna is rotated *360* degrees to record the received signal strength. The maximum and minimum signals are utilized to calculate the axial ratio. In addition, the measurement setup is shown in Fig. 5.19.

Fig. 5.18 Photograph of a half-wave dipole antenna perform as a receiving antenna in axial ratio measurement

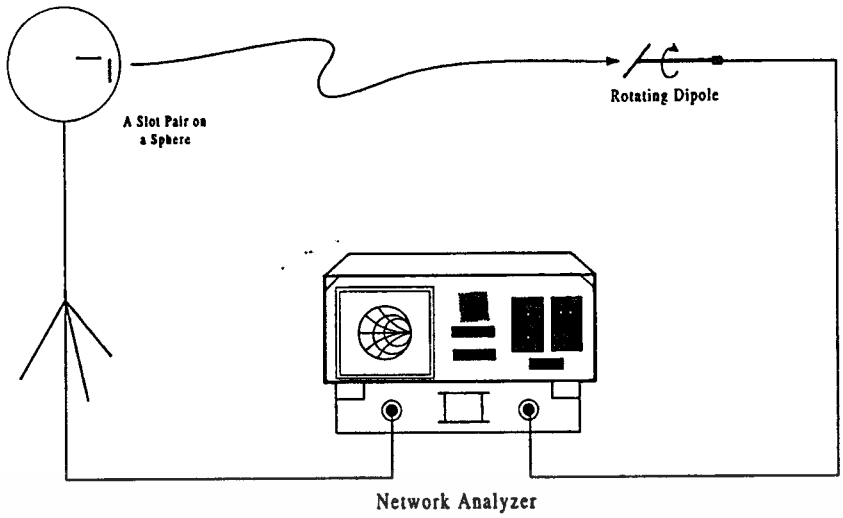

Fig. 5.19 Experiment setup to measure the axial ratio of a slot pair on a sphere

From the comparison results in the x-z plane of an axial ratio at $ka = 8$ with $\eta = 2.5$ and 3.0, as shown in Fig.5.20 and 5.21. The range of measurement starts from $\theta = 50^{\circ}$ to 130° because the range in the main beam direction is interested. As expected, the best axial ratio is occurred closely to $\theta = 90^{\circ}$ where at $\eta = 3.0$, $(AR)_{dB} = 2.4$ dB, also at $\eta = 3.0$, $(AR)_{dB} = 2.1$ dB and deteriorates on both sides of this point. The trend of the results for larger η, the rapid change of axial ratio can be significantly observed. Moreover, the discrepancy of the theoretical and experimental results has been observed because the cross polarization is still high. This may be occurred from the deviation from excitation phase and amplitude and also an imperfect fabrication of a prototype. In addition, the imperfect of free space test site will occur the reflected waves and disturb the accuracy of measurement results. However, the trend of measurement is in the similar way with the calculation. Reasonably, it is well to guarantee the accuracy of the theory.

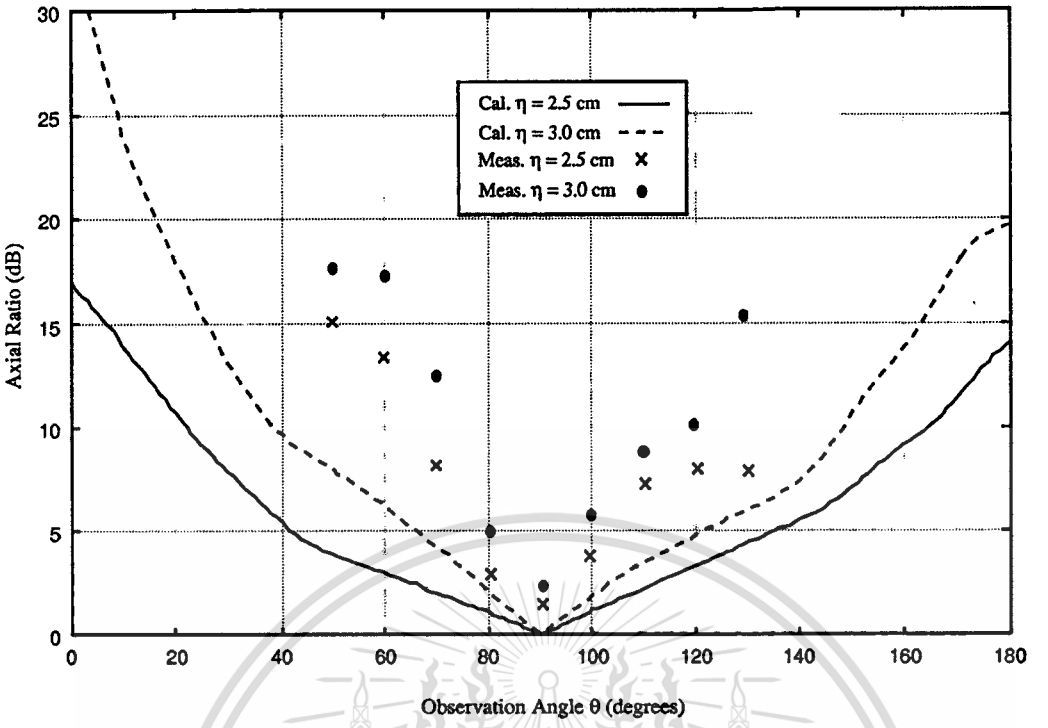

Fig. 5.20 Axial ratio comparison in the x-z plane between theory and experiment at $ka = 8\,(a = 7.64$ cm) with $\eta = 2.5$ and 3.0 cm

5.8 Conclusions

This chapter presents a theoretical approach for the analysis of a slot pair on a sphere. For the computation of the radiated fields, we used a coordinate transform from a previous chapter. The circular polarization has been obtained by exciting two orthogonal slots with *90* degrees phase difference. In addition, the derivation of the co- and cross-polarization and the axial ratio are presented. The prototype is constructed and measured the radiated wave. The experimental results have confirmed that for η become large, the cross-polarization increases proportionally with degrading the axial ratio. It should be pointed out that the best axial ratio is indicated at $\theta = 90$ degrees. Since the antenna under test still has high cross-polarization, many problems still remain such as the mutual coupling between the radiated slots, the cut-and-try to match the excitation. This problem will be left for further investigation and improvement.

CHAPTER 6

CONCLUSIONS

6.1 Summary of the Preceding Chapters

This thesis concerns with the analysis of a horizontal slot, an inclined slot and a slot pair on a sphere. The purpose of this study is to characterize the half-wave slot on a conducting sphere. The reason we consider this problem is to provide a fundamental theory of a slot as an array element of a spherical array antenna. Some principle backgrounds and the literature review on a slot antenna are addressed in chapter 1. The fundamentally analytical formulations of the electromagnetic waves of the spherical geometry are described in chapter 2. The derivation procedure is started with the Maxwell's equations and the continuity equation and then derived to the wave equation. The solutions are formulated via the Hertz vector potential by combining the *TE* and *TM* wave modes. In addition the method of separation of variables is used for solving the partial differential equations. The application of Lorentz reciprocity theorem is applied to solve the boundary value problem of an arbitrary aperture on a sphere. Then, the general solutions of the arbitrary aperture can be utilized to a slot on a sphere when the aperture is assumed to be a slot. The details of the derivation of a half-wave slot on a sphere are focused in chapter 3. It then starts from a narrow zonal slot by assuming the tangential field distribution on the aperture and applied to the half-wave slot on a sphere. The calculation results show the radiation patterns, directivity and front-to-back ratio. It is apparent from the results that the narrower the half-power beamwidth, the higher front-to-back ratio and the higher the directivity can be realized by selecting the larger effective radius. Next in chapter 4, the analysis in this chapter involves the radiation characteristics of an inclined slot on a sphere. Base on the application of the coordinate transformation, the space position in a difference coordinate system can be evaluated. This approach is expressed by the Euler rotation angle both on Cartesian and spherical coordinate systems. The relations between these coordinate systems are utilized to compute the radiation fields at various inclined angles. From the theoretical aspects as mentioned above, the investigation of a slot pair on a sphere is revealed in chapter 5. Two slots are perpendicularly located on the surface of a sphere to produce a circularly polarized radiation. Again, the contribution of coordinate transform is considered in the derivation. The plots of co- and cross-polarization pattern in addition to the axial ratio are demonstrated. In order to confirm the validity of the theoretical results, the experiment for some cases are set up and measured.

Finally, the summary of the material in this thesis and the discussion for the future works is included in chapter 6, the last chapter. Appendices consist of the vector analysis, the mathematical function in spherical coordinate. Additionally, the useful series expansions are presented at the end.

6.2 Remark for Future Research

Remarks for the further investigations are listed below :

1.) The improvement of the summation error in the numerical computation will be considered. The truncation and rounding error caused the unpredictable effects in computational results. The number of loops in each program will be equaled to $m \times n$, for example when $ka = 10$ the maximum m will be 14 and n will be up to 27, a number of loops is 378 but when $ka = 100$, m will become 98 and n will be maximized to 203, the number of loops will be $19{,}894$. This may be one factor that effects to the accuracy of the results.

2.) For ka larger than 100, the capacity of the computer is limited. In this work, we run program on Sun Ultra 10 workstation with Fortran 90 compiler. To overcome this obstruction, the ray techniques can be applied to reduce the summation of the program and will be continued in the future work.

3.) With the assumption of a tangential field distribution on the aperture, the analysis of electromagnetic wave in a sphere is neglected. For the rigorous investigation, the Method of Moment and the dyadic Green's function will be studied to combine the wave between the inner and outer of a sphere.

4.) In the model of a slot pair, it is assumed that the slot coupling is weak for reducing the complexity of the problem. However, to achieve the strong coupling, the model of the exciting structure must be considered to provide the exact solution.

5.) To form the spherical slot array antenna, the optimization of an arrangement and the dimension of the slots along the circumference of a sphere will be investigated.

REFERENCES

[1] Takada J., Ando M. and Goto N. "The bandwidth and the gain of radial line slot antenna with uniform slot density." IEICE Trans. Electron., vol. E73, Aug. 1990. pp. 1372-1377.

[2] Takahashi M., Takada J., Ando M., and Goto N. "A slot design for uniform aperture field distribution in single-layered radial line slot antennas." IEEE Trans. Antennas Propagat., vol. 39, Apr. 1991. pp. 954-959.

[3] Takada J., Tanisho A., Ito K., Ando M. and Goto N. "Radiation characteristics of a circularly polarized conical beam radial line slot antenna." 1994 Asia-Pacific Microwave Conf.Proc., Dec. 1994. pp. 101-104.

[4] Takada J., Yamamoto T., Ando M. and Goto N. "An azimuthal multibeam radial line slot antenna for mobile satellite communication." Proc. the 4th IEEE International Conf. On Universal Personal Communication, 1995. pp. 571-574.

[5] Horiguchi S., Ishizone T. and Mushiake Y. "Improvement on polarization property of turnstile spherical array antenna." IEICE Trans. Electron., vol. E67, Aug. 1984. pp. 451-453.

[6] Horiguchi S., Ishizone T. and Mushiake Y. "Radiation characteristics of spherical traingular array antenna." IEEE Trans. Antennas Propagat., vol. 33, Apr. 1985. pp. 473-476.

[7] Hori T., Terada N. and Kagoshima K. "Electronically steerable spherical array antenna for mobile earth station." Proc. of IEE. Conf. Antennas Propagat., 1987. pp. 55-58.

[8] Phongcharoenpanich C. "Electromagnetic Field Analysis of the Conducting Spherical Cavity and Segment." Master Thesis of King Mongkut's Institute of Technology Ladkrabang. 1998.

[9] Phongcharoenpanich C., Krairiksh M. and Takada J. "Investigations of radiation characteristics of a circularly polarized conical beam spherical slot array antenna." IEICE Trans. Electron., vol. E82-c, Jul. 1999. pp. 1242-1247.

[10] Bailin L.L. and Silver S. "Exterior electromagnetic boundary value problems for spheres and cones." IRE Trans. Antennas and Propagat., Jan. 1956. pp. 5-16.

[11] Mushiake Y. and Webster R.E. "Radiation characteristics with power gain for slots on sphere." IRE Trans. Antennas and Propagat., vol. 5, Jan. 1957. pp. 47-55.

[12] Sengupta D.L. "Experimental study of a spherical array of circularly polarized elements." Proceeding of IEEE, Nov. 1968. pp.2048-2051.

[13] Sengupta D.L., Smith T.M. and Larson R.W. "Radiation characteristics of a spherical array of circularly polarized elements." IEEE Trans. Antennas Propagat., vol. 16, Jan. 1968. pp. 2-7.

[14] Hoffman M. "Conventions for the analysis of spherical arrays." IEEE Trans. Antennas Propagat., vol. 11, Jul. 1963. pp. 390-393.

[15] Sadiku M.N.O. **Numerical Techniques in Electromagnetic Theory.** Boca Raton, FL: CRC Press. 1992.

[16] Taflove A. **Computational Electrodynamics the Finite-Difference Time-Domain Method.** Boston: Artech House. 1995.

[17] Harrington R.F. **Time-Harmonic Electromagnetic Fields.** New York: McGraw-Hill. 1961.

[18] Balanis C.A. **Antenna Theory: Analysis and Design.** 2nd edition. New York: John Wiley & Sons, Inc. 1997.

[19] Samii Y.R. "Useful coordinate transformations for antenna applications." IEEE Trans. Antennas Propagat., vol. 27, Jul. 1979. pp. 571-574.

[20] Arfken G.B. and Weber H.I. **Mathematical Methods for Physicists.** 4nd edition. San Diego, CA: Academic Press. 1995.

[21] Young E.C. **Vector and Tensor Analysis.** 2nd edition. New York: Dekker. 1993.

[22] Burger H. "Use of euler-rotation angles for generating antenna patterns." IEEE Antennas and Propagat. Mag., vol. 37, Apr. 1995. pp. 56-63.

[23] Milligan T. "More applications of euler rotation angles." IEEE Antennas and Propagat. Mag., vol. 41, Aug. 1999. pp. 78-83.

[24] Kawakami H., Sato G. and Wakabayashi R. "Research on circularly polarized conical-beam antennas." IEEE Antennas and Propagat. Mag., vol. 39, Jun. 1997. pp. 27-39.

[25] Huang J. "A technique for an array to generate circular polarization with linearly polarized elements." IEEE Trans. Antennas Propagat., vol. 34, Sep. 1986. pp. 1113-1124.

[26] Wong K.L. and Ke S.Y. "Cylindrical-rectangular microstrip patch antenna for circular polarization." IEEE Trans. Antennas Propagat., vol. 41, Feb. 1993. pp. 246-249.

[27] Ludwpig A.C. "The definition of cross polarization." IEEE Trans. Antennas Propagat., vol. 31, Jan. 1973. pp. 116-119.

[28] Stutman W.L. **Polarization in Electromagnetic Systems.** Norwood, MA: Artech House. 1992.

[29] Kraus J.D. **Antennas.** McGraw-Hill, New York, 1950.

[30] Mott H. **Polarization in Antennas and Radar.** John Wiley & Sons, Inc. 1986.

[31] Shavit R. "Circular polarization microstrip antenna on a conical surface." IEEE Trans. Antennas Propagat., vol. 45, Jul. 1997. pp. 1086-1092.

[32] Evans G.E. **Antenna Measurement Techniques.** Norwood, MA: Artech House. 1990.

[33] Hollis J.S., Lyon T.J. and Clayton L. **Microwave Antenna Measurements.** Atlanta, GA: Scientific-Atlanta, 1970.

[34] **IEEE Standard Test Procedure for Antennas** (IEEE Std. 149-1979), IEEE Inc., 1979.

[35] Marino R.A. and Hearst W. "Computation and measurement of the polarization ellipse." [Online]. Available : http://www.mwjournal.com/resources/oldarchive/ nov99/11M30.PDF. 1999.

[36] Kildal P.S. **Foundation of Antennas: A Unified Approach.** Lund, Sweden: Studentlitteratur. 2000.

[37] Pozar D.M. "Axial ratio of circularly polarized antennas with amplitude and phase errors." IEEE Antennas and Propagat. Mag., Oct. 1990. pp. 45-46.

[38] Parekh S.V. "Simple formulae for circular-polarization axial-ratio calculations." IEEE Antennas and Propagat. Mag., Feb. 1991. pp. 30-32.

APPENDICES

Appendix A

Vector Transformations and Operators in Spherical Coordinate

A.1 Vector Transformations

A.1.1 Vector Transformation between Rectangular and Spherical Coordinate

In this thesis, it required that the transformation be performed from rectangular-to-spherical components many times. The relation between rectangular and spherical coordinates can be written by

$$x = r\sin\theta\cos\phi \tag{A.1}$$

$$y = r\sin\theta\sin\phi \tag{A.2}$$

$$z = r\cos\theta \tag{A.3}$$

where

$$r = \sqrt{x^2 + y^2 + z^2} \tag{A.4}$$

$$\theta = \tan^{-1}\frac{z}{\sqrt{x^2 + y^2}} \tag{A.5}$$

$$\phi = \tan^{-1}\frac{y}{x} \tag{A.6}$$

The transformation matrix from rectangular-to-spherical components are accomplished by

$$\begin{bmatrix} A_r \\ A_\theta \\ A_\phi \end{bmatrix} = \begin{bmatrix} \sin\theta\cos\phi & \sin\theta\sin\phi & \cos\theta \\ \cos\theta\cos\phi & \cos\theta\sin\phi & -\sin\theta \\ -\sin\phi & \cos\phi & 0 \end{bmatrix} \begin{bmatrix} A_x \\ A_y \\ A_z \end{bmatrix} \tag{A.7}$$

and the spherical-to-rectangular components are related by

$$\begin{bmatrix} A_x \\ A_y \\ A_z \end{bmatrix} = \begin{bmatrix} \sin\theta\cos\phi & \cos\theta\cos\phi & -\sin\phi \\ \sin\theta\sin\phi & \cos\theta\sin\phi & \cos\phi \\ \cos\theta & -\sin\theta & 0 \end{bmatrix} \begin{bmatrix} A_r \\ A_\theta \\ A_\phi \end{bmatrix} \tag{A.8}$$

A.1.2 Vector Transformation between Cylindrical and Spherical Coordinate

We can write the relation between cylindrical and spherical components by

$$\rho = r\sin\theta \tag{A.9}$$

$$\phi = \phi \tag{A.10}$$

$$z = r\cos\theta \tag{A.11}$$

where

$$r = \sqrt{\rho^2 + z^2} \tag{A.12}$$

$$\theta = \tan^{-1}\frac{\rho}{z} \tag{A.13}$$

$$\phi = \phi \tag{A.14}$$

The transformation matrix from rectangular-to-spherical components are accomplished by

$$\begin{bmatrix} A_r \\ A_\theta \\ A_\phi \end{bmatrix} = \begin{bmatrix} \sin\theta & 0 & \cos\theta \\ \cos\theta & 0 & -\sin\theta \\ 0 & 1 & 0 \end{bmatrix} \begin{bmatrix} A_\rho \\ A_\phi \\ A_z \end{bmatrix} \tag{A.15}$$

and the spherical-to-cylindrical components are related by

$$\begin{bmatrix} A_\rho \\ A_\phi \\ A_z \end{bmatrix} = \begin{bmatrix} \sin\theta & \cos\theta & 0 \\ 0 & 0 & 1 \\ \cos\theta & -\sin\theta & 0 \end{bmatrix} \begin{bmatrix} A_r \\ A_\theta \\ A_\phi \end{bmatrix} \tag{A.16}$$

Note that the component A_ϕ and coordinate ϕ are the same in both systems.

A.2 Vector Differential Operators in Spherical Coordinate

Gradient:

$$\nabla\psi = \hat{a}_r \frac{\partial\psi}{\partial r} + \hat{a}_\theta \frac{1}{r}\frac{\partial\psi}{\partial\theta} + \hat{a}_\phi \frac{1}{r\sin\theta}\frac{\partial\psi}{\partial\phi} \tag{A.17}$$

Divergence:

$$\nabla\cdot\overline{A} = \frac{1}{r^2}\frac{\partial}{\partial r}\left(r^2 A_r\right) + \frac{1}{r\sin\theta}\frac{\partial}{\partial\theta}\left(\sin\theta A_\theta\right) + \frac{1}{r\sin\theta}\frac{\partial A_\phi}{\partial\phi} \tag{A.18}$$

Curl:

$$\nabla\times\overline{A} = \frac{\hat{a}_r}{r\sin\theta}\left[\frac{\partial}{\partial\theta}\left(A_\phi\sin\theta\right) - \frac{\partial A_\theta}{\partial\phi}\right] + \frac{\hat{a}_\theta}{r}\left[\frac{1}{\sin\theta}\frac{\partial A_r}{\partial\phi} - \frac{\partial}{\partial r}\left(rA_\phi\right)\right] + \frac{\hat{a}_\phi}{r}\left[\frac{\partial}{\partial r}\left(rA_\theta\right) - \frac{\partial A_r}{\partial\theta}\right] \tag{A.19}$$

Laplacian of a scalar:

$$\nabla^2\psi = \frac{1}{r^2}\frac{\partial}{\partial r}\left(r^2\frac{\partial\psi}{\partial r}\right) + \frac{1}{r^2\sin\theta}\frac{\partial}{\partial\theta}\left(\sin\theta\frac{\partial\psi}{\partial\theta}\right) + \frac{1}{r^2\sin^2\theta}\frac{\partial^2\psi}{\partial\phi^2} \tag{A.20}$$

Laplacian of a vector:

$$\nabla^2\overline{A} = \nabla(\nabla\cdot\overline{A}) - \nabla\times\nabla\times\overline{A} \tag{A.21}$$

$$\nabla^2\overline{A} = \hat{a}_r\left(\frac{\partial^2 A_r}{\partial r^2} + \frac{2}{r}\frac{\partial A_r}{\partial r} - \frac{2}{r^2}A_r + \frac{1}{r^2}\frac{\partial^2 A_r}{\partial\theta^2} + \frac{\cot\theta}{r^2}\frac{\partial A_r}{\partial\theta} + \frac{1}{r^2\sin^2\theta}\frac{\partial^2 A_r}{\partial\phi^2} - \frac{2}{r^2}\frac{\partial A_\theta}{\partial\theta} - \frac{2\cot\theta}{r^2}A_\theta - \frac{2}{r^2\sin\theta}\frac{\partial A_\phi}{\partial\phi}\right)$$

$$+\hat{a}_\theta\left(\frac{\partial^2 A_\theta}{\partial r^2}+\frac{2}{r}\frac{\partial A_\theta}{\partial r}-\frac{A_\theta}{r^2\sin^2\theta}+\frac{1}{r^2}\frac{\partial^2 A_\theta}{\partial\theta^2}+\frac{\cot\theta}{r^2}\frac{\partial A_\theta}{\partial\theta}+\frac{1}{r^2\sin^2\theta}\frac{\partial^2 A_\theta}{\partial\phi^2}+\frac{2}{r^2}\frac{\partial A_r}{\partial\theta}-\frac{2\cot\theta}{r^2\sin\theta}\frac{\partial A_\phi}{\partial\phi}\right)$$

$$+\hat{a}_\phi\left(\frac{\partial^2 A_\phi}{\partial r^2}+\frac{2}{r}\frac{\partial A_\phi}{\partial r}-\frac{1}{r^2\sin^2\theta}A_\phi+\frac{1}{r^2}\frac{\partial^2 A_\phi}{\partial\theta^2}+\frac{\cot\theta}{r^2}\frac{\partial A_\phi}{\partial\theta}+\frac{1}{r^2\sin^2\theta}\frac{\partial^2 A_\phi}{\partial\phi^2}+\frac{2}{r^2\sin\theta}\frac{\partial A_r}{\partial\phi}+\frac{2\cot\theta}{r^2\sin\theta}\frac{\partial A_\theta}{\partial\phi}\right)$$

(A.22)

Appendix B

Special Function in Spherical Coordinate and Useful Series Expansions

B.1 Spherical Bessel and Hankel Functions

The spherical Bessel and Hankel functions is another set of the Bessel and Hankel functions which satisfied the spherical Bessel's differential equation that can be written that

$$\frac{d^2}{dx^2}(xz_\nu(x))+\left[1-\frac{n(n+1)}{x^2}\right]xz_\nu(x)=0 \tag{B.1}$$

where $z_\nu(x)$ are

$j_n(x)$: Spherical Bessel function of the first kind of order n,

$y_n(x)$: Spherical Bessel function of the second kind of order n,

$h_n^{(1)}(x)$: Spherical Hankel function of the first kind of order n,

$h_n^{(2)}(x)$: Spherical Hankel function of the second kind of order n.

The spherical Bessel and Hankel functions of order n are relate, respectively, to the regular Bessel and Hankel of order $n+1/2$ by

$$j_n(x)=\sqrt{\frac{\pi}{2x}}J_{n+1/2}(x) \tag{B.2}$$

$$y_n(x)=\sqrt{\frac{\pi}{2x}}Y_{n+1/2}(x) \tag{B.3}$$

$$h_n^{(1)}(x)=\sqrt{\frac{\pi}{2x}}H_{n+1/2}^{(1)}(x) \tag{B.4}$$

$$h_n^{(2)}(x) = \sqrt{\frac{\pi}{2x}} H_{n+1/2}^{(2)}(x) \tag{B.5}$$

Recurrence Relation and Differentiation Formulas:

$$z_{v-1}(x) + z_{v+1}(x) = \frac{2v+1}{x} z_v(x) \tag{B.6}$$

$$z_v'(x) = \frac{1}{2v+1}\left[v z_{v-1}(x) - (v+1) z_{v+1}(x)\right] \tag{B.7}$$

Small-Argument Approximations:

$$j_n(x) \approx \frac{x^n}{1 \cdot 3 \cdot 5 \cdots (2n+1)} \tag{B.8}$$

$$y_n(x) \approx -1 \cdot 3 \cdot 5 \cdots (2n-1) x^{-(n+1)} \tag{B.9}$$

$$h_n^{(1)}(x) \approx j_n(x) + j y_n(x) \tag{B.10}$$

$$h_n^{(2)}(x) \approx j_n(x) - j y_n(x) \tag{B.11}$$

Large-Argument Approximations:

$$j_n(x) \approx \frac{1}{x} \sin\left(\frac{n\pi}{2} - x\right) \tag{B.12}$$

$$y_n(x) \approx \frac{1}{x} \cos\left(\frac{n\pi}{2} - x\right) \tag{B.13}$$

$$h_n^{(1)}(x) \approx \frac{j^{-(n+1)}}{x} e^{jx} \tag{B.14}$$

$$h_n^{(2)}(x) \approx \frac{j^{n+1}}{x} e^{-jx} \tag{B.15}$$

B.2 Associated Legendre Functions

The associated Legendre functions are the functions that satisfied the associated Legendre's differential equation as

$$(1-x^2)\frac{d^2Y_n^m}{dx^2} - 2x\frac{dY_n^m}{dx} + \left[n(n+1) - \frac{m^2}{1-x^2}\right]Y_n^m = 0 \tag{B.16}$$

Its general solution is of the form

$$Y_n^m(x) = A_{mn}P_n^m(x) + B_{nm}Q_n^m(x) \tag{B.17}$$

Where n and m is the nonnegative integer values. $P_n^m(x)$ and $Q_n^m(x)$ are called the associated Legendre functions of the first and second kind, respectively. The associated Legendre functions $P_n^m(x)$ and $Q_n^m(x)$ are related to the first kind Legendre functions $P_n(x)$ and the second kind $Q_n(x)$ by

$$P_n^m(x) = (1-x^2)^{m/2}\frac{d^m P_n(x)}{dx^m} \tag{B.18}$$

$$Q_n^m(x) = (1-x^2)^{m/2}\frac{d^m Q_n(x)}{dx^m} \tag{B.19}$$

where

$$P_n(x) = \frac{1}{2^n n!}\left(\frac{d}{dx}\right)^n (x^2-1)^n \tag{B.20}$$

$$Q_n(x) = P_n(x)\left\{\frac{1}{2}\ln\left(\frac{1+x}{1-x}\right) - \psi(n)\right\} + \sum_{m=1}^{n}\frac{(-1)^m(n+m)!}{(m!)^2(n-m)!}\psi(m)\left(\frac{1-x}{2}\right)^m \tag{B.21}$$

where

$$\psi(n) = 1 + \frac{1}{2} + \frac{1}{3} + \ldots + \frac{1}{n} \tag{B.22}$$

Note that the Legendre functions $Q_n(x)$ of the second kind are singular at $x = \pm 1$.

Properties and Identities of Associated Legendre Functions are :

Special Value when n and m are integers:

$$P_n^m(x) = 0, \qquad m > n \tag{B.23}$$

$$P_n^m(-x) = (-1)^{n-m} P_n^m(x) \tag{B.24}$$

$$P_n^m(x) = P_{-n-1}^m(x) \tag{B.25}$$

Differential Formulas:

$$\frac{d}{dx} P_n^m(x) = \frac{(n+m)P_{n-1}^m(x) - nxP_n^m(x)}{1-x^2} \tag{B.26}$$

$$\frac{d}{d\theta} P_n^m(x) = \frac{1}{2}\left[(n-m+1)(n+m)P_n^{m-1}(x) - P_n^{m+1}(x)\right] \tag{B.27}$$

$$\frac{d}{d\theta} P_n^m(x) = -(1-x^2)^{1/2} \frac{d}{dx} P_n^m(x) \tag{B.28}$$

$$\frac{d}{dx} P_n^m(x) = -\frac{mxP_n^m(x)}{1-x^2} + \frac{(1-x^2)^{m/2}}{2^n} \sum_{k=0}^{\left[\frac{m-n}{2}\right]} \frac{(-1)^k (2n-2k)!\, x^{n-2k-m-1}}{k!(n-k)!(n-2k-m)!} \tag{B.29}$$

Recurrence Formulas:

$$P_n^m(x) = \frac{(2n-1)xP_{n-1}^m(x) - (n+m-1)P_{n-2}^m(x)}{n-m} \tag{B.30}$$

$$P_n^m(x) = \frac{2(m-1)x}{(1-x^2)^{1/2}} P_n^{m-1}(x) - (n-m+2)(n+m-1)P_n^{m-2}(x) \tag{B.31}$$

Integrals:

$$\int_{-1}^{1} P_n^m(x) P_k^m(x)\, dx = \frac{2}{2n+1} \frac{(n+m)!}{(n-m)!} \delta_{nk} \tag{B.32}$$

$$\int_{-1}^{1} \frac{P_n^m(x) P_n^k(x)}{1-x^2}\, dx = \frac{1}{m} \frac{(n+m)!}{(n-m)!} \delta_{mk} \tag{B.33}$$

B.3 Useful Series Expansions

$$\frac{1}{1+x} \approx 1-x+x^2 \qquad when\ x << 1 \qquad (B.34)$$

$$\frac{1+x}{1-x} \approx 1+2x+2x^2 \qquad when\ x << 1 \qquad (B.35)$$

$$e^x \approx 1+x+\frac{1}{2}x^2 \qquad when\ x << 1 \qquad (B.36)$$

$$e^{-jk\Delta} \approx 1-jk\Delta-\frac{1}{2}(k\Delta)^2 \qquad when\ k\Delta << 1 \qquad (B.37)$$

$$\ln(1+x) \approx x-\frac{1}{2}x^2 \qquad when\ x << 1 \qquad (B.38)$$

$$\log(1+x) = (\log e)\ln(1+x) = \log e(x-\frac{1}{2}x^2) \qquad when\ x << 1 \qquad (B.39)$$

$$\sqrt{z^2+\Delta^2} \approx z+\frac{1}{2}\frac{\Delta^2}{z} \qquad when\ \Delta^2 << z^2 \qquad (B.40)$$

$$10^x = e^{x\ln 10} \approx (1+x\ln 10) \qquad when\ x << 1/\ln 10 = 0.43 \qquad (B.41)$$

$$A = 10^{A_{dB}/10} = e^{A_{dB}\ln 10/10} \approx 1+A_{dB}\ln 10/10 \approx 1+0.23A_{dB} \qquad when\ A_{dB} << 4.3 \qquad (B.42)$$

AUTHOR BIOGRAPHY

Author: Chaiwat Leekpai

Date of Birth: November 19, 1974

Place of Birth: Trang Province, Thailand

Bachelor Degree: B.Eng. in Computer Engineering

Institution: Department of Computer Engineering
Faculty of Engineering
King Mongkut's University of Technology Thonburi

Year of Graduation: 1997

Interested Researches: Slot array antenna, Microstrip antenna, Asymptotic function and numerical techniques in electromagnetic

Related Publications:

1. **C.Leekpai,** C.Phongcharoenpanich and M.Krairiksh "Theoretical investigation of a slot on spherical surface" 21st Electrical Engineering Conference (EECON-21), Bangkok, Thailand, Nov. 1998, pp.513-516.